INHIBITED BOVINE TRYPSIN, AND BOVINE TRYPSINOGEN: THE REFINED STRUCTURE AND MECHANISM OF A NOT-TOO-SERENE PROTEASE

Thesis by

John L. Chambers

In Partial Fulfillment of the Requirements

for the Degree of

Doctor of Philosophy

California Institute of Technology

Pasadena, California

1977

(Submitted 4 May 1977)

TO MY GRANDFATHER

PREFACE

This thesis is in large part an introduction to and summary of the work described in detail in the appendices. The central theme of this work has been the elucidation of the detailed, high-resolution three-dimensional structures of inhibited derivatives of bovine trypsin and of bovine trypsinogen, and the implications of these studies for protease mechanism, and for structure and function of enzymes in general.

Chapter I is a historical sketch concerning protease structure and mechanism, and introduces the present work on diisopropylphosphoryl (DIP)-, Ag^{+}-, and Cu^{2+}-inhibited trypsins. This work is described more fully in Appendices 1 and 6, and in Chapter IV. Chapter II and Appendices 4 and 5 deal with trypsinogen and the structural basis for the inactivity of this precursor of trypsin, as well as its mechanism of activation.

In order for these structures to be interpreted reliably, extension of their resolution and structure refinement were necessary. A major portion of this thesis work has thus been development of techniques for routine, inexpensive refinement of macromolecular structures. These techniques and their application in the case of DIP-trypsin are presented in Chapter III and Appendix 6. The reliability of even the most highly refined structure is, however, affected by the accuracy of the data. Improved methods of correcting protein data for background radiation, with a corresponding improvement in

accuracy, were developed in the course of this thesis work, and are presented in Appendix 2.

Portions of the DIP-trypsin structure at its current level of refinement (R = 21.5% at 1.5 Å resolution) are shown in Appendix 7, and protease mechanism is discussed in detail in Appendix 3.

ACKNOWLEDGMENTS

I would like to thank my fellow graduate students and colleagues, Tony Kossiakoff, Monty Krieger, Steve Spencer, Mike Ross, Roger Koeppe, Dave Agard, Mel Jones, Gary Christoph and Steve Skedzeleski, in addition to those identified in the appendices, for their help and suggestions during the course of this work.

I am grateful for the assistance of Dee Barr in typing the manuscripts of this thesis and of the papers appearing in the appendices (these latter ones several times each, as I remember). Her patience and advice during my stay at Caltech have been very helpful.

My deep appreciation goes to C.L. Borders, Jr., S.E. Anderson, L.W. Haynes, T.R. Williams, R.H. Bromund, D.L. Powell, W.F. Kieffer, J.W. Chittum and J.D. Reinheimer. Their instruction and encouragement during my undergraduate years have proven invaluable.

I thank the National Institutes of Health for financial support during my graduate career.

My parents, grandparents, and the other members of my family gave me their support and encouragement throughout this work, for which I am extremely grateful. Special thanks go to my brother, Scott, for staying in Ohio during the last five years.

Most of all I would like to thank my advisor, Robert Stroud, who taught me to ask whether it is better "to suffer the slings and arrows of outrageous torsions, or by opposing bend them?" His

guidance has been most valuable, and working in his laboratory has been a unique experience as well as a very rewarding one.

ABSTRACT

Refined three-dimensional structures of diisopropylphosphoryl (DIP)-inhibited bovine trypsin and of bovine trypsinogen are described, as determined by x-ray crystallography. A constrained difference Fourier method for rapid, economical protein structure refinement was developed and applied to these structures. The refinement system, which has been written to operate on a minicomputer, has reduced the standard crystallographic R-factor for DIP-trypsin from 47.2% at 2.7 Å resolution to 21.5% at 1.5 Å resolution, making it one of the most highly and inexpensively refined protein structures to date. For trypsinogen, R is 31% at 1.9 Å resolution, and refinement of both structures is nearing completion. The refined structures, the mechanism of serine proteases, and the mechanism of activation of their zymogens are discussed.

During data collection for the studies described, new, more efficient techniques of correction for background radiation in protein data measured by x-ray diffractometry were developed.

Also presented are the structures of trypsin inhibited by the metal ions Ag^{+} and Cu^{2+}. These ions, which are powerful trypsin and chymotrypsin inhibitors, bind tightly and specifically at the active site of the enzyme, between Asp 102 O_{δ_1} and His 57 N_{δ_1}. They may thus be used as specific probes of the active site of serine proteases.

TABLE OF CONTENTS

Chapter I

Serine Protease Structure and Mechanism: Introduction and Background

The wide occurrence of the family of peptide-bond splitting enzymes, the serine proteases, along with their participation in a variety of important physiological processes, has placed them among the most extensively studied proteins. The digestive enzymes, trypsin, chymotrypsin, and elastase, have been especially well studied. Other members of the serine protease family include thrombin, which is important in blood clotting (1); enzymes of the complement system (2); acrosomal protease, important in fertilization (3); and plasmin, which is involved in dissolution of blood clots (4). Increased plasmin activity has also been shown to be responsible for a number of morphological changes in the transformation of cancer cells (5,6,7). Study of the serine proteases has resulted in not only a better understanding of these physiological processes, but also development of general principles of enzyme catalysis and specificity.

The reaction catalyzed by these enzymes is schematized below:

$$E + S \rightleftharpoons ES \rightleftharpoons ES^{T} \rightleftharpoons EA \rightleftharpoons EP_2^{T} \rightleftharpoons EP_2 \rightleftharpoons E + P_2$$

$$+$$

$$P_1$$

where E, S, P_1 and P_2 are respectively free enzyme, substrate, the amine (or alcohol in ester hydrolysis) product, and carboxylic acid product. ES and EP_2 are Michaelis complexes, ES^{T} and EP_2^{T} are tetrahedral intermediates, and EA is the acyl-enzyme intermediate (8-14).

These enzymes work optimally near pH 8 (15). While the kinetics of peptide or ester hydrolysis are very similar for different members of the family, each member exhibits its own substrate specificity. For example, trypsin, chymotrypsin, and elastase preferentially hydrolyze peptide bonds to the carboxyl side of residues with long positively-charged side chains, large hydrophobic side chains, and small side chains, respectively (16).

The side chains of residues Ser 195 and His 57 (using the chymotrypsinogen numbering system), conserved throughout the serine protease family, were demonstrated to be essential for enzymatic activity by chemical modification (17,18). Solution of the three-dimensional structure of tosyl-α-chymotrypsin at pH 4.2 and 2 Å resolution by Blow and coworkers showed that these two residues were in fact adjacent to one another in the catalytic site, with Ser 195 Oγ hydrogen-bonded to His 57 Nε, and indicated the importance of a third residue, Asp 102, whose carboxyl group was hydrogen bonded to the other side of the His 57 imidazole ring (19,20). In 1966, Oppenheimer et al. (9) had shown the importance of the amino terminus in the reactivity of chymotrypsin. Matthews et al. (19) noted that the amino terminus formed a salt bridge to Asp 194, stabilizing the conformation of the protein around the active-site serine. Henderson (21) and Robertus et al. (22) later suggested the importance of hydrogen bonds from the N—H groups of Gly 193 and Ser 195 to the substrate carbonyl oxygen in stabilization of reaction intermediates.

Subsequently the structure of diisopropylphosphoryl (DIP)-trypsin at pH 7 was solved at 2.7 Å resolution by Stroud, Kay, and Dickerson (23). Diisopropylfluorophosphate is a very powerful general inhibitor of serine proteases. The DIP group becomes covalently attached to the active-site serine, and probably resembles a tetrahedral intermediate in the proteolytic reaction (24). In spite of a sequence identity between trypsin and chymotrypsin in only 40% of the residues, their overall three-dimensional folding was shown to be remarkably similar (23,24). These authors also noted that the carboxyl group of Asp 189 (serine in chymotrypsin) is in an ideal position to form a hydrogen bond to the positively charged side chain of a specific substrate. Krieger, Kay and Stroud showed that this interaction does indeed give trypsin its specificity, when they solved the structure of trypsin reversibly inhibited by the specific side chain analog, benzamidine (25).

Elastase at pH 5, solved at 3.5 Å resolution by Shotton and Watson (26), is also remarkably similar in structure to trypsin and chymotrypsin. Residue 216, which is Gly in these latter two enzymes, is valine in elastase. This valine side chain blocks access to the lower portion of the specific binding pocket, thus giving elastase its specificity for small side chains.

The pH-rate profiles for these enzymes were shown in early experiments to depend upon deprotonation of a group with a pK_a between 6 and 7 (27,28). Since this is the normal range for ionization of a histidine imidazole, His 57 was generally assumed responsible for this

limb of the profile (11,18,29,30). However, in the mechanism suggested by Blow and coworkers Asp 102, in its unusual environment, acts as a base rather than simply to stabilize a positive charge on the His 57 imidazole, or to maintain structure, and accepts a proton from the imidazole while the imidazole in turn receives a proton from Ser 195 Oγ (31). The explanation of the pH-rate profile given such a mechanism and the assumed normal pK_a's of Asp 102 and His 57, however, was then unclear. In 1973, Hunkapiller et al. (32), from ^{13}C nmr studies of α-lytic protease, presented strong evidence that His 57 remained neutral throughout the pH range 4 - 9, and suggested that the pK_a of 6.8 observed in the rate profile arose from Asp 102. Koeppe and Stroud, using difference infrared titration, were able to assign directly a pK_a of 6.8 to the carboxyl group of Asp 102 (33).

One of the studies presented in this thesis is the crystallographic determination of the inhibitory site for Ag^+ and Cu^{2+} in trypsin. These ions are strong inhibitors of trypsin and chymotrypsin ($K_I \sim 10^{-4}$ M), which impair catalysis without hindering substrate binding (34,35). Using a difference Fourier technique, we found that the major binding site for these ions is between Asp 102 $O\delta_1$ and His 57 $N\delta_1$, with approximately linear coordination of the metal ion. The resulting disruption of the charge-relay system greatly diminishes the activity of the enzyme. Not only did an understanding of the inhibition mechanism result from this study, but also the idea of using Ag^+ and Cu^{2+} as highly specific reversible probes of the catalytic site of serine proteases. These ions were subsequently used by Koeppe and

Stroud to assign the peaks corresponding to titration of Asp 102 in the difference infrared spectra (33). The Ag^{+}-trypsin study is presented in more detail in Appendix 1 of this thesis. The Cu^{2+}-trypsin project is reported in Chapter IV.

During the collection of data from silver trypsin, we developed new techniques for accurate approximation of background measurements. Use of these methods greatly reduces the time spent measuring backgrounds, increasing the useful x-ray exposure life of the crystal, and is particularly advantageous in protein crystallography, where the crystals often decay rapidly in the x-ray beam. The methods are substantial improvements over earlier techniques used for proteins which assumed that the background depends only on scattering angle. This work is reported in Appendix 2.

The mechanism of serine proteases at our current level of understanding is described in Appendix 3.

References

1. Magnusson, S. In The Enzymes (P.D. Boyer, Ed.), Vol. 3, pp. 277-321. Academic Press, New York, 1971. 886 pages.
2. Muller-Eberhard, H.J. (1969), Ann. Rev. Biochem. 38, 389-414.
3. Stambaugh, R., Brackett, B., and Mastroianni, L. (1969), Biol. Reprod. 1, 223-227.
4. Goodnight, S.H. In Cold Spring Harbor Symposium on Proteases and Biological Control (E. Reich, D.B. Rifkin, and E. Shaw, Eds.),

pp. 191-197. Cold Spring Harbor Laboratory, New York, 1975. 1021 pages.

5. Quigley, J.P. Ossowski, L., and Reich, E. (1974), J. Biol. Chem. 249, 4306-4311.
6. Quigley, J.P., Ossowski, L., and Reich, E. (1974), J. Biol. Chem. 249, 4312-4320.
7. Tobler, J., Krieger, M., and Stroud, R.M., unpublished results.
8. Zerner, B., Bond, R.P., and Bender, M.L. (1964), J. Amer. Chem. Soc. 86, 3674-3679.
9. Oppenheimer, H.L., Labouesse, B., and Hess, G.P. (1966), J. Biol. Chem. 241, 2720-2730.
10. Caplow, M. (1969), J. Amer. Chem. Soc. 91, 3639-3645.
11. Hess, G.P., McConn, J., Ku, E., and McConkey, G. (1970), Phil. Trans. Roy. Soc. (Lond.) B257, 89-104.
12. Fersht, A.R. and Requena, Y. (1971), J. Amer. Chem. Soc. 93, 7079-7087.
13. Fastrez, J. and Fersht, A.R. (1973), Biochemistry 12, 2025-2034.
14. Fersht, A.R. and Renard, M. (1974), Biochemistry 13, 1416-1426.
15. Northrop, J.H. and Kunitz, M. (1932), J. Gen. Physiol. 16, 295-311.
16. Stroud, R.M. (1974), Scientific American 231, 74-88.
17. Jansen, E.F., Nutting, M.D.F., and Balls, A.K. (1949), J. Biol. Chem. 179, 201-204.
18. Schoellman, G. and Shaw, E. (1963), Biochemistry 2, 252-255.

19. Matthews, B.W., Sigler, P.B., Henderson, R., and Blow, D.M. (1967), Nature 214, 652-656.

20. Steitz, T.A., Henderson, R., and Blow, D.M. (1969), J. Mol. Biol. 46, 337-348.

21. Henderson, R. (1970), J. Mol. Biol. 54, 341-354.

22. Robertus, J.D., Kraut, J., Alden, R.A., and Birktoft, J.J. (1972), Biochemistry 11, 4293-4303.

23. Stroud, R.M., Kay, L.M., and Dickerson, R.E. (1971), Cold Spring Harbor Symposium on Quant. Biol. 36, 125-140.

24. Stroud, R.M., Kay, L.M., and Dickerson, R.E. (1974), J. Mol. Biol. 83, 185-208.

25. Krieger, M., Kay, L.M., and Stroud, R.M. (1974), J. Mol. Biol. 83, 209-230.

26. Shotton, D.M. and Watson, H.C. (1970), Phil. Trans. Roy. Soc. (Lond.) B257, 111-118.

27. Hartley, B.S. and Kilby, B.A. (1954), Biochem. J. 56, 288-297.

28. Hammond, B.R. and Gutfreund, H. (1955), Biochem. J. 61, 187-189.

29. Weil, L., James, S., and Buchert, A.R. (1953), Arch. Biochem. Biophys. 46, 266-278.

30. Bender, M.L. and Kezdy, F.J. (1964), J. Amer. Chem. Soc. 86, 3704-3714.

31. Blow, D.M., Birktoft, J.J., and Hartley, B.S. (1969), Nature 221, 337-340.

32. Hunkapiller, M.W., Smallcombe, S.H., Whitaker, D.E., and Richards, J.H. (1973), Biochemistry 12, 4732-4743.

33. Koeppe, R.E. II and Stroud, R.M. (1976), Biochemistry 15, 3450-3458.

34. Martinek, K., Vill, Kh., Streltsova, Z.A., and Berezin, I.V. (1969), Molek. Biol. 3, 554-565.

35. Martinek, K., Savin, Y.V., and Berezin, I.V. (1971), Biokhimiya 36, 806-815.

Chapter II

The Structure and Activation Mechanism of Bovine Trypsinogen

Physiological control over hydrolysis by the digestive serine proteases, and in other systems as well, is maintained by presence of specific inhibitors and by synthesis of these enzymes as inactive precursors, called zymogens or proenzymes. The digestive serine protease zymogens are activated by a single tryptic split, between Lys 15 and a hydrophobic residue, 16 (1,2). Loss of these few residues from the N-terminus results in conformational changes which make the enzyme catalytically active (3).

The three-dimensional structure of chymotrypsinogen was solved by Freer et al. (4) and was further interpreted by Wright (5,6). Although the structure of the zymogen, including orientation of the catalytic site residues Asp 102, His 57, and Ser 195, was very similar to the chymotrypsin structure of Birktoft and Blow (7), the specific binding pocket (residues 187-194 and 214-220) was somewhat less open and accessible to a substrate side chain than in the active enzyme. Lack in the zymogen of the Ilu 16 - Asp 194 salt bridge resulted in a very different conformation for residues 191-194, according to the study.

This chapter of the thesis is concerned with the determination of the high resolution structure of bovine trypsinogen, carried out primarily by Tony Kossiakoff, and by Bob Stroud and the author. This study indicates that trypsin and trypsinogen are structurally significantly more alike than chymotrypsin and chymotrypsinogen. This may be partly due to the existence of chymotrypsin as a dimer in the pH 4.2 crystals (8), and to the fact that those structures are in a lower

state of refinement that the trypsin/trypsinogen pair. This work is discussed in detail in Appendices 4 and 5.

An additional observation made from this study is that relatively small structural changes (on the order of an angstrom) can be very important to the function of a protein. Moreover, in low-resolution electron density maps the possibility of errors in interpretation is high. Refinement of protein structures can greatly improve the accuracy in determination of such changes, and is the subject of the next chapter of this thesis.

References

1. Neurath, H. and Dixon, G.H. (1957), Fed. Proc. 16, 791-801.
2. Northrop, J.H., Kunitz, M., and Herriot, R.M. Crystalline Enzymes, p. 96. Columbia Univ. Press, New York, 1948. 352 pages.
3. Neurath, H., Rupley, J.A., and Dreyer, W.J. (1956), Arch. Biochem. Biophys. 65, 243-259.
4. Freer, S.T., Kraut, J., Robertus, J.D., Wright, H.T., and Xuong, Ng. H. (1970), Biochemistry 9, 1997-2009.
5. Wright, H.T. (1973), J. Mol. Biol. 79, 1-11.
6. Wright, H.T. (1973), J. Mol. Biol. 79, 13-23.
7. Birktoft, J.J. and Blow, D.M. (1972), J. Mol. Biol. 68, 187-240.
8. Sigler, P.B., Jeffery, B.A., Matthews, B.W., and Blow, D.M. (1966), J. Mol. Biol. 15, 175-192.

Chapter III

Protein Structure Refinement:

The Refined High-Resolution Structures of DIP-Trypsin and Trypsinogen

Ever since the method of multiple isomorphous replacement (MIR) enabled the first protein structure, that of hemoglobin, to be solved by Perutz and coworkers (1), MIR has been the traditional method for solution of new macromolecular structures. The technique has enabled protein crystallography in a short time to become one of the most powerful methods for elucidation of biochemical problems. However, the errors in such a structure determination, arising from interpretation of the electron density map, and from difficulties in building and measuring atomic coordinates from a skeletal model of the protein with reference to such a map, can be substantial (2). The MIR electron density map unfortunately provides no feedback concerning the correctness of interpretation.

It has become apparent that small positional changes (on the order of an angstrom or less) can be highly significant mechanistically, for example in evaluating differences between oxidized and reduced forms of a protein, between an enzyme and its zymogen, between members of an enzyme family, or in comparing homologous proteins from different species. Structure refinement is now performed routinely on structures of small molecules, and has recently been applied to some protein structures (3-8), although the size of the problem makes most of the methods normally applied to small molecules unfeasible or prohibitively expensive for large structures (6,9). Refinement greatly improves the accuracy with which the types of differences mentioned above, as well as other important structural features, can be described. It is moreover particularly valuable in the case of proteins,

where these differences may lie well within the resolution of the data, in obtaining the maximum amount of information from the limited diffraction patterns typically available from protein crystals.

Generally, in structure refinement the disagreement (e.g., a weighted sum of the squared differences) between the observed structure factor amplitudes (F_o) and those calculated from the model of the structure (F_c) is minimized with respect to the positional and thermal parameters for each atom. The most commonly quoted index of this disagreement is the standard crystallographic R-factor ($R = \Sigma|F_o-F_c|/\Sigma F_o$). For a small molecule R is often in the range 30% - 40% prior to refinement, and can fall to around 4% for a well-refined structure. In the case of a protein, R usually depends strongly on the resolution and overall temperature factor of the data, but is typically about 45% - 50% for a medium-resolution unrefined structure, falling to less than 25% for most of the refined structures to date.

The most spectacular refinement of a protein structure currently is that of rubredoxin (3) for which R is 11% at 1.2 Å resolution (11). However, the structure-factor least squares procedure used for this small protein (molecular weight 6000), which forms unusually well-ordered crystals, is expensive (9), and would be prohibitively so for a large structure.

Presently, the most widely used technique for protein structures is real-space refinement, in which use is made of the programs written by Diamond (12,13) for fitting a model with standard bond lengths and

angles to a measured coordinate set (model-building), and for optimizing the fit of a set of model coordinates to an electron density map (real-space refinement). These programs are, however, very complex and require very large amounts of storage and time on a large computer. While these requirements do not increase as rapidly for large structures as is the case with least squares refinement, many more cycles are required to produce a refined structure, and the method is still extremely costly. Refinement by difference Fourier methods is potenially much more economical. The method has previously been used effectively for proteins in conjunction with Diamond's programs (5-8, 14,15).

In the present study the three-dimensional structures of DIP-trypsin and trypsinogen were refined with a constrained difference Fourier technique. The project was undertaken for several reasons. It was felt that the changes between these two proteins, leading to a model for the relative inactivity of the zymogen, could be much more accurately described with reference to high-resolution, refined structures, and this is in fact the case. In addition, the DIP-trypsin structure was an excellent candidate for revealing fine details of general protein structure upon refinement. The crystals are well ordered, diffract to at least 1.1 Å resolution, and can be grown to relatively large size (about 0.75 x 0.75 x 1.5 mm). It was expected that features such as nonplanar amide groups and proline rings, distortions in helices and sheet structures, solvent structure, and unusual values of bond lengths and angles, could be accurately

identified in the refined structure. There were, moreover, several regions in the MIR-phased map where interpretation was ambiguous, particularly near the surface of the molecule and in some of the tight loops in the structure. Extension of the resolution of the map and refinement of the structure were necessary to insure correct interpretation in these regions, and to remove the errors arising from construction and measurement of the wire model. Finally, because of the dramatic improvements in description of a structure which can be gained through refinement, development of a system for efficient, inexpensive, and routine refinement of macromolecular structures was highly desirable.

The author has written a series of programs for routine refinement of protein structures, which can operate entirely on a minicomputer (with the current exception of computation of density maps). Use of this system has enabled the DIP-trypsin refinement to proceed at an extremely low cost from a starting R of 47% at 2.7 Å resolution to 21.5% at 1.5 Å resolution (the best statistics to date for a refined enzyme structure). This work is described in Appendix 6. Some additional stereo figures of points of interest in the refined structure, generated with this system, are presented in Appendix 7.

This series of programs has also been used for refinement of the trypsinogen structure to an R of 31% at 1.9 Å resolution. The results and comparison with the trypsin structure are discussed in Appendices 4 and 5. As part of this work, I developed a similar system for protein refinement for use on the CDC-7600 computer at Brookhaven

National Laboratory, and refinement of the trypsinogen structure is being continued there by Dr. A. Kossiakoff.

Parts of the system have also been used recently in optimizing the fit of coordinates for oxidized and reduced forms of tuna heart cytochrome c to the MIR electron density (16). Bob Almassy is currently using the system with the structure of cytochrome c_{551} (17).

References

1. Green, D.W., Ingram, V.M. and Perutz, M.F. (1954), Proc. Roy. Soc. A225, 287-307.
2. Chambers, J.L. and Stroud, R.M. (1977), Acta Crystallogr.--in press (Appendix 6 of this thesis).
3. Watenpaugh, K.D., Sieker, L.C., Herriot, J.R., and Jensen, L.H. (1973), Acta Crystallogr. B29, 943-956.
4. Diamond, R. (1974), J. Mol. Biol. 82, 371-391.
5. Moews, P.C. and Kretsinger, R.H. (1975), J. Mol. Biol. 91, 201-228.
6. Freer, S.T., Alden, R.A., Carter, C.W. Jr., and Kraut, J. (1975), J. Biol. Chem. 250, 46-54.
7. Deisenhofer, J. and Steigemann, W. (1975), Acta Crystallogr. B31, 238-250.
8. Bode, W. and Schwager, P. (1975), J. Mol. Biol. 98, 693-717.
9. Konnert, J.H. (1976), Acta Crystallogr. A32, 614-617.

10. Stout, G.H. and Jensen, L.H. X-ray Structure Determination: A Practical Guide, pp. 395-397. Macmillan, New York, 1968. 466 pages.

11. Watenpaugh, K.D., Sieker, L.C., and Jensen, L.H. (1977), American Crystallographic Association Abstracts, Series 2, 5(1), 17.

12. Diamond, R. (1966), Acta Crystallogr. 21, 253-266.

13. Diamond, R. (1971), Acta Crystallogr. A27, 436-452.

14. Huber, R., Kukla, D., Bode, W., Schwager, P., Bartels, K., Deisenhofer, J., and Steigemann, W. (1974), J. Mol. Biol. 89, 73-101.

15. Epp, O., Lattman, E.E., Schiffer, M., Huber, R., and Palm, W. (1975), Biochemistry 14, 4943-4952.

16. Mandel, N., Mandel, G., Trus, B.L., Carlson, G., and Dickerson, R.E. (1977), J. Biol. Chem.--in press.

17. Almassy, R.J., personal communication.

Chapter IV

A Crystallographic Study of Trypsin Inhibition by Cu^{2+}

Introduction

The metal ions Ag^+ and Cu^{2+} are strong inhibitors of trypsin and chymotrypsin (1,2). These ions compete with one another for binding to the enzyme in an inhibitory fashion. As described in Chapter I and Appendix 1 of this thesis, Ag^+ inhibits these enzymes by disrupting the catalytic site, binding between the Asp 102 and His 57 side chains. In the difference infrared titration experiment of Koeppe and Stroud (3), the peaks corresponding to titration of the Asp 102 carboxyl with a pK_a of 6.8 were assigned with the use of Cu^{2+} ions, since the experimental difficulties with Ag^+ are considerably greater.

We wished to determine directly the site of Cu^{2+} binding to trypsin, since the fact that Cu^{2+} and Ag^+ compete in the kinetic experiments does not necessarily mean that they bind at the same site in the enzyme. The determination was made using x-ray crystallographic techniques by Roger Koeppe, Lois Kay, and the author. In addition, Mel Jones and the author are currently attempting to locate the Cu^{2+} binding site in benzamidine-inhibited trypsin.

Experimental

DIP-trypsin was crystallized as described by Stroud et al. (4). The Cu^{2+} derivative was prepared by placing the DIP-trypsin crystals in a pH 6.9, 0.05 M cacodylate buffer containing 17 mM $Cu(NO_3)_2$ (Merck reagent) and 0.66 M $MgSO_4$.

Reflection intensities were measured with a Syntex $P\bar{1}$ diffractometer using graphite-monochromatized CuK_α radiation, and equipped with a helium tube between the crystal and detector. Tube voltage and current were 40 KV and 20 ma, respectively. The step-scan method of Wyckoff et al. (5) was employed to record intensities from a single crystal to 2.53 Å ($2\theta = 35.5°$). Background corrections were made with the anisotropic interpolation method of Krieger et al. (6). Further data reduction and scaling were performed according to Stroud et al. (4). The intensities of five standard reflections were monitored throughout the data collection as an indication of crystal decay arising from x-ray exposure. At the termination of data collection none of these intensities had fallen by more than 15% from their initial value. Of the 7704 independent reflections in the 2.53 Å sphere, those 6905 with structure factors greater than twice their standard deviation were included in the final data set.

A 2.7 Å difference electron density map was computed with coefficients $m\ (F_{CuDIP} - F_{DIP})\ e^{i\phi}$, where F_{CuDIP} and F_{DIP} are respectively the structure factor amplitude for Cu^{2+}-DIP-trypsin and DIP-trypsin, and ϕ and m are the 'best' phase and figure of merit (7) determined by Stroud et al. (4)

Results and Discussion

The section of the difference density map obtained in this study, shown in Figure 1, is very similar to that obtained for the Ag^+ derivative (8). These are the only significant peaks in the map, the larger one arising from a copper ion bound between Asp 102 $O\delta_1$ and His 57 $N\delta_1$, and the smaller one from movement of the His 57 imidazole to accommodate the copper ion. This determination therefore indicates that the site of Cu^{2+} inhibition of trypsin is the same as for Ag^+, confirming the method of assignment of difference infrared peaks by Koeppe and Stroud (3).

References

1. Martinek, K., Vill, Kh., Streltsova, Z.A., and Berezin, I.V. (1969), Molek. Biol. 3, 554-565.
2. Martinek, K., Savin, Y.V., and Berezin, I.V. (1971), Biokhimiya 36, 806-815.
3. Koeppe, R.E. II, and Stroud, R.M. (1976), Biochemistry 15, 3450-3458.
4. Stroud, R.M., Kay, L.M., and Dickerson, R.E. (1974), J. Mol. Biol. 83, 185-208.
5. Wyckoff, H.W., Tsernoglou, D., Hanson, A.W., Knox, J.R., Lee, B., and Richards, F.M. (1970), J. Biol. Chem. 245, 305-328.

6. Krieger, M., Chambers, J.L., Christoph, G.G., Stroud, R.M., and Trus, B.L. (1974), Acta Crystallogr. A30, 740-748 (Appendix 2 of this thesis).

7. Dickerson, R.E., Kendrew, J.C., and Strandberg, B.E. (1961), Acta Crystallogr. 14, 1188-1195.

8. Chambers, J.L., Christoph, G.G., Krieger, M., Kay, L., and Stroud, R.M. (1974), Bioch. Bioph. Res. Commun. 59, 70-74 (Appendix 1 of this thesis).

9. Henderson, R. and Moffat, J.K. (1971), Acta Crystallogr. B27, 1414-1420.

Figure Legend

FIGURE 1. A view down the y-axis of the 2.7 Å F_{CuDIP}-F_{DIP} difference Fourier map described in the text. Four sections of the map, giving a total thickness of about 5 Å, are represented. Positive density is indicated by solid contours, negative density by dotted contours. Contour levels begin at ±0.2 electrons/Å^3 with intervals of ±0.1 e/Å^3. The RMS error in this map (9) is 0.08 e/Å^3. The bars at the lower right indicate distances of 2 Å.

The only significant peaks in the map are shown, the larger corresponding to a Cu^{2+} ion positioned between H57Nδ_1 and D102Oδ_1, and the smaller one to the movement of the H57 imidazole out toward the solvent to accommodate the copper ion. The positions of the Ag^+ and H57 movement peaks in the Ag^+-DIP-trypsin difference map (8) are marked with asterisks (*).

Figure 1

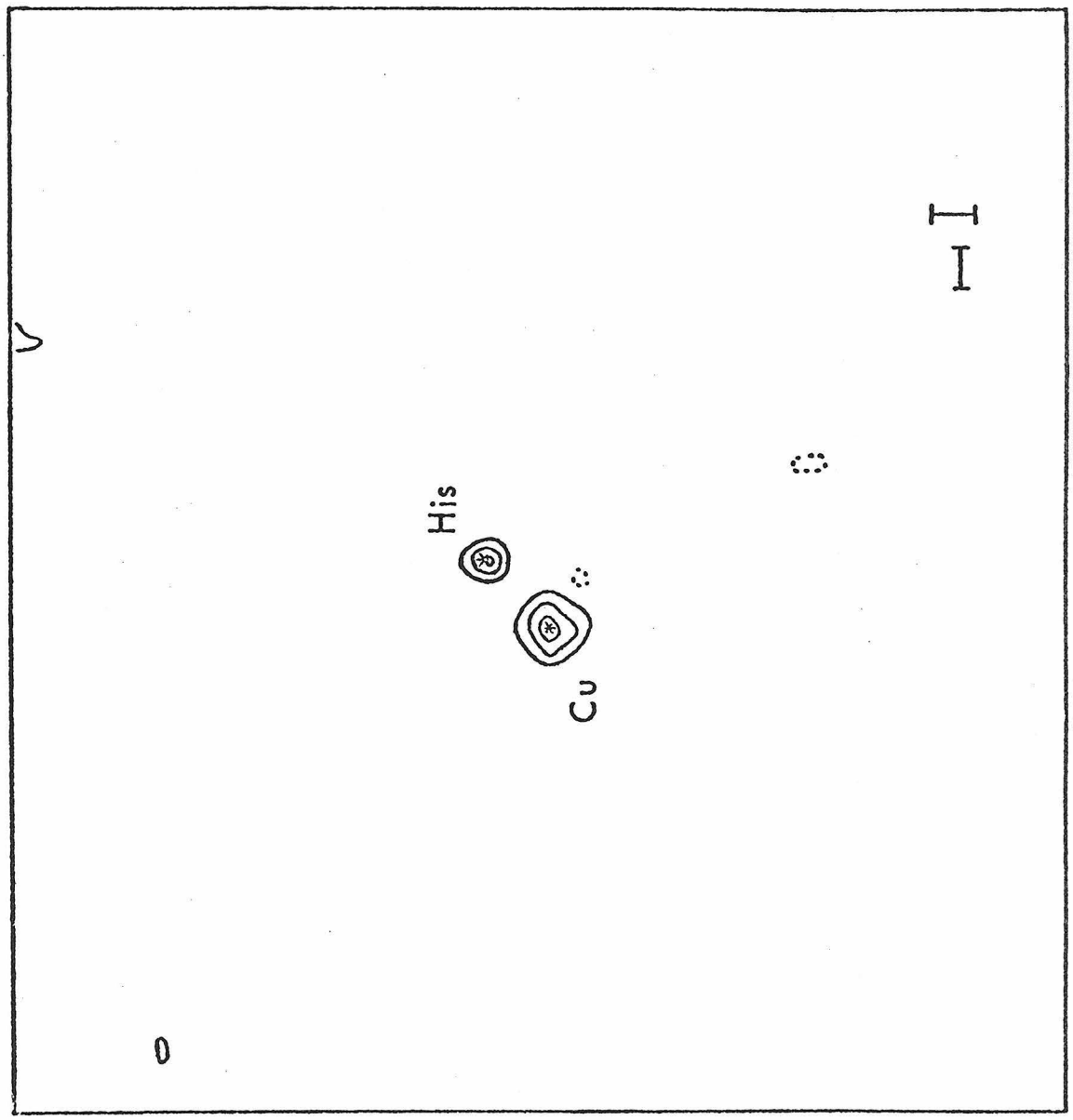

Appendix 1

Silver Ion Inhibition of Serine Proteases: Crystallographic Study of Silver-Trypsin

Vol. 59, No. 1, 1974 BIOCHEMICAL AND BIOPHYSICAL RESEARCH COMMUNICATIONS

SILVER ION INHIBITION OF SERINE PROTEASES: CRYSTALLOGRAPHIC STUDY OF SILVER–TRYPSIN

J. L. Chambers, G. G. Christoph, M. Krieger, L. Kay, and R. M. Stroud

Norman W. Church Laboratory of Chemical Biology
California Institute of Technology
Pasadena, California 91109 U.S.A.

Received May 3,1974

Summary

Silver ion is a potent inhibitor of trypsin and chymotrypsin, with K_I's of 4×10^{-5} M. and 3×10^{-5}, respectively. A crystallographic study shows that the primary silver ion binding site on trypsin is at the active center between the carboxyl group of Asp 102 and the δ-nitrogen of His 57. This result is correlated with the fact that Ag^+ interferes primarily with the acylation rate constant, k_2, and does not significantly affect the binding constant, K_s. The location of this site explains the potent inhibitory effect of silver (I) ions on trypsin activity: The imidazole ring of His 57 is repositioned 1.8 Å further out into the solvent to accommodate the silver ion, preventing its normal interaction with the hydroxyl group of Ser 195. Consequently, His 57 cannot directly assist the proton transfer in the catalyzed reaction.

Since silver ion binds to the catalytic site in this highly specific manner, silver may be used as a specific probe of the active site of serine proteases.

This communication reports the 2.7 Å resolution structure of the isomorphous silver derivative of bovine trypsin inhibited by diisopropyl-fluorophosphate (DIP). Martinek et al.[1,2] found that silver ion is a potent trypsin (or chymotrypsin) inhibitor with a K_I 4×10^{-5} M. They concluded, first, that silver ion prevents the acylation of the enzyme while not appreciably interfering with substrate binding. Second, silver ions compete with protons for the binding site and the silver binding depends on a group with an apparent pK_a of 7.1, which they suggested was the imidazole of His 57. In light of more recent evidence, however, the pK_a reflected in those experiments is more likely that of Asp 102[3,4].

EXPERIMENTAL

To prepare the silver (I) derivative crystals of DIP-trypsin[5] were soaked in solutions containing 0.012 M $AgNO_3$ for periods of four to eight days. Three-dimensional, 2.7 Å data sets for both the native DIP-trypsin

and the silver (I) derivative were collected using a Syntex $P\bar{1}$ automated diffractometer. Data reduction and scaling were accomplished using standard techniques.[5]

RESULTS AND DISCUSSION

From our data and the phases previously determined for DIP-trypsin,[5] a difference Fourier map was obtained. The region of this map in the area of the active site is shown in Fig. 1. The large peak "A" corresponds to the position of the fully occupied, primary silver ion binding site. In addition, there is a smaller region of positive density, "B", above and behind the primary site. This peak results from a movement of the imidazole ring of the catalytic site residue His 57 into the solvent by approximately 1.8 ±(≤0.2) Å. A secondary silver ion binding site of 35% refined occupancy was found elsewhere on the surface of the molecule, in the vicinity of His 40.

Fig. 2 shows an ORTEP[6] representation of the catalytic site in the silver (I) trypsin derivative. The silver ion is coordinated in an approximately linear fashion between the lower carboxyl oxygen of Asp 102 and the δ-nitrogen of His 57. Bond distances are: Oδ1 (Asp 102)-Ag^+, 2.3±0.2 Å; Ag^+-Nδ (His 57), 2.3 ±0.2 Å. This suggests that the silver ion is in a two coordinate sigma-bonded complex characteristic of silver (I)[7]. This configuration is also structurally very similar to complexes of silver (I) with free amino acids.[8]

The silver DIP-trypsin structure provides a model for the mechanism of the silver (I) inhibition of trypsin. The distance between the ε-nitrogen of His 57 and the position of the γ-oxygen of Ser 195 found previously for benzamidine-trypsin (where the serine oxygen was hydrogen bonded to the εN of His 57) is 4.2 ±0.2 Å in the silver derivative. This long distance, coupled with the unfavorable directionality between these two atoms, prevents proton transfer from the hydroxyl group of Ser 195 to the His 57 imidazole. The effect of Ag^+ on k_2, the acylation rate constant, thus gives an indication of the contribution of His 57 and Asp 102 to enhancement of the catalytic rate of serine proteases.

As well as defining the mechanism of the silver ion inhibition, the silver derivative data have been incorporated into the phase refinement

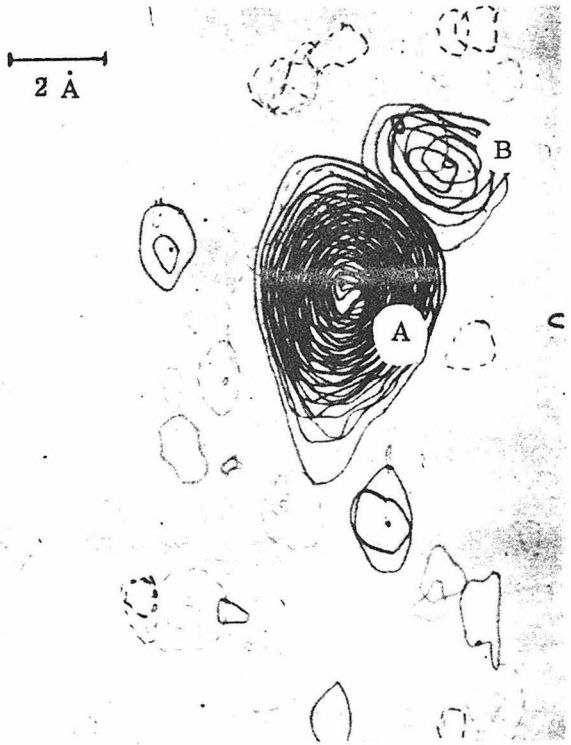

Figure 1. A view parallel to the crystallographic a-axis of the active site region of a difference Fourier map calculated using coefficients $|F_{silver}| - |F_{native}|$. The view shown is a projection through 12 sections, each 1.1 Å apart. Solid contours enclose regions of positive density; the broken lines, regions of negative density. Peak "A" corresponds to the location of the main silver ion binding site. Peak "B" results from the movement of the His 57 imidazole ring. Contours begin at ± 2.5 standard deviations and the contour interval is one standard deviation in the difference electron density.

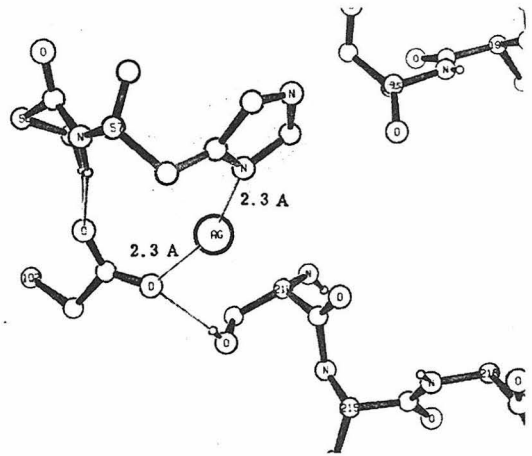

Figure 2. An ORTEP drawing of the catalytic site of silver DIP-trypsin, viewed approximately down the crystallographic b-axis. The DIP group has been omitted for clarity. The γ-oxygen of Ser 195 is in the position found for DIP-trypsin, close to that found in tetrahedral intermediates or in acyl enzymes.

of the 2.7 Å structure of DIP-trypsin. The overall mean figure of merit of the 2.7 Å phases increased to 0.83 during this refinement. The details of this refinement will be discussed elsewhere.

One of the key problems in the assignment of microscopic pK_a's to residues at the active center of serine proteases lies in the requirement that one should be examining the "native" enzyme rather than a modified derivative of it. Two familiar problems are thus apparent: 1) presence of a covalent label near the active site perturbs the system under study in an unknown fashion; 2) spectroscopic techniques which study the native enzyme often have problems of assignment to particular residues.

Silver ion can be used to assign peaks to the active center residues by perturbation of the native enzyme spectrum, primarily affecting peaks due to Asp 102 and His 57. We are currently applying this technique to assign peaks associated with carboxylic acid groups in the difference infrared titration spectra of native serine proteases.[9]

ACKNOWLEDGEMENT

This work is contribution no. 4850 from the Norman W. Church Laboratory of Chemical Biology of the California Institute of Technology. This work has been carried out with the support of the United States Public Health Service Grants GM-19984 and GM-12121, whose help is gratefully acknowledged. One of us (MK) is the recipient of a Danforth Graduate Fellowship, another (RMS) is the recipient of a National Institutes of Health Career Award (GM-70469), and another (GGC) is a National Institutes of Health Postdoctoral Fellow.

REFERENCES

1. Martinek, K., Savin, Y.V., and Berezin, I.V., Biokhimiya 36, 806-815 (1971).
2. Martinek, K., Vill, K., Strel'tsova, Z.A., and Berezin, I.V., Molekulyarnaya Biol. 3, 554-565 (1969).
3. Krieger, M., Kay, L.M., and Stroud, R.M., J. Mol. Biol. 83, 209-230 (1974).

4. Hunkapiller, M. W., Smallcombe, S. H., Whitaker, D. R., and Richards, J. H., Biochemistry 12, 4732-4743 (1973).
5. Stroud, R. M., Kay, L. H., and Dickerson, R. E., J. Mol. Biol. 83, 185-208 (1974).
6. Johnson, C. K., "ORTEP: A Fortran Thermal Ellipsoid Plot Program for Crystal Structure Illustrations", Oak Ridge National Laboratory, Oak Ridge, Tenn., Publ. No. ORNL-3794, revised 1965.
7. Cotton, F. A. and Wilkinson, G. "Advanced Inorganic Chemistry", Interscience, New York, 2nd ed., 1966, p. 1040.
8. Acland, C. B. and Freeman, H. C., J. Chem. Soc. D1971, 1016-1017.
9. Koeppe, R. and Stroud, R. M. --in preparation.

Appendix 2

Data Collection in Protein Crystallography: Capillary Effects and Background Corrections

Reprinted from *Acta Crystallographica*, Vol. A 30, Part 6, November 1974

PRINTED IN DENAMRK

Acta Cryst. (1974). A30, 740

Data Collection in Protein Crystallography: Capillary Effects and Background Corrections*

BY M. KRIEGER†, J. L. CHAMBERS, G. G. CHRISTOPH‡, R. M. STROUD§

Crellin Laboratory of Chemistry

AND B. L. TRUS¶

Norman W. Church Laboratory of Chemical Biology, California Institute of Technology, Pasadena, California 91109, *U.S.A.*

(*Received* 16 *January* 1974; *accepted* 24 *May* 1974)

In protein crystallography, observed diffraction intensities must be corrected for background radiation due to scatter from air and scatter and absorption by capillary, crystal and mother liquor. A systematic study shows that a major contribution to background intensity is air scatter arising from the air intercepted by the direct X-ray beam as 'seen' by the receiving-counter aperture. As a result there is a first-order dependence of background on the 2θ angle. The second-order variations in this function are principally due to absorption of the direct beam or air-scattered radiation by the capillary and to diffraction by the glass in the direct beam. To reduce data collection time and crystal exposure, individual background measurements may be approximated by interpolation from empirical background curves or, alternatively, by collecting background intensities for short times and fitting these data with a multidimensional function. If isotropic interpolation is used, *i.e.*, if background is considered to be a function of 2θ alone, systematic errors of up to about 30% can be introduced into the interpolated backgrounds. Methods of accounting for the anisotropy in the background are derived and shown to reduce this error to 1–2%.

Introduction

Because protein crystals are quite susceptible to radiation damage, crystallographers have been exploring different methods for accurate data collection which minimize the X-ray exposure of the crystal. With automated diffractometers, one widely used method of data collection involves counting the background on one or both sides of each measured reflection. There are several methods of reducing the time of data collection and thereby increasing the number of reflections collected per crystal (*e.g.*, Wyckoff, Tsernoglou, Hanson, Know, Lee & Richards, 1970; Watson, Shotton, Cox & Muirhead, 1970). In one method, the observation of individual backgrounds is omitted and background corrections for the measured intensities are calculated from an empirical curve of background *versus* $\sin\theta/\lambda$ measured for each crystal.

If the backgrounds do not vary significantly during the time of collection, almost all of the crystal exposure time can be devoted to intensity data collection, and empirical background curves can be measured after the intensity data have been collected. Empirical background curves have generally been obtained from background values measured with long counting times for points along one lattice row, and applied using the approximation that the background depends only on the Bragg angle and not on the other setting angles (Matthews, Levine & Argos, 1972; Jensen, 1972; Salemme, Freer, Xuong, Alden & Kraut, 1973; Wyckoff, Doscher, Tsernoglou, Inagami, Johnson, Hardman, Allewell, Kelly & Richards, 1967). This approximation can give rise systematic errors of about 30% between interpolated and observed backgrounds.

Hill & Banaszak (1973) have reported observing an additional, 2θ-invariant φ dependence. Our experiments show that the background radiation can vary systematically with φ and χ in addition to 2θ, and furthermore that such φ and χ dependences are functions of 2θ. These dependences can be accounted for by additional components in a simple interpolative procedure. In contrast to Hill & Banaszak, we conclude that the variation with φ arises primarily from capillary absorption and scattering rather than absorption of background radiation by the protein crystal and its mounting to the capillary. There is substantial improvement in interpolated backgrounds if the φ and χ-dependent variations are accounted for.

A second approach to streamlining data collection involves observing very short backgrounds with each reflection, and fitting, by least squares, a function of the diffractometer setting angles to all of the data. Such a function must include cross terms between χ and 2θ, and φ and 2θ, and can vary in complexity depending upon the range of 2θ and the experimental conditions. By pooling the data in this manner, the resulting backgrounds are more accurate than the individual short measurements from which the background function was constructed.

* Contribution No. 4726. Supported by U.S. Public Health Service Grants GM-19984 and GM-12121.

† Danforth Foundation Fellow.

‡ National Institutes of Health Postdoctoral Fellow.

§ National Institutes of Health Career Development Awardee, U.S. Public Health Service Grant No. GM-70469.

¶ Jane Coffin Childs Memorial Fellow.

It should be noted that systematic variations between real and interpolated values for the background can give rise to systematic errors in phase determination, in ΔF terms used in calculating difference maps, and in scaling. Phases and ΔF's free from such errors are crucial to accurate descriptions of molecular shifts from difference maps (Dickerson, Kopka, Varnum & Weinzierl, 1967; Henderson & Moffat, 1971; Krieger, Kay & Stroud, 1973). Furthermore, with protein crystals whose reflection intensities are small, a reflection which is only twice as intense as the background may be ten standard deviations above background. Therefore, well determined reflection intensities ($\gtrsim 3\sigma$) may be in error by as much as 30% if anisotropy in the background is not accounted for.

As the background intensity is independent of crystal absorption, the backgrounds, estimated or measured, should be subtracted from the observed diffraction intensities before applying the standard absorption and Lp corrections.

In this paper we describe two methods for obtaining background corrections of similar quality to individually measured backgrounds, but at significant savings in the time spent on observing backgrounds. Although it is desirable to minimize the background present (*i.e.*, improve the signal-to-noise characteristics of the experiments), we are primarily concerned here with developing background correction methods whose use would be applicable to a wide variety of existing four-axis diffractometers, without modification of the experimental hardware. As a result of this analysis, and the consideration of the origins of components in the background intensity, experimental methods of reducing the background, and thereby increasing the signal-to-noise ratio, are suggested.

Experimental

Measurements were made on several different diffractometers both with and without a monochromator. Details of each experimental arrangement used are described in Table 1. Each machine will henceforth

Table 1. *Characteristic data for diffractometers used in this study*

In all cases the basic four-circle machines have been rebuilt and modified; in all cases except *A* and *D* modifications have been extensive to the point of total remachining.

	(*A*) Syntex *P*$\bar{1}$	(*B*) GE XRD-490	(*C*) Datex–GE hybrid	(*D*) Hilger Watts*	(*E*) Buerger Supper†	(*F*) S. Samson‡ hybrid
Source						
Target size (mm)	10 × 1	12·5 × 0·8	12·5 × 0·8	10 × 1	8 × 0·4	12·5 × 0·8
Voltage (kV)	40	45	45	46	33	45
Current (mA)	20	18·5	15	16	20	18
Radiation	Cu *Kα*	Cu *Kα*	Cu *Kα*	Cu *Kα*	Cu *Kα*	Mo *Kα*
Geometry						
Take-off-angle	6°	–	3°	3°	3°	–
Monochromator type	Graphite	Graphite	None	None	Graphite	Graphite
Monochromator mounting (ϱ)§	90°	90°	–	–	–	0°
Monochromator dispersion	0·3°	0·3°	–			0·3–0·4°
Source to crystal						
Distance from source to:						
1st aperture(cm) (size in mm)	5·5 (2·0)	4·5 (1·0)	–		8·0 (2·0)	4·0 (1·0)
Monochromator crystal	6·8	5·0	None	None	9·0	5·5
Aperture (size)	19·8 (1·0–1·5)	8·0 (1·0)	4·5 (1·5)	~4·0 (1·0)	11·5 (0·6)	12·0 (1·5)
Aperture (size)	21·3 (1·5–2·0)	14·5 (1·8)	14·3 (1·8)	~9·5 (1·0)	15·9 (0·6)	20·8 (1·8)
Crystal	27·3	15·5	15·0	23·5	19·4	22·5
Crystal to counter ¶						
Distances from crystal to:						
Aperture (size)	32·5 (2·5)	4·0 (1·0–1·5)	9·2 (1·0)	17·0 (3·0)	6·0 (2·2)	8·0 (2·11)
Aperture (size)	38·5 (1·0–2·0)	12·0 (2·0–2·5)	–	22·5 (3·0)	11·8 (1·5–2·0)	11·4 (5·04)
Counter	40·5	16·0	22·2	25·0	13·5	21·6
Noise count rate with X-rays off (per 100 s)	35	55	25	38	30	13

* Standard four-circle machine with no monochromator.

† This machine was essentially redesigned by, and rebuilt under the direction of, R. M. Stroud, and uses Datex automation for operation in a φ-step scan mode (two-circle Weissenberg geometry).

‡ Four-circle diffractometer assembled locally under the direction of S. Samson. Electronics and Alloys goniostat, Varian computer, Datex resoverdynes, and Ortec counter chain.

§ ϱ is the angle between the normals to the planes of incidence at the monochromator.

¶ Counter type: all diffractometers use scintillation counter. Hermetically sealed Tl-drifted NaI crystals are individually selected and checked regularly for decay and damage.

be referred to by a letter (*A–F*) which in turn corresponds to one arrangement in Table 1. Each of the figures refers to a specific case, although the discussion considers results obtained from many different experiments. It should be noted that these different arrangements include diffractometers both with and without monochromators, with both of the generally used monochromator settings, with copper and molybdenum $K\alpha$ radiation, and with or without helium-filled pathways to the counter.

Glass capillaries were 0·3–1·0 mm in diameter with walls approximately 0·01 mm thick. Crystals of trypsin, trypsinogen, cytochrome *c* and their derivatives with dimensions ranging from 0·1 × 0·1 × 0·35 mm to 0·4 × 0·4 × 0·7 mm were used in the crystal–capillary experiments. Trypsin crystals grow with acicular habit, cytochrome crystals are rectangular prisms, and trypsinogen crystals grow as approximately equidimensional trigonal bipyramids. Thus crystals of the most commonly encountered morphological forms have been used.

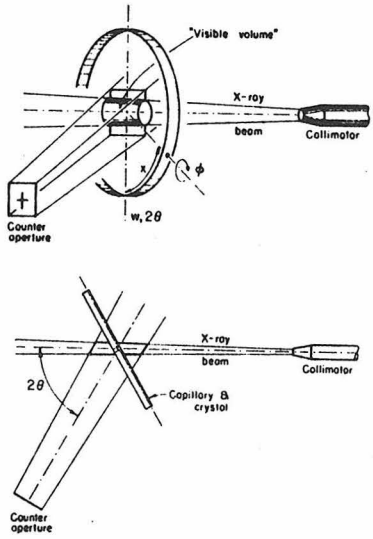

Fig. 1. The usual diffractometer data-collection arrangement. The 'visible volume' is the volume of air irradiated by the direct beam that is seen by the receiving-counter aperture. This volume changes only with 2θ, and governs the 2θ dependence of the air-scattered part of the background. Portions of the 'visible volume' are at times hidden from the X-ray beam and at times from the counter by the interposition of the capillary and crystal. The overall background will be affected by changes in the capillary–crystal setting angles, as well as the amount of capillary glass in the direct beam.

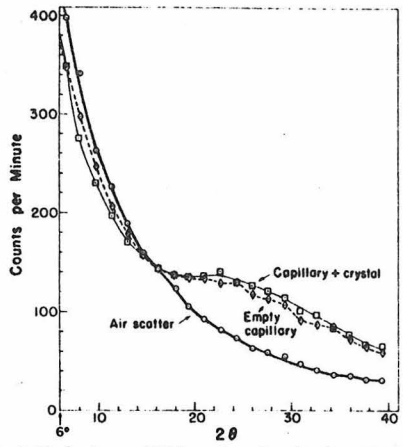

Fig. 2. The background 2θ dependence for: (*a*) air scatter only (○, 5 min/point), (*b*) an empty capillary (◇, 3 min/point), and (*c*) for a trypsinogen crystal, mounted in the same 0·5 mm diameter capillary (□, 3 min/point). All measurements were made at $\chi = 90°$, using diffractometer *A* as described in the text.

Backgrounds were measured under the following conditions:

(1) without crystal or capillary in the beam;

(2) with a well centered capillary (mounted coaxially with φ) in the beam;

(3) with a capillary miscentered, but mounted parallel to the φ axis; and

(4) with a crystal in a capillary such that the crystal, but not the capillary, is centered in the beam (the standard data-collection condition).

Background counting times were usually 3 to 5 min per point for the empirical background curves, and 10 to 120 s for individual backgrounds used for comparison. Reflection intensities were measured in both the ω scan and the Wyckoff step-scan (Wyckoff *et al.*, 1967) modes. Measurements were made over the ranges $0 \le 2\theta \le 46°$; $0 \le \varphi \le 360°$; and $0 \le \chi \le 360°$. Attenuators were used to obtain data for small 2θ angles down to 0°.

Results

Fig. 1 shows the usual diffractometer data collection arrangement and illustrates the origins of the different variations in the background intensity.

Primary effects: 2θ *dependence*

Fig. 2 shows the overall background as a function of 2θ: (*a*) with no crystal, no capillary; (*b*) for a well centered capillary; and (*c*) for a capillary containing a trypsinogen crystal (dimensions approximately 0·3 ×

0·25 × 0·35 mm). The intrinsic absorption of a glass capillary was measured and found to be generally less than 25%. The absorptive component due to the glass which affects the curves of Fig. 2 must consequently be less than about 25%. It is much less where 'visible volume' dimensions (see Fig. 1) are greater than the diameter of the capillary which is often the case. It is therefore clear that scattering by air is a major contributing factor to the background. In the presence of a capillary the background is reduced by absorption by the glass capillary. The background intensity increases at higher 2θ angles where scatter from the glass predominates over its absorption. Variations in the orientation of the capillary lead to φ- and χ-dependent secondary perturbations in the background.

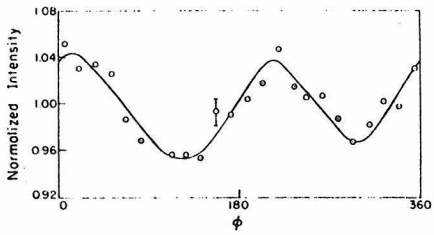

Fig. 3. The background φ dependence observed at $2\theta = 22{\cdot}6°$ and $\chi = 90°$ for a DIP-trypsin crystal. The average intensity is normalized to 1·0 (Diffractometer *A*).

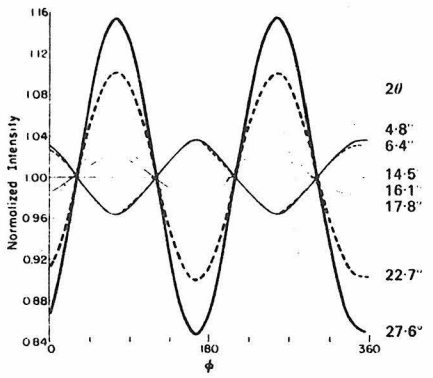

Fig. 4. The φ dependence of the background for an eccentrically mounted empty capillary at various 2θ values ($\chi = 90°$ in all cases). While the amplitude and sign of the variations change with 2θ, the phase is constant. The curves were measured at $2\theta = 27{\cdot}6°$, 22·7°, 17·8°, 16·1°, 14·5°, 6·4°, and 4·8°. The traces, except for $2\theta = 14{\cdot}5°$, represent the best least-squares fit of 24 points measured at 15° intervals to the function: Normalized intensity $= 1{\cdot}0 + a \cos 2(\varphi - \varphi_0)$. The average intensity at each 2θ is normalized to 1·0. The curve for $2\theta = 14{\cdot}5°$ is the best straight line through the data at this 2θ value. Measurements were made on diffractometer *A*.

Secondary effects: φ dependence

When it is necessary to collect data with a crystal mounted in a capillary whose *diameter* is greater than the radius of the X-ray beam, there can be a significant systematic variation of the background radiation with the diffractometer φ setting. Because there is little difference between the angular distribution of the background of an empty capillary and that of a capillary containing a crystal and its mother liquor, the φ dependence must be almost wholly due to the eccentricity of the capillary about the φ axis.

Fig. 3 shows typical φ dependence of background intensity for a capillary containing a protein crystal, and Fig. 4 shows this dependence for an eccentrically mounted empty capillary at different 2θ values. A well centered capillary shows no φ dependence, while with eccentrically mounted capillaries the background variation is an approximately sinusoidal function of 2φ as the capillary rotates in and out of the beam. At low 2θ values the background, primarily due to air scatter, is modulated by absorption of the eccentric capillary; therefore, the background is greatest when the capillary blocks the direct beam least ($\varphi = 0$ and 180° in Fig. 5). At higher 2θ angles the capillary scatters more radiation than it absorbs, and backgrounds are highest at $\varphi = 90$ and 270° in Fig. 5. At intermediate 2θ values, near the crossing point of Fig. 2, the absorption and scattering of the capillary are nearly equal and the backgrounds are essentially φ-independent. The extent of the background variation with φ will depend on the eccentricity and diameter of the capillary and the value of 2θ. The curves in Fig. 6 depict the background as a function of 2θ measured at two values of φ; one when the low-angle background is a minimum [curve $A_{\varphi_0, \chi_{90}}(2\theta)$] and the other when the low-angle background is a maximum [curve $B_{\varphi_1, \chi_{90}}(2\theta)$]. The magnitude of the differences between the two curves is the amplitude of the φ-dependent variation. There may be circumstances under which these curves would not cross, although we have not observed this. In such a case the amplitude of the φ-dependent variation with 2θ would not change sign.

For a DIP-trypsin crystal in a 0·6 mm capillary and a 1 mm beam, the background at 23° in 2θ varied 11% in intensity with rotation about φ. The average reflection intensity in the shell $22 < 2\theta < 26°$ for this crystal was seven times the background level. For a reflection with this 'average' intensity, using interpolated backgrounds uncorrected for the φ dependence would produce a systematic error up to 1·6% in its net intensity. Weaker reflections, which are still important for heavy-atom refinement and difference maps, are subject to substantially larger errors: a reflection with raw intensity twice background, *although at least* 10 σ (*standard deviations*) *above background*, would be in error by as much as 11%. These errors are systematic and must be corrected for, if accurate phases are to be calculated.

The following scheme was tested for generating interpolated backgrounds corrected for φ dependence:

(1) Measure the φ dependence at a low 2θ value ($\sim 6°$) with a φ scan at $\chi = 90°$.

(2) Measure the 2θ dependence, $A_{\varphi_0, \chi_{90}}(2\theta)$, at the φ value (φ_0) for which the background is a minimum on the φ scan.

(3) Measure the 2θ dependence, $B_{\varphi_1, \chi_{90}}(2\theta)$, at the φ value ($\varphi_1 = \varphi_0 + 90°$) for which the background is a maximum on the φ scan.

(4) Tabulate the difference, $D_\varphi(2\theta) = B_{\varphi_1, \chi_{90}}(2\theta) - A_{\varphi_0, \chi_{90}}(2\theta)$. [Normally, it is convenient to interpolate the values between the observed backgrounds on the $A_{\varphi_0, \chi_{90}}(2\theta)$ and $B_{\varphi_1, \chi_{90}}(2\theta)$ curves at intervals in $\sin(\theta)/\lambda$.]

(5) Calculate the backgrounds, $BG(2\theta, \varphi)$. For background corrections (just as for absorption corrections) the φ setting angle, φ_s must be modified to account for geometrical contributions to rotation with respect to the incident beam from χ and ω.*

$$BG(2\theta, \varphi_s) = A_{\varphi_0, \chi_{90}}(2\theta) + D_\varphi(2\theta) \sin^2(\varphi_c - \varphi_0) \quad \text{(I)}$$

where

$$\varphi_c = \varphi_s - \tan^{-1}(\cos\chi \tan\omega) . \quad \text{(II)}$$

For 1500 reflections observed over a wide range of 2θ, φ, and χ for a DIP-trypsin crystal ($0{\cdot}25 \times 0{\cdot}3 \times 0{\cdot}4$ mm) mounted in a 1 mm capillary on diffractometer *A*, the agreement between observed and interpolated backgrounds typically improved by 40% when φ-dependent anisotropic, rather than isotropic, interpolation was used. This scheme assumes that the φ dependence is sinusoidal† and that the amplitude of the variation is the difference $[D_\varphi(2\theta)]$ between the $A_{\varphi_0, \chi_{90}}(2\theta)$ and $B_{\varphi_1, \chi_{90}}(2\theta)$ curves of Fig. 6. If possible, crystals should be mounted only in capillaries whose diameters are smaller than the radius of the X-ray beam. Under these conditions there is no observable φ dependence.

* Any additional correction for a 2θ component in φ_c (due to rotation with respect to the counter) is much less significant in general where the visible volume (Fig. 1) is larger than the irradiated portion of the capillary. The correction for χ and ω deals with the source of scattering directly, while the 2θ correction deals with only a small component of the scattered radiation. In any case an additional 2θ correction would be asymmetric and complex and is usually unnecessary.

† We have always observed a certain asymmetry in the φ scans which we presume to be due to the difference in position of the eccentrically mounted capillary with respect to the counter at φ and $\varphi + 180°$. In order to account for this asymmetry, we have calculated backgrounds using the expression:

$$BG(2\theta, \varphi) = A_{\varphi_0, \chi_{90}}(2\theta) + D_\varphi(2\theta) \left[\frac{F(\varphi_c) - F(\varphi_0)}{F(\varphi_1) - F(\varphi_0)} \right]$$

where, for example,
$F(\varphi) = a(x - x_0)^2 + b(y - y_0)^2 + c(x - x_0)(y - y_0)$: $x = \sin\varphi$, $y = \cos\varphi$, and x_0, y_0, a, b, and c are refinable parameters. Alternatively, one could use an interpolated φ curve for $F(\varphi)$. However, we have obtained the best results using the sine function in equation (I).

χ dependence

The background χ dependence is analogous to the φ dependence, but a rigorous definition of the problem is more difficult as a result of more complex geometry. However, the χ dependence may be understood qualitatively. As χ varies from 0 to 90°, the amount of glass in the equatorial plane increases approximately as the secant of χ. This, in turn, increases the absorption of air-scattered radiation. The exact nature of this angular background variation with χ depends strongly on the experimental conditions.‡

‡ We have observed that each diffractometer has a characteristic χ–2θ dependence, as shown in Figs. 7 and 8. Subtle differences in the geometry of the diffractometers (*e. g.*, collimator-to-crystal distance) are apparently responsible for the difference in these patterns. The correction scheme outlined below has proven effective for data collected on different diffractometers with different χ–2θ patterns.

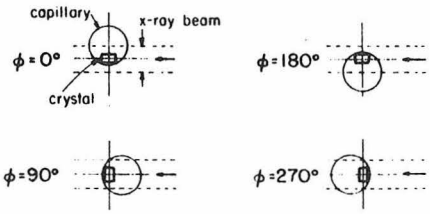

Fig. 5. View parallel to the φ axis of a capillary and crystal, showing the amount of direct-beam radiation they intercept at various φ settings. The capillary diameter is greater than the radius of the X-ray beam.

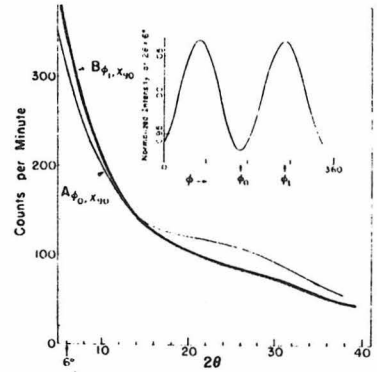

Fig. 6. Curves $A_{\varphi_0, \chi_{90}}$ and $B_{\varphi_1, \chi_{90}}$, the background 2θ dependence observed at two φ settings, 90° apart, for a capillary-mounted DIP-trypsin crystal. Inset, a φ scan for this crystal taken at $2\theta = 6°$, showing the positions of the φ_0 and φ_1 settings (Diffractometer *A*).

Figs. 7 and 8 show the 2θ dependence of the background radiation for DIP-trypsin and cytochrome c crystals at $\chi=0°$ [$C_{\varphi_0,\chi_0}(2\theta)$] and $\chi=90°$ [$A_{\varphi_0,\chi_{90}}(2\theta)$], and the variation of the χ dependence for several values of 2θ. Just as with the φ dependence, the amplitude of the χ variation depends upon the difference between the backgrounds at the extremes, $\chi=0$ and $\chi=90°$. Depending upon the experimental conditions, it is possible to observe a crossover of the $A_{\varphi_0,\chi_{90}}(2\theta)$ and $C_{\varphi_0,\chi_0}(2\theta)$ curves analogous to that for the φ curves. In such cases, the high-angle background increases as χ goes from 0 to 90°, and the shape of the curve can vary from that observed at low 2θ (Fig. 8).

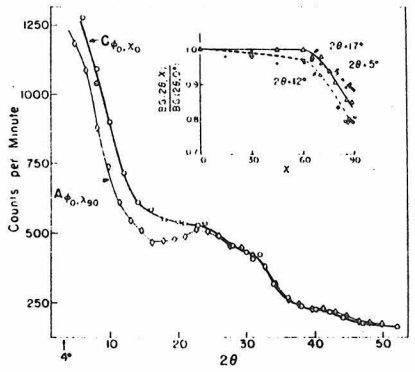

Fig. 7. Curves $A_{\varphi_0,\chi_{90}}$ and C_{φ_0,χ_0}: the background 2θ dependence observed at $\chi=90$ and $\chi=0°$ on diffractometer A for a DIP-trypsin crystal mounted in a 1 mm capillary. Each data point was counted for 4 min. Inset: the χ dependence observed at several 2θ values. Each point was measured for 5 min.

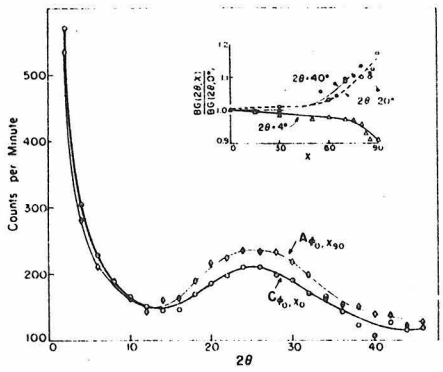

Fig. 8. Curves $A_{\varphi_0,\chi_{90}}$ and C_{φ_0,χ_0}: the background 2θ dependence observed at $\chi=90$ and $\chi=0°$ for a cytochrome c crystal using diffractometer B. Inset: background χ dependence at several 2θ values. All points were measured for 4 min.

The χ-dependent background variation can represent a significant fraction of the total background. We have routinely observed 15% differences in backgrounds between $\chi=0$ and $\chi=90°$, and differences as high as 25% are not uncommon. The following interpolation scheme, analogous to that used for φ, was used to correct for the χ dependence:

(1) Measure the 2θ dependence, $C_{\varphi_0,\chi_0}(2\theta)$, at $\chi=0°$.

(2) Measure the 2θ dependence, $A_{\varphi_0,\chi_{90}}(2\theta)$, at $\chi=90°$.

(3) Tabulate the differences, $D_\chi(2\theta)=C_{\varphi_0,\chi_0}(2\theta)-A_{\varphi_0,\chi_{90}}(2\theta)$.

(4) Measure the χ dependence at a $2\theta=2\theta_m$ for which the difference, $D_\chi(2\theta)$, is large. If possible, $2\theta_m$ should be representative of the 2θ's in the data set.

(5) Calculate the backgrounds from:

$$\mathrm{BG}(2\theta,\chi)=A_{\varphi_0,\chi_{90}}(2\theta)+D_\chi(2\theta)\left[\frac{F(\chi)-F(90°)}{F(0°)-F(90°)}\right]_{2\theta_m} \quad \text{(III)}$$

where $F(\chi)$ is either an empirical function representing the χ dependence or an interpolated χ curve at $2\theta_m$. Our best results have been obtained with:

$$F(\chi)=a\exp\{-b/(\cos\chi+c)\} \quad \text{(IV)}$$

where the coefficients a,b,c are determined by a least-squares fit. If the background shown in Fig. 7, for example, is not corrected for χ dependence, *i.e.*, if isotropic interpolated backgrounds (depending only on 2θ) are used, systematic errors of up to 30% of the background can result. χ-dependent (anisotropic) interpolation can be improved upon by subdividing the data into smaller 2θ ranges and applying appropriate χ curves to the data in each range.

When both φ and χ dependences are present, backgrounds may be approximated by combining the φ and χ corrections:

$$\mathrm{BG}(2\theta,\varphi,\chi)=A_{\varphi_0,\chi_{90}}(2\theta)+D_\varphi(2\theta)\sin^2(\varphi_c-\varphi_0)+D_\chi(2\theta)\left[\frac{F(\chi)-F(90°)}{F(0°)-F(90°)}\right]_{2\theta_m}. \quad \text{(V)}$$

Non-linear least squares

A different approach to the estimation of backgrounds is the use of non-linear least squares to approximate backgrounds as some function of 2θ, φ, and χ. This function is determined by fitting backgrounds measured for short times in the vicinity of each reflection. The reliability of such a procedure depends on the choice of a well behaved function with a relatively small number of parameters. Its accuracy also depends on the number of data and time spent on measuring the individual backgrounds.

The dependence of background intensity on 2θ may be satisfactorily accounted for by a third-order function of 2θ:

$$\mathrm{BG}(2\theta) = a + bT + cT^2 + dT^3, \quad \text{(VI)}$$

where $T = 2\theta$ and the lower case letters a, b, c, *etc.*, are parameters to be determined. Some improvement can be achieved when the data are separated into low, middle, and high-angle regions in 2θ. Other terms are added to $\mathrm{BG}(2\theta)$ to account for the variation of BG (2θ) as functions of φ and χ.

In any region of reciprocal space (not necessarily over all 2θ ranges), it is sufficient to approximate the changing magnitude and sign of the φ correction with a third-order polynomial:

$$\Delta B_1(\varphi,2\theta) = \sin^2(\varphi-\varphi_0)(e+fT+gT^2+hT^3) \quad \text{(VII)}$$

where φ_0 is a parameter corresponding to the φ value for minimum or maximum background. If the background does not have a φ dependence, $\Delta B_1(\varphi,2\theta)$ is zero.

Since the magnitude, curvature, and sometimes the sign of the χ correction are also 2θ-dependent, we have tried various combinations of terms of the form $T^i\chi^j$; $i = 1$ to 4; $j = 1$ to 4 to determine which terms are useful to best correct for the χ dependence. An expression of the form

$$\Delta B_2(\chi,2\theta) = iT\chi + jT\chi^2 + kT\chi^3 + lT^2\chi^2 + mT^3\chi \quad \text{(VIII)}$$

provides the best compromise between the number of refined parameters and the overall quality of fit.

The overall expression for least-squares refinement is:

$$\mathrm{BG}(2\theta,\varphi,\chi) = \mathrm{BG}(2\theta) + \Delta B_1(\varphi,2\theta) + \Delta B_2(\chi,2\theta)\,. \quad \text{(IX)}$$

This function can be used in any 2θ range. However, $\mathrm{BG}(2\theta)$ and $\Delta B_2(\chi,2\theta)$ can often be simplified for middle and high 2θ ranges with essentially no loss of accuracy: for middle or high 2θ, $\mathrm{BG}(2\theta) = a + bT$ suffices; for the middle range, $\Delta B_2(\chi,2\theta) = iT\chi + jT\chi^2 + kT\chi^3 + lT^2\chi^2$; and for the high range $\Delta B_2(\chi,2\theta) = iT\chi + jT\chi^2 + kT\chi^3$.

Discussion

The anisotropic interpolation (AI) and non-linear least-squares (LS) techniques have been used routinely to compare and measure background intensities for crystals of several proteins on different diffractometers. Data for the comparison to be discussed first were taken from a DIP-trypsin crystal using diffractometer *A*. The data shown in Table 2 and Fig. 9 compare the isotropic interpolation (II), AI and LS methods of estimating background intensity with individual backgrounds, BG_{obs}, each measured for 40 s.

Fig. 9 shows the distribution of errors, $\Delta\mathrm{BG}/\sigma_{obs}$, where

$$\Delta\mathrm{BG} = (\mathrm{BG}_{obs} - \mathrm{BG}_{calc}) \text{ and } \sigma_{obs} = \sqrt{\mathrm{BG}_{obs}}\,,$$

for each of the three methods and for a perfectly normal distribution. For the II method the distribution of error is far from normal because of the systematic error introduced by ignoring the anisotropy in the background. The error distribution is skewed and distorted regardless of the setting angles used for observing the 2θ curve (see Fig. 10).

The error distributions for the AI and LS methods, on the other hand, are very nearly Gaussian,* indi-

Table 2. *Error analysis of background-approximation techniques*

Estimated backgrounds compared to backgrounds measured for 40 s per point.*

Method	$\langle\Delta\mathrm{BG}^2\rangle^{1/2}$†	s‡	R_{BG}%§	GOF¶	R_F%**
II	61·7	55·3	10·0	2·22	1·76
AI	41·2	30·8	6·0	1·38	0·88
LS	32·3	17·1	5·3	1·19	0·87

* Results are for 1956 reflections measured on diffractometer (*A*) as described in the text. The average observed background was 501 counts per min, and the rms σ (BG_{obs}) was 27·4 counts per min. The comparisons are all tabulated in counts per min.

† $\Delta\mathrm{BG} = \mathrm{BG}_{obs} - \mathrm{BG}_{calc}$.

‡ s is the error component due to errors arising from the II, AI or LS methods, $s^2 = \langle\Delta\mathrm{BG}^2\rangle - \langle\sigma^2_{obs}\rangle$.

§ $R_{BG} = \sum|\Delta\mathrm{BG}| / \sum \mathrm{BG}_{obs}$.

¶ $\mathrm{GOF} = \left[\dfrac{\sum(\Delta\mathrm{BG}/\sigma_{obs})^2}{1956 \text{ pts.}}\right]^{1/2}$, the 'goodness-of-fit'.

** $R_F = \sum|F_{BGobs} - F_{BGcalc}| / \sum|F_{BGobs}|$.

* We have shown this in two ways: least-squares fitting a Gaussian to the error frequency curves in Fig. 9, and by direct comparison to perfectly normal distributions by means of normal probability plots (Abrahams & Keve, 1968).

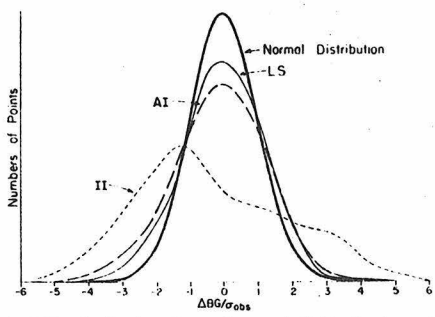

Fig. 9. The distribution of errors between individually observed (40 s) backgrounds and backgrounds calculated using the three techniques described in the text. The statistics plotted are the numbers of points within intervals of $\Delta\mathrm{BG}/\sigma_{obs}$, where $\Delta\mathrm{BG} = \mathrm{BG}_{obs} - \mathrm{BG}_{calc}$ and $\sigma_{obs} = \sqrt{\mathrm{BG}_{obs}}$. The total area under each curve is equivalent to 1956 data points. The curves are frequency distributions for the errors of the II, or isotropic interpolated backgrounds, the AI, or anisotropic interpolated backgrounds, and the LS, or least-squares backgrounds. The heavy curve represents an ideal Gaussian distribution of error for the same number of points. (DIP-trypsin crystal on diffractometer *A*).

cating that the systematic errors resulting from the II method have been largely eliminated. The slightly increased breadth of the AI and LS error distributions relative to the perfectly normal distribution is a consequence of the errors introduced by these methods. We can estimate the extent of these errors, s, using the approximation:

$$s^2 \simeq \langle \Delta BG^2 \rangle - \langle \sigma^2_{obs} \rangle \qquad (X)$$

where $\langle \Delta BG^2 \rangle$ is the mean squared ΔBG and $\langle \sigma^2_{obs} \rangle$ is the mean squared error in the individually observed backgrounds. For the data illustrated in Fig. 9 the estimated average error for backgrounds calculated using the AI technique, with empirical background curves observed for 4 min per point, is roughly equivalent to that which would be obtained by measuring each background for 32 s. For LS, s is equivalent to error expected for backgrounds measured for 91 s each. The value of s for AI depends upon the time spent measuring each point for the interpolated curves, while that for LS depends on the counting times for individually measured backgrounds. In this example, individual 40 s backgrounds were used to calculate the LS function. In another case results were essentially identical when 10 s backgrounds were used, and this method is clearly most useful when still shorter times are used.

We have compared the effects of the II, AI and LS methods on the structure factors by calculating the R values (R_F) between the data sets obtained using observed and calculated backgrounds (see Table 1). The R_F value for the II corrected data is approximately twice as large as that calculated for the AI and LS corrected data. Applying absorption corrections to the scan intensities *before* subtracting II backgrounds, as recommended by Hill & Banaszak, increases the R_F value to 1·95%. Clearly the AI and LS methods are substantial improvements over the II method.

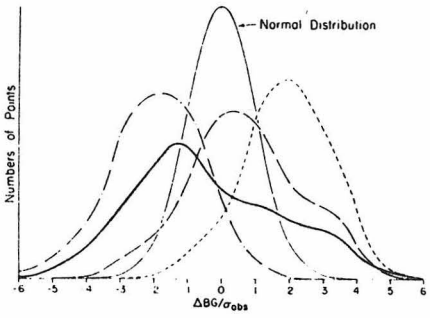

Fig. 10. The distribution of errors when different empirical 2θ curves are used in the II method. The frequency distributions are for backgrounds calculated using: a 2θ curve measured at $\varphi=\varphi_0$, $\chi=0°$ (· · ·), a 2θ curve measured at $\varphi=\varphi_1$, $\chi=90°$ (– – –), a 2θ curve measured at $\varphi=\varphi_0$, $\chi=90°$ (——); and a 2θ curve calculated from the φ_1,χ_{90} and φ_0,χ_{90} curves, representing a 2θ curve which would be obtained if $\varphi \sim \frac{1}{2}(\varphi_0+\varphi_1)$ (– · –). The light curve (– – –) represents an ideal Gaussian distribution of error. As in Fig. 9, the area under each curve represents 1956 data points distributed over the range $4·6° < 2\theta < 46°$.

Conclusion

The most significant conclusions to be drawn from these studies of background intensity are:

(1) The principal 2θ-dependent component of background intensity arises from X-rays scattered by the volume of air illuminated by the direct beam and 'seen' by the receiving-counter aperture. Modulation of this air scatter by capillary absorption and scatter gives rise to φ and χ-dependent variations in the background.

(2) The background intensity is essentially uncorrelated with the crystal absorption. Under certain experimental conditions the two phenomena may appear to be correlated; for example, where a flat crystal rests on the side of the capillary such that its long axis lies parallel to the φ axis of the diffractometer.

(3) As a consequence of (2), the background intensity should always be subtracted from the scan intensity before the absorption corrections are applied, contrary to the suggestion of Hill & Banaszak (1973).

(4) The anisotropy of background scatter as a function of 2θ, φ, and χ can be satisfactorily accounted for by using a simple interpolative procedure, or by fitting a suitable function to many backgrounds measured for short times near each reflection.

(5) The use of an isotropic background interpolation is usually unsatisfactory for accurate data reduction. This method can introduce systematic errors of up to 30% in the estimated background intensities. Errors of this sort lead to systematic errors in phases and increase the noise levels in difference maps.

Both the AI and LS methods substantially reduce the systematic errors inherent in the II method. As a result, the differences between observed backgrounds and estimated backgrounds closely follow a normal distribution. Both methods represent significant savings in time and are improvements over the II method. The overall accuracy of either method is limited by the extent and duration of the background sampling, and is generally commensurate with that obtained for individual backgrounds. When deciding between the two methods, one must choose between the greater savings in time provided by the AI method, or the somewhat better accuracy of the LS technique at the cost of increased crystal exposure and decay.

Our results identify the principal sources of background intensity. Consequently, there are several experimental steps which can be taken to reduce background intensity: (1) Capillaries should ideally be chosen to be smaller in diameter than the radius of the incident X-ray beam. This renders φ dependence insignificant, diminishes χ dependence of the background and reduces the high-angle background due to capillary

scatter. (2) Helium-filled tubes are often used to reduce absorption by air in the input or output beam directions. However, as the main problem is generally one of peak-to-background ratio, these measures only slightly affect this ratio, and in any case do not reduce background intensity significantly. It would seem highly advantageous to fill the 'visible volume' with helium, so affecting the background intensity directly. This is obviously difficult to do as it implies either a helium-filled enclosure over the entire diffractometer, or a helium-filled chamber mounted around the φ axis which surrounds the capillary and crystal completely. There are obvious mechanical difficulties in building such a device. First, it must be almost X-ray transparent over the angular ranges used. Second, it must be moderately well sealed to minimize leakage of helium if it encloses the φ drive shaft bearing. A mylar cylinder with solid supports mounted onto the top of the goniometer head would seem to be a good compromise allowing for rigid support of the top and bottom in the X-ray shadow.

(3) Any means of restricting the visible volume will reduce the background in almost direct proportion to the volume change. This can be achieved by placing the final restricting aperture and the scatter cap on the input collimator as close to the crystal as possible. Similarly, there should be a defining aperture as close to the crystal as possible in the crystal–counter pathway, and a second one close to the counter.

We thank Drs A. Kossiakoff and R. Swanson for generously supplying background data, Mr R. Almassy for helpful assistance, and Dr R. E. Marsh and Mr J. Greif for valuable discussions. We are grateful to Dr Sten Samson for allowing us to collect data on diffractometer *F*, a machine designed in the most part by himself, and for his supervision in the redesign of diffractometer *B*. We also recognize his constant attention in the redesign and improvements made to diffractometer *C*.

References

ABRAHAMS, S. C. & KEVE, E. T. (1971). *Acta Cryst.* A**27**, 157–165.

DICKERSON, R. E., KOPKA, M. L., VARNUM, J. & WEINZIERL, J. E. (1967). *Acta Cryst.* **23**, 511–522.

HENDERSON, R. & MOFFATT, J. K. (1971). *Acta Cryst.* B**27**, 1414–1420.

HILL, E. J. & BANASZAK, L. J. (1973). *Acta Cryst.* B**29**, 372.

JENSEN, L. (1972). Personal communication.

KRIEGER, M., KAY, L. M. & STROUD, R. M. (1974). *J. Mol. Biol.* **83**, 209–230.

MATHEWS, F. S., LEVINE, M. & ARGOS, P. (1972). *J. Mol. Biol.* **64**, 449–464.

SALEMME, F. R., FRIER, S. T., XUONG, Ng. H., ALDEN, R. & KRAUT, J. (1973). *J. Biol. Chem.* **248**, 3910–3921.

WATSON, H. C., SHOTTON, D. M., COX, J. M. & MUIRHEAD, H. (1970). *Nature, Lond.* **225**, 806–811.

WYCKOFF, H. W., DOSCHER, M., TSERNOGLOU, D., INAGAMI, T., JOHNSON, L. N., HARDMAN, K. D., ALLEWELL, N. M., KELLY, D. M. & RICHARDS, F. M. (1967). *J. Mol. Biol.* **27**, 563–578.

WYCKOFF, H. W., TSERNOGLOU, D., HANSON, A. W., KNOX, J. R., LEE, B. & RICHARDS, F. M. (1970). *J. Biol. Chem.* **245**, 305–328.

Appendix 3

Structure-Function Relationships in the Serine Proteases

Structure-Function Relationships in the Serine Proteases

Robert M. Stroud, Monty Krieger, Roger E. Koeppe II, Anthony A. Kossiakoff and John L. Chambers

Norman W. Church Laboratory of Chemical Biology
California Institute of Technology, Pasadena, California 91109

Of the many ways available to control the biological activity of proteins, e.g., induction or repression of their synthesis at the translational (Jacob and Monod 1961) or transcriptional levels (Tomkins et al. 1969), specific modification or destruction are the most direct. Many biological systems are controlled by methods such as these, and the serine protease family of enzymes plays a major role in many of these systems (Stroud 1974). The pancreatic serine proteases are digestive enzymes which show optimal activity around the neutral pH region. Their function in hydrolyzing peptide bonds and the systems of physiological control over their activity have close homology in many other biological processes, e.g., blood clotting (Owren and Stormorken 1973; Magnusson 1971), bacterial sporulation (Leighton et al. 1973), fertilization (Stambaugh, Brackett and Mastroianni 1969), etc. Many of the enzymes of biological control have been recognized as serine proteases, which in nearly all documented cases have amino acid sequence homology to the pancreatic serine proteases. It is therefore to be expected that these enzymes will have closely homologous tertiary structures and will share the same catalytic mechanism of action. The mechanisms by which such enzymes are activated or inhibited will also share many common features with the digestive serine proteases. In many cases the degrees to which these principles can be extended may be predicted by recognition of the chemical and structural features of the pancreatic serine proteases which appear to define their properties. In this article we will discuss recent advances in the understanding of aspects of the structures and functions of the mammalian serine proteases.

THE PANCREATIC DIGESTIVE ENZYMES: TRYPSIN, CHYMOTRYPSIN, ELASTASE

Intrinsic to the process of digestion in mammals is the breakdown of dietary protein by the pancreatic serine proteases. These pancreatic digestive enzymes

are among the most thoroughly studied of all enzymes, principally because they are extracellular enzymes that are easily separated and purified in large quantities (Kunitz and Northrop 1935). They originate in the pancreas as inactive precursors, or proenzymes, which are secreted into the duodenum. There they are activated (Kunitz and Northrop 1936; Northrop, Kunitz and Herriot 1948; Maroux, Baratti and Desnuelle 1971) by the cleavage of one critical peptide bond near the amino-terminal end of the polypeptide chain (Davie and Neurath 1955). This cleavage in turn permits a conformational change (Neurath and Dixon 1957; Sigler et al. 1968) which converts the proenzymes to active enzymes. Once activated, these enzymes catalyze the breakdown of proteins, first into fragments and ultimately into individual amino acids.

Kinetic studies on a variety of amide and ester substrates have shown that the mechanism of serine protease catalysis (Eq. 1) involves a number of intermediates (Zerner, Bond and Bender 1964; Oppenheimer, Labouesse and Hess 1966; Caplow 1969; Hess et al. 1970; Fersht and Requena 1971a; Fastrez and Fersht 1973a,b; Fersht and Renard 1974):

$$E + S \rightleftharpoons ES \rightleftharpoons ES^T \rightleftharpoons \underset{+\ P_1}{EP_2^a} \rightleftharpoons EP_2^T \rightleftharpoons EP_2 \rightleftharpoons E + P_2. \qquad (1)$$

Here, E represents free enzyme; S, the substrate; ES and EP_2, enzyme substrate and product complexes; ES^T and EP_2^T, tetrahedral intermediates; EP_2^a, an acyl enzyme; P_1, the amino or alcohol portion of the product; and P_2, the carboxylic acid portion of the product. For amides, the rate-determining step is generally acylation, $E + S \rightarrow EP_2^a$, whereas deacylation, $EP_2^a \rightarrow E + P_2$, is usually rate-determining for esters (Zerner and Bender 1964). The characteristic differences between each of the digestive serine proteases—trypsin, chymotrypsin and elastase—lie in their specificity for hydrolyzing the peptide bonds between different amino acids in the protein substrate. Trypsin, the most sharply specific of the digestive enzymes, hydrolyzes those peptide bonds that immediately follow either of the two basic amino acids, lysine or arginine. Chymotrypsin hydrolyzes peptide bonds that follow several of the amino acids with larger hydrophobic side chains, and elastase binds the small side chains of glycine, alanine or serine at the equivalent binding site (Naughton and Sanger 1961; Brown, Kauffman and Hartley 1967; Sampath Narayanan and Anwar 1969). The complete amino acid sequences and three-dimensional molecular structures have now been worked out for chymotrypsin (Sigler et al. 1968) and its proenzyme (Freer et al. 1970), elastase (Shotton and Watson 1970), and DIP (diisopropylphosphoryl)-trypsin (Stroud, Kay and Dickerson 1971, 1974) and the proenzyme (Kossiakoff, Kay and Stroud, unpubl.). These structures, along with that of the bacterial serine protease subtilisin (Wright, Alden and Kraut 1969; Alden, Wright and Kraut 1970), have been uniquely valuable in developing an understanding of how these enzymes bind a substrate and how they catalyze the subsequent chemical reaction.

Activating the Proenzyme

The first key to activation of the pancreatic proenzymes is enterokinase, an enzyme secreted in small amounts by the mucous membrane of the stomach. Its prime function is to convert some trypsinogen to trypsin, which then activates all of the proenzymes (including more trypsinogen) (Kunitz and Northrop 1936; Northrop, Kunitz and Herriot 1948; Maroux, Baratti and Desnuelle 1971). In each case, activation involves the cleavage of a few amino acid residues from the amino-terminal end of the proenzyme (Davie and Neurath 1955; Neurath and Dixon 1957).

With the formation of the new amino terminus at Ile-16[1] (Oppenheimer, Labouesse and Hess 1966), the protein undergoes conformational changes (Neurath, Rupley and Dreyer 1956) leading to a catalytically active configuration. A comparison of the high-resolution structure of chymotrypsinogen with that of chymotrypsin (Freer et al. 1970; Wright 1973) and of the high-resolution structure of DIP-trypsin with the recently determined high-resolution structure of trypsinogen (Kossiakoff, Kay and Stroud, unpubl.) helps us to understand the exact nature of these conformational changes. (A detailed description of the trypsinogin structure will be published later.) In both cases,

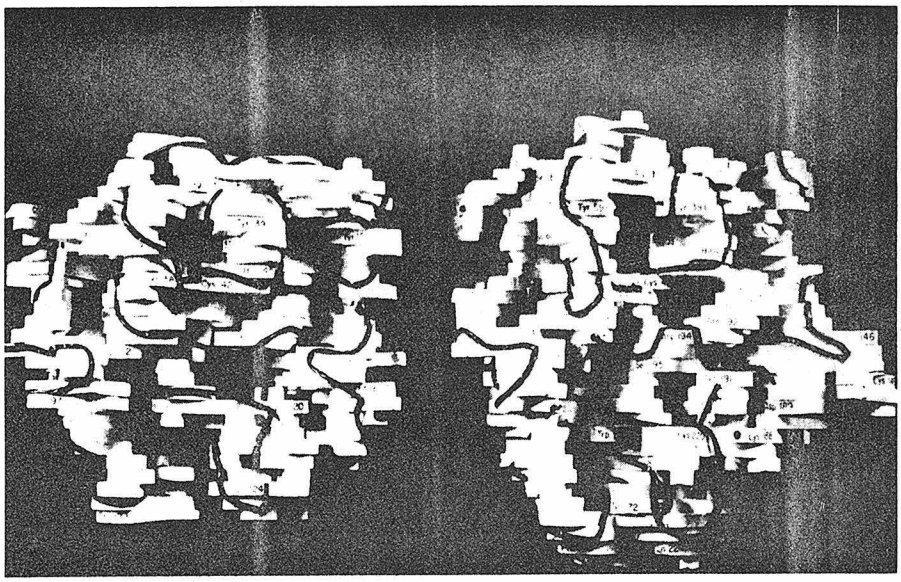

Figure 1
A comparison of the 5-Å models of trypsinogen (*left*) and DIP-trypsin (*right*) shows close structural homology in most areas of the molecule. Striking structural differences are observed in only two areas of the molecule. The first is in the binding pocket region, which is formed by residues 214–220 and 189–192, and the second is along a loop of chain containing residues 140–151 located on the right-hand side of the molecule. The small difference in size of the models is due to a difference in scale and orientation.

[1] The numbering system referred to is that of chymotrypsin, which will be adopted here as a standard for comparison of sequences.

clipping the proenzyme tail permits the new, positively charged α-amino terminus at residue 16 to fold into the interior of the globular structure and form an ion pair with the negative carboxyl group of Asp-194 (Matthews et al. 1967; Sigler et al. 1968). While this change is accompanied by movements in the region of the specificity binding pocket, there appears to be little change in the interaction between Asp-102, His-57 and Ser-195 at the catalytic site (Freer et al. 1970; see also Fig. 1). Thus the arrangement of these catalytic residues is preformed in the proenzyme. One major factor which contributes to the relative inactivity of the zymogen is that the binding of the normal substrates is impaired (Kassell and Kay 1973; Gertler, Walsh and Neurath 1974).

Enzyme Specificity and Substrate Binding

The serine proteases differ in their specificities because of differences in their substrate binding sites. Trypsin, chymotrypsin and elastase all have specific side-chain binding pockets on the surface of the protein close to the catalytic site (see Fig. 2). This pocket is lined by residues 214–220 and 189–192 and

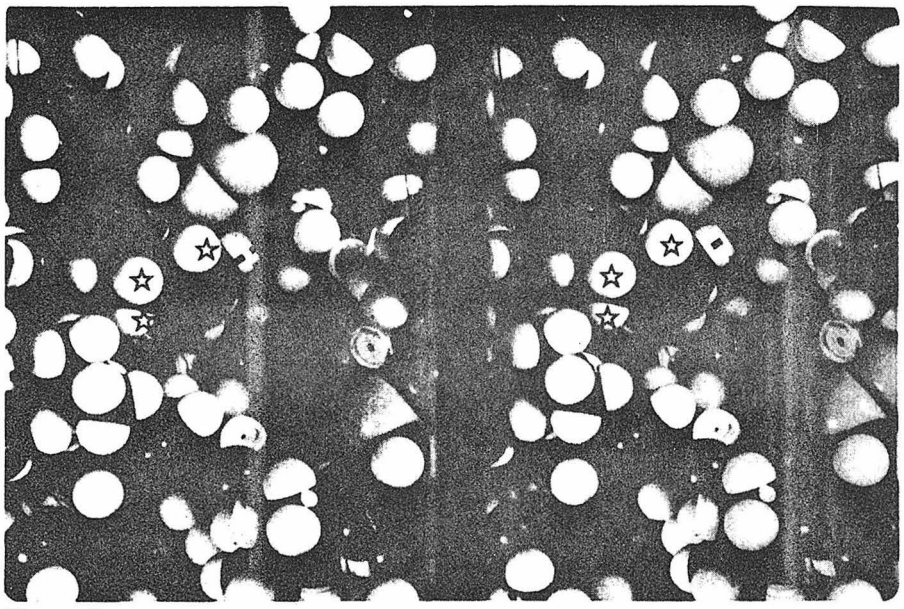

Figure 2

Stereoscopic photograph of a space-filling model showing the active site and specificity pocket in trypsin (see Stroud, Kay and Dickerson 1971, 1974). The imidazole side chain of His-57 is visible; however, the carboxylic acid side chain of Asp-102 is hidden from view by several amino acid residues. The viewing direction is approximately the same as that of Figures 4 and 7. The side-chain binding pocket is located beneath and to the right of the catalytic site.

Stars are placed near the active site as markers. They are located (reading from left to right) at the following positions: the Asp-102/His-57 hydrogen bond, the β-carbon protons of His-57, one of the ring protons on His-57, and the Ser-195 γ-hydroxyl.

defines the primary specificity toward substrate side chains immediately prior to the peptide bond which is to be cleaved. Cysteine residues 220 and 191 are linked by a disulfide bond. In trypsin, residue 189 is an aspartic acid, and its negatively charged carboxyl group ($pK_{it} = 4.6$) (East and Trowbridge 1968) lies at the bottom of the pocket (Stroud, Kay and Dickerson 1974). Trypsin has primary specificity for basic amino acids because their positively charged side chains bind tightly in this pocket (Mares-Guia and Shaw 1965; Ruhlmann et al. 1973; Blow, Janin and Sweet 1974; Sweet et al. 1974; Krieger, Kay and Stroud 1974). In an attempt to determine the manner in which amino acid side chains bind, we determined the structure of benzamidine trypsin. Benzamidine is a competitive, specific and reversible inhibitor of trypsin. Figure 3 shows how benzamidine, an amino acid side chain analog, binds in the specificity binding pocket (Krieger, Kay and Stroud 1974). In the case of trypsin, there is evidence that when side chains are bound in this pocket, they induce small conformational changes in the enzyme-substrate complex which help to accelerate catalysis (Inagami and Murachi 1964; Inagami and York 1968). In chymotrypsin, residue 189 is a serine (Hartley 1964). The pocket is now relatively hydrophobic and uncharged at neutral pH's, thus explaining chymotrypsin's specificity. In both trypsin and chymotrypsin, residue 216, a glycine, lies at the entrance to the binding pocket. In elastase, valine replaces glycine at position 216 (Shotton and Hartley 1970). The larger hydrophobic side chain blocks the entrance to the pocket and only allows the binding of amino acids with small side chains at the primary binding site (Shotton and Watson 1970).

Other parts of the enzyme are involved in binding other parts of the substrate molecule as well as the side chain, so that the susceptible substrate bond is aligned appropriately on the surface. Secondary specificity toward other

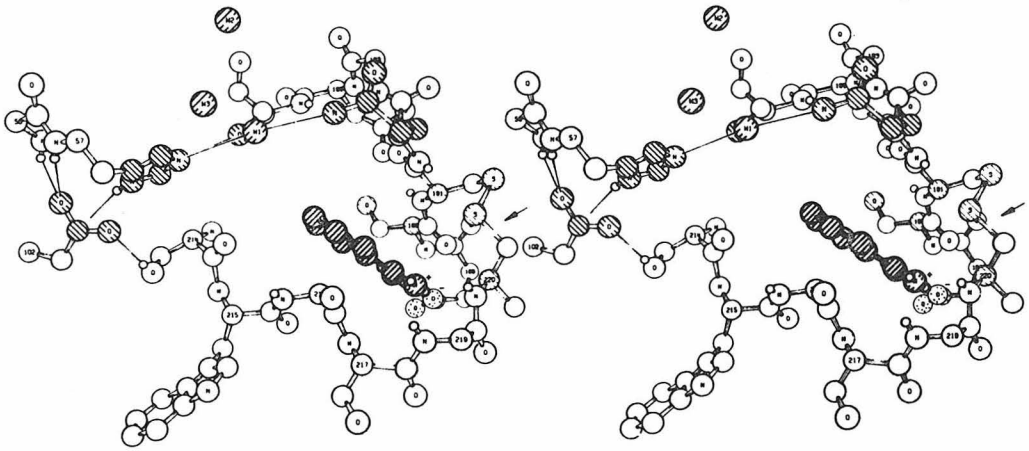

Figure 3

The figure shows the structure of the trypsin binding pocket in benzamidine-trypsin. (The phenyl amidinium is depicted by heavy shading.) This view is approximately the same as that of Figure 2. (Reprinted, with permission, from Krieger, Kay and Stroud 1974.)

side chains in the physiological substrate molecules can also be correlated with enzyme structure (Fersht, Blow and Fastrez 1973), although the role of secondary specificity in the digestive enzymes is clearly much less significant than it is in highly specific enzymes of biological control.

Ideally, one would like to study the three-dimensional structure of an enzyme-substrate complex by X-ray crystallography and in so doing, gain new insights into the mechanism of serine protease catalysis. Unfortunately, this has not yet been possible because the catalyzed reaction takes place almost immediately after the substrate is bound and the system becomes an enzyme-plus-product complex. Data for a three-dimensional structure analysis cannot generally be collected in so short a time. Fersht and Renard (1974) have pointed out, however, that it may be possible to use equilibrium methods to trap intermediates in the reaction pathway and study their structures. Until the structures of such intermediates have been determined, crystallographers will be limited to studying the binding of substrate analogs and inhibitors, which in some limited respects resemble true substrates. Nevertheless, from such studies inferences can be drawn about the structural transformations which occur during the catalyzed reaction.

Among the best analogs to true trypsin substrates are the naturally occurring trypsin inhibitors. They have evolved in parallel with the enzymes so that they bind extremely tightly to the active site. Such protein inhibitors are crucial to physiological control of the serine proteases (Tschesche 1974). For example, if pancreatic secretory trypsin inhibitors were not synthesized along with the pancreatic serine proenzymes, one prematurely activated molecule of trypsin could start an autocatalytic chain reaction which would activate the other serine proenzymes and destroy any nearby proteins. Inhibitors are present to prevent such catastrophes and to control physiological processes mediated by proteolytic enzymes. The structure of an intracellular 6500 molecular weight trypsin inhibitor (PTI) isolated from bovine pancreas and other organs was determined by R. Huber et al. (1970, 1971). Chemical modifications had already shown that Lys-15 of this inhibitor was involved in the trypsin-PTI association (Chauvet and Acher 1967; Kress and Laskowski 1967; Fritz et al. 1969). By combining models of PTI with the known structures of trypsin and chymotrypsin, substrate binding models (Fig. 4) were developed by us (Stroud, Kay and Dickerson 1971; Krieger, Kay and Stroud 1974) and independently by Huber et al. (1971) and Blow et al. (1972). High-resolution structures of the PTI-trypsin complex (Ruhlmann et al. 1973) and of a soybean trypsin inhibitor-trypsin complex (Blow, Janin and Sweet 1974; Sweet et al. 1974) have since been determined. Several hydrogen bonds and stereochemical complementarity between enzyme and inhibitor orient the susceptible bond at the active site. There is one very important difference between the predicted substrate binding models and the structures of the trypsin-inhibitor complexes; the inhibitor and trypsin are covalently bound together via an oxygen-carbon bond between the hydroxyl of Ser-195 and the carbonyl group of Lys-15 in the trypsin-PTI complex and between the serine hydroxyl and the carbonyl carbon of Arg-63 in the trypsin-STI (soybean trypsin inhibitor) complex. These complexes have been shown to exist as tetrahedral adducts which probably resemble normal intermediates ($ES^{\ddagger}$) in serine protease catalysis.

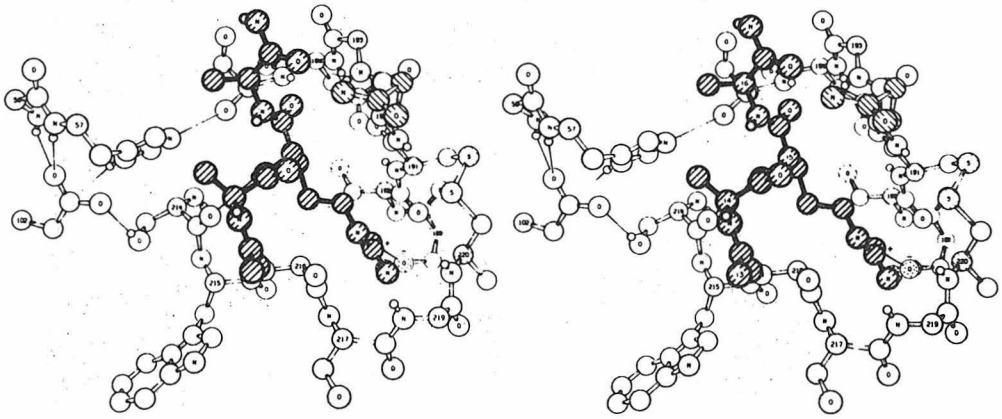

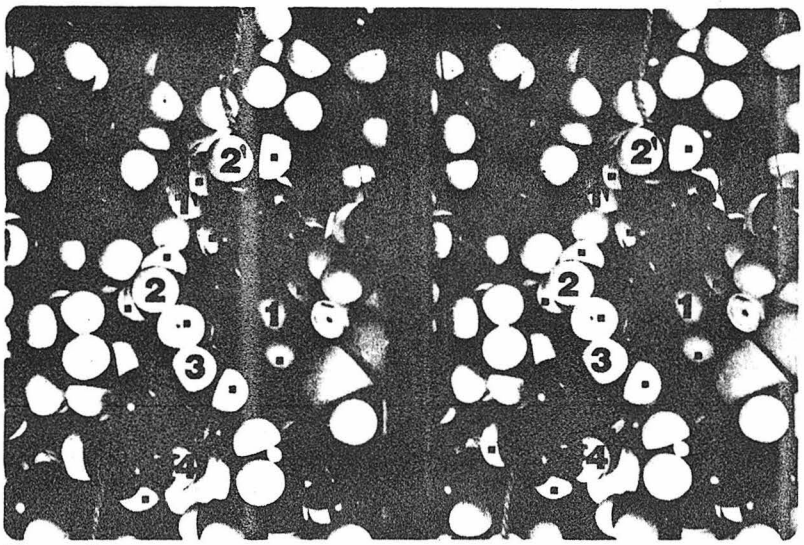

Figure 4

(*Top*) A model for the binding of a portion of the bovine pancreatic trypsin inhibitor (heavy shading) to trypsin in which the side chain of the inhibitor's Lys-15 has been replaced by an arginine side chain. The model was constructed so that the "Arg-15" side chain fitted the electron density for benazmidine in benzamidine-trypsin. This model for enzyme-substrate interaction embodies a substrate conformation that evolved to bind tightly to the enzyme and an enzyme conformation which is presumably like that induced by the binding of specific substrate side chains. (Reprinted, with permission, from Krieger, Kay and Stroud 1974.)

(*Bottom*) Stereoscopic view of a space-filling model of the trypsin-substrate complex described in the text. This view (approximately as above) should be compared with the same region of the enzyme alone shown in Figure 2. This figure beautifully demonstrates the intimate stereochemical compatibility between enzyme and substrate. The woolen threads indicate the end points of the portion of the oligopeptide substrate chain which is included in the model. Protons in the substrate are labeled with square dots, and atoms attached to the α-carbon atoms of the substrate fragment are labeled 4-3-2-1-1′-2′ (along the sequence in the substrate). The peptide bond between 1 and 1′ is the one to be hydrolyzed.

These and other crystallographic and chemical studies have produced detailed models for the association of enzyme and substrate prior to catalysis. Although based on inferences drawn from substrate analogs or inhibitor binding studies, such models do suggest ways that chemical groups on the enzyme may participate in catalysis.

The Active Center: pH-Activity Correlations

The X-ray crystal structures of the serine proteases have shown that their active sites are almost identical. The catalytic site of all serine proteases is characterized by a serine hydroxyl group (residue 195). Diisopropylfluorophosphate (DFP) (Jansen, Nutting and Balls 1949; Hartley 1960) and phenyl methane sulfonyl fluoride (PMSF) (Fahrney and Gold 1963; Kallos and Rizok 1964) react with this hydroxyl and irreversibly inhibit serine proteases, regardless of their substrate specificity. In the free enzyme, this hydroxyl is hydrogen bonded to the N-ϵ_2 of His-57. N-δ_1 of His-57 is hydrogen bonded to the carboxyl group of Asp-102, which in turn is not directly accessible to solvent (Blow, Birktoft and Hartley 1969; Wright, Alden and Kraut 1969; Alden, Wright and Kraut 1970; Birktoft and Blow 1972; Stroud, Kay and Dickerson 1974). The direct participation of these three groups in catalysis has been established, and chemical modification of any of them can greatly diminish or abolish catalysis (Jansen, Nutting and Balls 1949; Hartley 1960; Fahrney and Gold 1963; Kallos and Rizok 1964; Ong, Shaw and Schoellmann 1964; Shaw, Mares-Guia and Cohen 1965; Henderson 1971; Martinek, Savin and Berezin 1971; Chambers et al. 1974).

The pH-activity profiles for hydrolysis of peptides, amides or esters by trypsin or chymotrypsin are bell shaped and reflect maximal enzymatic activity at about pH 8. The high pH limb of the curve depends on an apparent pK_a of 8.8 for α-chymotrypsin (Fersht and Requena 1971b) or 10.1 for trypsin (Spomer and Wootton 1971). Fersht and Requena have demonstrated that this ionization, which controls enzyme conformation and substrate binding (K_m), is directly associated with titration of the α-amino terminus of Ile-16. The internal salt bridge formed between this amino group and the side chain of Asp-194 in the active enzyme is broken at high pH, where deprotonation of the amino group was shown to favor an alternate conformation for the enzyme.

The low pH limb of the profile depends on a single group of pK_a about 6.7 in both enzymes; protonation of this group adversely affects both acylation and deacylation (Bender and Kezdy 1964). It has often been assumed that this group corresponds to His-57. Jencks (1969), however, has pointed out that this group need not be His-57, but might be some other group on the enzyme either controlling conformation or effecting a change in rate-determining step near this pH. The aspartic-histidine-serine system *as a whole* has been shown to take up a single proton as the pH is lowered below 7.0. Fersht and Renard (1974) have also demonstrated that for the hydrolysis of acetyl phenylalanine-*p*-nitrophenyl ester by δ-chymotrypsin, k_{cat} or k_{cat}/K_m depends on a single ionization between pH 9.0 and pH 2.0. Thus it would seem that only one group at the active center has a pK_a in the range pH 2–9 which can be detected kinetically.

Richards and his colleagues (Hunkapiller et al. 1973) have shown by

nuclear magnetic resonance studies that the imidazole of His-57 in α-lytic protease (a bacterial homolog of the pancreatic serine proteases) does not ionize until the pH is lowered below 4.0. Their research led them to propose that the group of pK_a 7.0 was Asp-102.

In order to study the ionization of Asp-102 in trypsin (Koeppe and Stroud, unpubl.), we monitored infrared absorbance arising from the carboxyl C=O stretch at 1570 cm^{-1} and 1710 cm^{-1} (Timasheff and Rupley 1972) as a function of pH. To diminish the number of titratable carboxyls, accessible carboxyl groups in trypsin were modified with semicarbazide (Fersht and Sperling 1973). The modified enzyme was found to contain 2.5 molar equivalents of free carboxyl groups. These were identified as Asp-102, Asp-194 (1.0 molar equivalent each) and the α-carboxyl terminus of Asn-245 (0.5 equivalent).

The spectrum shown in Figure 5 indicates differential absorbance at 1600 cm^{-1} and at 1680 cm^{-1} between semicarbazide-trypsin solutions of pD 6.50 and 7.13. Each peak is shifted toward the other by about 30 cm^{-1} from the value found for other carboxyls—a result which is to be expected for hydrogen-bonded carboxyls (Susi 1972) such as Asp-102. The titration curve of semicarbazide-trypsin compiled from a series of infrared difference spectra is shown in Figure 6. Based on the number of free carboxyl groups, we assume that the low pH titration of average pK_a 2.9 corresponds to titration of 1.5 carboxyl groups, while the titration of average pK_a 6.8 corresponds to one carboxyl. The gradient of the low pH titration is approximately 1.5 times that of the upper one, which is consistent with the assumption. Both titrations, however, appear sharper than expected for single or noninteracting groups.

Binding of Cu^{++} ions displaces the upper limb of the titration downward from pH 6.8. Martinek et al. (1969, 1971) have shown that Ag^{+} ions are powerful competitive inhibitors of trypsin, and that Cu^{++} and Ag^{+} compete with each other in inhibiting chymotrypsin. Either species competes with pro-

Figure 5
Infrared difference spectrum for semicarbazide-trypsin. The path length was 0.150 mm. The sample cell was at pD 7.13, and the reference cell at pD 6.50. pD values in all cases correspond to uncorrected pH meter readings. Concentrations were 1.5 mM enzyme, 6 mM $NaNO_3$, and 12 mM benzamidine. The peak positions at 1680 cm^{-1} for C=O in COOD and at 1600 cm^{-1} for C—O in COO^{-} are closer together than for other trypsin carboxyls due to the effect of hydrogen bonding. The detected difference in species concentration judged from peak heights corresponds to about 0.4 carboxyl equivalent.

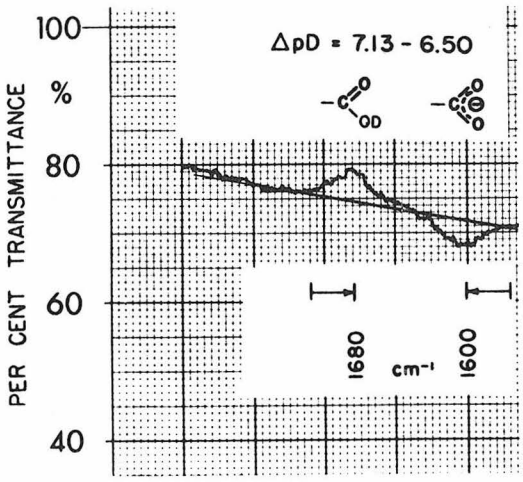

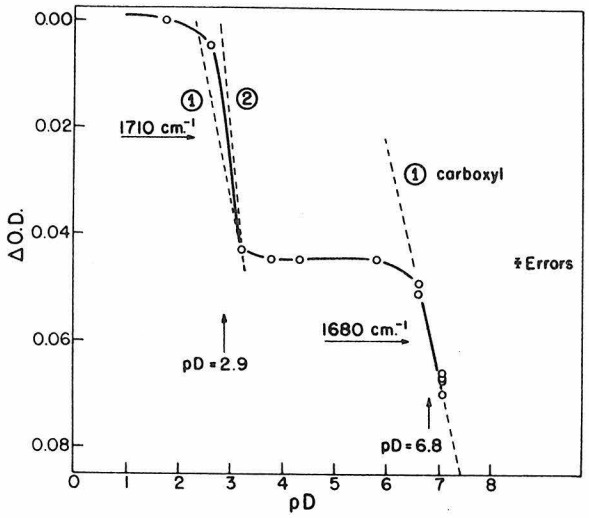

Figure 6
Titration curve for free carboxyls in semicarbazide-trypsin obtained by plotting differential absorbance at 1710 cm^{-1} and 1680 cm^{-1} from a series of infrared difference spectra. Reference solutions were at pD 3.2, 3.8, 4.4 and 6.6. The gradient of the titration at low pD was 1.5–2.0 times greater than the gradient for the group of pKa 6.8 and corresponds to titration of about 1.5 carboxyls.

tons for a site on the enzyme with $pK_{app} \simeq 7.0$. Since we have shown that Ag^+ binds specifically between Asp-102 and His-57 in the orthorhombic crystal form of DIP-trypsin (Chambers et al. 1974 and Fig. 7), in trypsinogen and in trigonal DIP-trypsin (Kossiakoff, Kay and Stroud, unpubl.), the pK_a of 6.8 has tentatively been assigned to the carboxyl of Asp-102. (A detailed description of the experimental procedures and results will be published elsewhere.) Copper ion binding shows that Asp-194 and Asn-245 cannot be responsible for this pK_a. These data suggest that the average apparent pK_a of Asp-194 and Asn-245 is 2.9.

Control experiments eliminate the possibility that imidazole-stretching frequencies could account for the infrared bands at 1680 cm^{-1} and 1600 cm^{-1} in Figure 5. However, imidazole titration may perturb a neighboring carbonyl and thereby conceivably be responsible for the infrared difference peaks observed around pD 6.8. This possibility is the subject of continuing investigations in our laboratory.

There are two arguments against this possibility and in support of the assignment of a pK_a of about 7.0 to Asp-102. First, using an average extinction coefficient for the other seven carboxyl groups in β-trypsin, derived from infrared difference spectra of the unmodified enzyme, the low pH limb of the titration shown in Figure 6 corresponds to 1.5 carboxyl equivalents. This implies that the remaining carboxyl group must titrate outside of the range pH 2–pH 5. Second, in the presence of Cu^{++} ions, there is no differential

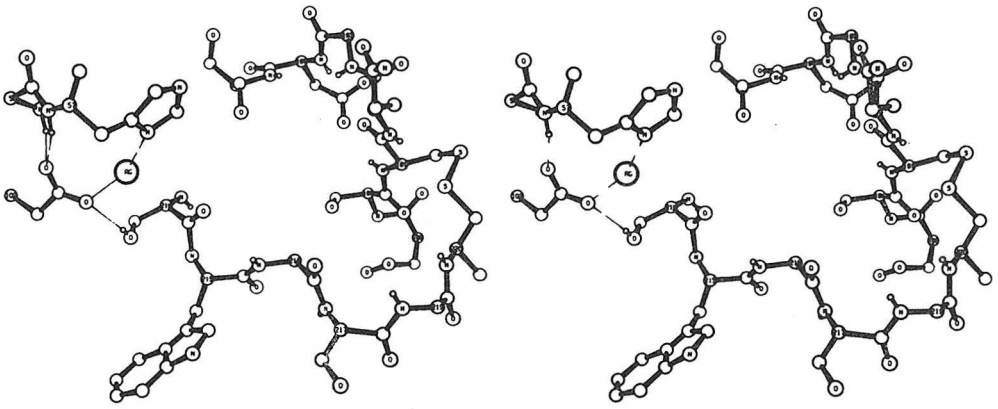

Figure 7
A stereo ORTEP drawing of the catalytic site of silver DIP-trypsin, shown in the same orientation as Figure 1. The DIP group has been omitted for clarity. The γ-oxygen of Ser-195 is in the position found for DIP-trypsin, close to that found in tetrahedral intermediates or in acyl enzymes (see text). (Reprinted, with permission, from Chambers et al. 1974.)

absorbance in the region of pH 7.0, which suggests that either of the two imidazoles at His-40 or His-91 which may titrate around pH 7.0 do not induce changes in their neighboring carbonyl groups which would be detected by the technique.

The Mechanism of Hydrolysis by Serine Proteases

Following their determination of the active-site structure of chymotrypsin, Blow, Birktoft and Hartley (1969) first proposed that proton transfers between His-57 and Asp-102 were important in catalysis. The studies of the microscopic pK_a's of His-57 and Asp-102 referred to in the previous section are consistent with this proposal. From their studies of the histidine ionization in α-lytic protease, Hunkapiller et al. (1973) explained the sequence of proton transfers between Asp-102 and His-57, discussed here and included in Figure 9 (below), in terms of pK_a's.

In this discussion we assume (see previous section) that the pK_a of Asp-102 is 6.8, and that the imidazole of His-57 is essentially neutral above pH 4.0. This leads to the ionization of the active center around pH 7.0 (Fig. 8). The mechanistic importance of these assignments is that the aspartate ion of residue 102 can act as a chemical base which can readily accept a proton from the histidine side chain during catalysis (Hunkapiller et al. 1973). Together, Asp-102 and His-57 shuttle protons back and forth from enzyme to substrate, and so the mechanism can best be described as nucleophilic attack with general base catalysis by His-57 (Bender and Kezdy 1964; Inward and Jencks 1965) and Asp-102. The important differences between this reaction and a non-enzymatic hydrolysis are the binding to the enzyme and the efficient proton shuttle.

Interfering with this shuttle inhibits catalysis. For example, by methylating the N-ϵ_2 of His-57 in chymotrypsin, the shuttle can no longer operate normally

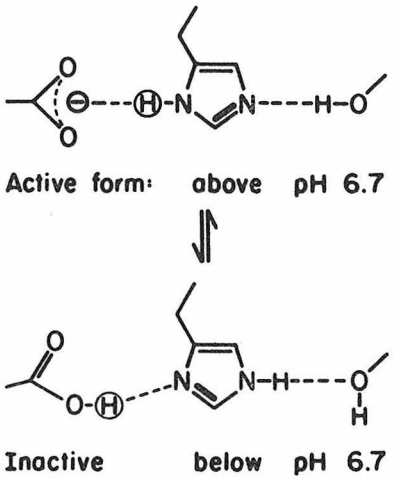

Figure 8
Ionization of the active center in the range pH 4.0–8.0 as discussed in the text.

and the rate of catalysis drops by a factor of 5000 to 200,000 for specific substrates (Henderson 1971). Silver ions bind specifically to trypsin between Asp-102 and His-57 (Chambers et al. 1974). By adding silver, the shuttle is blocked and catalysis is inhibited (Martinek, Savin and Berezin 1971).

The mechanistic scheme shown in Figure 9 is consistent with most experimental data relating to hydrolysis of peptides, esters or amides by trypsin or chymotrypsin. In the first step (I), substrate and enzyme form a Michaelis complex. Nucleophilic attack by the hydroxyl group of Ser-195 follows. As the reaction proceeds, the hydroxyl twists around the C_α—C_β bond and forms a covalent chemical bond to the substrate carbon at step I–II (Steitz, Henderson and Blow 1969). Concerted with this, a proton is transferred from the serine hydroxyl group to the N-ϵ_2 of His-57. From there, it is eventually delivered to the nitrogen of the peptide bond in the substrate. As a result of this proton transfer, the proton previously bound to the N-δ_1 of His-57 is transferred to the carboxyl group of Asp-102, which acts as a base in this reaction (Hunkapiller et al. 1973). Although these proton transfers are rapid, deuterium isotope effects show that proton transfer is involved in the rate-determining step of the catalysis (Bender et al. 1964; Pollock, Hogg and Schowen 1973).

Whether the Asp-His-Ser proton shuttle is concerted or stepwise remains in question. If the mechanism is concerted, the negative charge of Asp-102 would be neutralized while negative charge develops on the carbonyl oxygen of the substrate. The imidazole would remain neutral throughout the reaction; thus unstable intermediates due to charge separation would be avoided (Jencks 1971; Hunkapiller et al. 1973). In fact, charge development in the transition state in chymotrypsin catalysis does appear to be small (Jencks 1971). The shuttle may be stepwise if the energy requirements of charge separation (negative charges on the substrate and Asp-102 and a positive charge on His-57) are offset by a more favorable entropy of activation in a two-step process (Jencks 1972).

One might favor the concerted mechanism because it might be expected that the precise alignment of the shuttle, which has been observed in all serine protease structures, evolved so that the entropic advantage of the

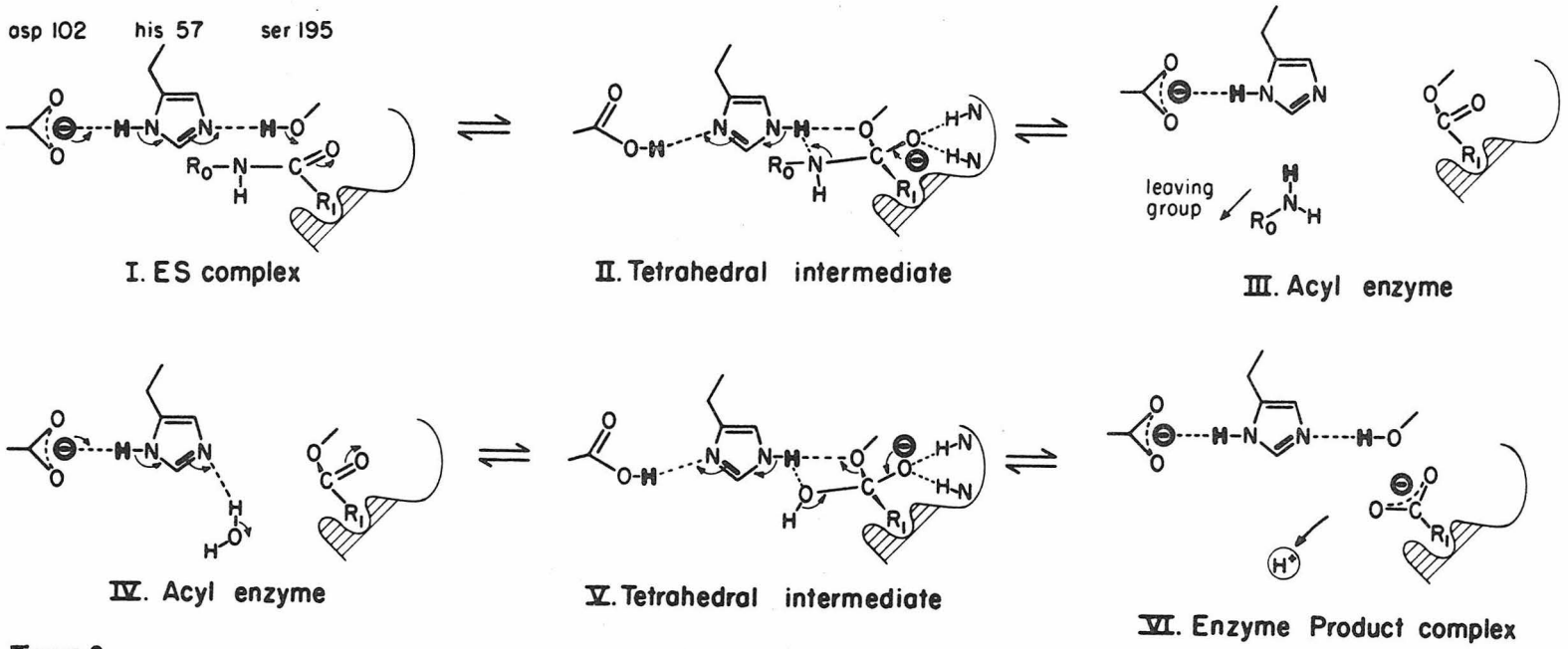

Figure 9
A mechanism for serine protease hydrolysis of peptides or amides. In this representation, the proton shuttle is concerted.

two-step process over the concerted process was minimized. Thus the enzyme could exploit for increased reaction rate the energy saved in eliminating charge separation. If this were not the case, it would seem unnecessary to use both an Asp and an His for the general base catalysis. The Asp could be eliminated and the His could act as the base.

After the attack by the serine on the substrate, a short-lived tetrahedral intermediate is formed (II). This intermediate is stabilized by the covalent bond to the enzyme and by a number of hydrogen bonds. The following structural features of the tetrahedral intermediate are primarily based on the crystallographic determination of many different protease-inhibitor structures.

The negatively charged substrate oxygen in the tetrahedral intermediate is stabilized by hydrogen bonds from the amide nitrogens of residues 195 and 193. The importance of the amides of Ser-195 and Gly-193 was first noted by Steitz, Henderson and Blow (1969), and their role in transition-state stabilization was postulated by Henderson (1970) and by Robertus et al. (1972). Another hydrogen bond forms between the carbonyl group of Ser-214 and the α-N of the substrate (Steitz, Henderson and Blow 1969; Segal et al. 1971). Comparison of the kinetics of hydrolysis of specific trypsin and chymotrypsin substrates with and without the hydrogen bonding capacity of the α-N suggests that the Ser-214—α-N bond may not form in the Michaelis complex (Ingles and Knowles 1968; Caplow and Harper 1972; Kobayashi and Ishi 1974). These results show, however, that this hydrogen bond does play a role in the transition states between intermediates and possibly in the tetrahedral and acyl enzyme intermediates.

One explanation for the exceptional catalytic powers of enzymes is that enzymes have evolved so that they can optimally bind the transition-state structures in the reactions they catalyze rather than the substrates themselves (Pauling 1946; Wolfenden 1972). The hydrogen-bonded structure in the serine protease-substrate transition state may be an example of transition-state stabilization, for the oriented hydrogen bonds can help to speed up the reaction by smoothing down the highest energy barriers between intermediate states. The stability of the tetrahedral adduct in the trypsin-trypsin inhibitor complexes is consistent with the transition-state stabilization hypothesis.

At step II–III, the now unstable carbon-nitrogen bond is broken, and the first product of hydrolysis, an amine, is free to diffuse away, taking with it a proton from the enzyme. At the same time, the bound part of the substrate rearranges to a covalently modified acyl enzyme intermediate (III). At pH 8, N^{14}/N^{15} kinetic isotope effects (O'Leary and Kluetz 1972) show that the C—N bond rupture is partially rate-determining for the hydrolysis of acetyl tryptophanamide by chymotrypsin. The rate-determining step for amide hydrolysis, however, may vary from the formation of the tetrahedral intermediate to its breakdown, depending upon the pH and the structure of the substrates (Fastrez and Fersht 1973a).

The breakdown of the acyl intermediate (IV–VI) is the microscopic reverse of steps I–III; this time water is the attacking group. At step V–VI, the second product is formed. It is an acid which loses a proton to the solution and becomes negatively charged. For the first time (if the proton shuttle is concerted), there are two charges in the system. These two negative charges repel each other and so help to dissociate the second product from the enzyme (Johnson and Knowles 1966), regenerating free enzyme.

The presence of a carboxyl group of high pK_a and a neutral side chain of His-57 with a low pK_a would suggest two compelling evolutionary reasons why the Asp-His-Ser arrangement should be universal to serine proteases (Hunkapiller et al. 1973). First, by neutralizing a negative charge on Asp-102, rather than generating a positive charge on His-57, during formation of the tetrahedral intermediate, there would be no unfavorable charge separation. This would contribute to reducing transition-state internal energies, and thus to rate enhancement (Jencks 1971). Second, if the charged Asp-102 is to be a proton acceptor at physiological pH values, its pK_a must be raised and it must have access to the proton donor. The imidazole of His-57 is ideally suited both to insulate Asp-102 from solvent (so raising the pK_a of the buried carboxyl group) and to serve as a proton conductor, transferring charge from the carboxyl group to the substrate. It is also important to note that both the reverse separation of the pK_a values of Asp-102 and His-57 and the structure of trypsin at pH 7 and pH 8 (Stroud, Kay and Dickerson 1974; Krieger, Kay and Stroud 1974; Huber et al. 1974; Sweet et al. 1974), which shows a symmetric interaction between the charge on Asp-102 and His-57 (see Fig. 3), are unlike the situation expected in aqueous solution and reflect a unique microenvironment for these groups.

As far as we know, all the serine proteases use the same three chemical groups to hydrolyze peptide bonds. They, like trypsin, are active catalysts only when the aspartic acid is negatively charged. Against the active site, the reaction goes on in an unique way as the enzyme smoothes the transition from one intermediate state to another. This emphasizes the importance of exact stereochemical fit and correct orientation (Koshland 1958) of the substrate as the reaction takes place, rather than simply the generation of an especially reactive site. After all, a very reactive site could react in many less specific ways. It is better to have a moderately efficient catalytic site coupled with a very selective binding requirement (Fersht and Sperling 1973). With this in mind, the subtle differences between serine proteases involved in biological control can be understood in terms of differences in their specific substrate binding properties.

Acknowledgments

This is contribution number 4990 from the Norman W. Church Laboratory of Chemical Biology. We would like to acknowledge our indebtedness to the National Institutes of Health for their support by means of grants GM-19984 and GM-70469. R.M.S. is the recipient of an NIH Career Development Award, M.K. is the recipient of a Danforth Foundation Fellowship, R.K. and J.C. are recipients of NIH Predoctoral Traineeships, and A.K. is the recipient of an NIH Postdoctoral Fellowship.

REFERENCES

Alden, R. A., C. S. Wright and J. Kraut. 1970. A hydrogen-bond network at the active site of subtilisin BPN'. *Phil. Trans. Roy. Soc. London* B **257**:119.

Bender, M. L. and F. J. Kezdy. 1964. The current state of the α-chymotrypsin mechanism. *J. Amer. Chem. Soc.* **86**:3704.

Bender, M. L., G. E. Clement, F. J. Kezdy and H. D'A. Heck. 1964. The correlation of the pH (pD) dependence of the stepwise mechanism of α-chymotrypsin-catalyzed reactions. *J. Amer. Chem. Soc.* **86:**3680.

Birktoft, J. J. and D. M. Blow. 1972. Structure of crystalline α-chymotrypsin. V. The atomic structure of tosyl-α-chymotrypsin at 2 Å resolution. *J. Mol. Biol.* **68:**187.

Blow, D. M., J. J. Birktoft and B. S. Hartley. 1969. Role of a buried acid group in the mechanism of action of chymotrypsin. *Nature* **221:**337.

Blow, D. M., J. Janin and R. M. Sweet. 1974. Mode of action of soybean trypsin inhibitor (Kunitz) as a model for specific protein-protein interactions. *Nature* **249:**54.

Blow, D. M., C. S. Wright, D. Kukla, A. Ruhlmann, W. Steigemann and R. Huber. 1972. A model for the association of bovine pancreatic trypsin inhibitor with chymotrypsin and trypsin. *J. Mol. Biol.* **69:**137.

Brown, J. R., D. L. Kauffman and B. S. Hartley. 1967. The primary structure of porcine pancreatic elastase: The N-terminus and disulphide bridges. *Biochem. J.* **103:**497.

Caplow, M. 1969. Chymotrypsin catalysis. Evidence for a new intermediate. *J. Amer. Chem. Soc.* **91:**3639.

Caplow, M. and C. Harper. 1972. Discrete effects of the acylamino proton in a chymotrypsin substrate on different processes in catalysis. *J. Amer. Chem. Soc.* **94:**6508.

Chambers, J. L., G. G. Christoph, M. Krieger, L. Kay and R. M. Stroud. 1974. Silver ion inhibition of serine proteases: Crystallographic study of silver trypsin. *Biochem. Biophys. Res. Comm.* **59:**70.

Chauvet, J. and R. Acher. 1967. The reactive site of the basic trypsin inhibitor of pancreas. *J. Biol. Chem.* **242:**4274.

Davie, E. W. and H. Neurath. 1955. Identification of a peptide released during autocatalytic activation of trypsinogen. *J. Biol. Chem.* **212:**515.

East, E. J. and C. G. Trowbridge. 1968. Binding of benzamidine and protons to trypsin as measured by difference spectra. *Arch. Biochem. Biophys.* **125:**334.

Fahrney, D. E. and A. M. Gold. 1963. Sulfonyl fluorides as inhibitors of esterases. *J. Amer. Chem. Soc.* **85:**997.

Fastrez, J. and A. R. Fersht. 1973a. Mechanism of chymotrypsin. Structure, reactivity, and nonproductive binding relationships. *Biochemistry* **12:**1067.

———. 1973b. Demonstration of the acyl-enzyme mechanism for the hydrolysis of peptides and anilides by chymotrypsin. *Biochemistry* **12:**2025.

Fersht, A. R. and M. Renard. 1974. pH dependence of chymotrypsin catalysis. *Biochemistry* **13:**1416.

Fersht, A. R. and Y. Requena. 1971a. Mechanism of the α-chymotrypsin hydrolysis of amides. pH dependence of k_c and K_m. Kinetic detection of an intermediate. *J. Amer. Chem. Soc.* **93:**7079.

———. 1971b. Equilibrium and rate constants for the interconversion of two conformations of α-chymotrypsin. *J. Mol. Biol.* **60:**279.

Fersht, A. R. and J. Sperling. 1973. The charge relay system in chymotrypsin and chymotrypsinogen. *J. Mol. Biol.* **74:**137.

Fersht, A. R., D. M. Blow and J. Fastrez. 1973. Leaving group specificity in the chymotrypsin catalyzed hydrolysis of peptides. A stereochemical interpretation. *Biochemistry* **12:**2035.

Freer, S. T., J. Kraut, J. D. Robertus, H. T. Wright and Ng.- H. Xuong. 1970. Chymotrypsinogen: 2.5 Å crystal structure, comparison with α-chymotrypsin, and implications for zymogen activation. *Biochemistry* **9:**1997.

Fritz, H., H. Schult, R. Meister and E. Werlo. 1969. Herstellung und eigenschaften

von derivaten des Trypsin-Kallikrein-Inhibitors aus Rinderorganen. *Z. Physiol. Chem.* **350:**1531.

Gertler, A., K. A. Walsh and H. Neurath. 1974. Catalysis by chymotrypsinogen. Demonstration of an acyl-zymogen intermediate. *Biochemistry* **13:**1302.

Hartley, B. S. 1960. Proteolytic enzymes. *Annu. Rev. Biochem.* **29:**45.

———. 1964. Amino acid sequence of bovine chymotrypsinogen A. *Nature* **201:**1284.

Henderson, R. 1970. Structure of crystalline α-chymotrypsin. IV. Structure of indoleacryloyl-α-chymotrypsin and its relevance to the hydrolytic mechanism of the enzyme. *J. Mol. Biol.* **54:**341.

———. 1971. Catalytic activity of α-chymotrypsin in which histidine-57 has been methylated. *Biochem. J.* **124:**13.

Hess, G. P., J. McConn, E. Ku and G. McConkey. 1970. Studies of the activity of chymotrypsin. *Phil. Trans. Roy. Soc. London* B **257:**89.

Huber, R., D. Kukla, A. Ruhlmann and W. Steigemann. 1971. Pancreatic trypsin inhibitor: Structure and function. *Cold Spring Harbor Symp. Quant. Biol.* **36:**141.

Huber, R., D. Kukla, A. Ruhlmann, O. Epp and H. Formanek. 1970. The basic trypsin inhibitor of bovine pancreas. I. Structure analysis and conformation of the polypeptide chain. *Naturwissenschaften* **57:**389.

Huber, R., D. Kukla, W. Steigemann, J. Deisenhofer and A. Jones. 1974. Structure of the complex formed by bovine trypsin and bovine pancreatic trypsin inhibitor. In *Bayer Symposium V: Proteinase Inhibitors* (ed. H. Fritz et al.), p. 497. Springer Verlag, Heidelberg.

Hunkapiller, M. W., S. H. Smallcombe, D. R. Whitaker and J. H. Richards. 1973. Carbon nuclear magnetic resonance studies of the histidine residue in α-lytic protease. *Biochemistry* **12:**4732.

Inagami, T. and T. Murachi. 1964. The mechanism of the specificity of trypsin catalysis. *J. Biol. Chem.* **239:**1395.

Inagami, T. and S. S. York. 1968. The effect of alkylguanidines and alkylamines on trypsin catalysis. *Biochemistry* **7:**4045.

Ingles, D. W. and J. R. Knowles. 1968. The stereospecificity of α-chymotrypsin. *Biochem. J.* **108:**561.

Inward, P. W. and W. P. Jencks. 1965. The reactivity of nucleophilic reagents with furoyl-chymotrypsin. *J. Biol. Chem.* **240:**1986.

Jacob, F. and J. Monod. 1961. Genetic regulatory mechanisms in the synthesis of proteins. *J. Mol. Biol.* **3:**318.

Jansen, E. F., M. D. F. Nutting and A. K. Balls. 1949. Mode of inhibition of chymotrypsin by diisopropylfluorophosphate. I. Introduction of phosphorous. *J. Biol. Chem.* **179:**201.

Jencks, W. P. 1969. *Catalysis in Chemistry and Enzymology,* p. 218. McGraw-Hill, New York.

———. 1971. Reactivity correlations and general acid-base catalysis in enzymic transacylation reactions. *Cold Spring Harbor Symp. Quant. Biol.* **36:**1.

———. 1972. General acid-base catalysis of complex reactions in water. *Chem. Rev.* **72:**705.

Johnson, C. H. and J. R. Knowles. 1966. The binding of inhibitors to α-chymotrypsin. *Biochem. J.* **101:**56.

Kallos, J. and D. Rizok. 1964. Heavy atom labeling of the serine of the active center of chymotrypsin: Pipsyl-chymotrypsin. *J. Mol. Biol.* **9:**255.

Kassell, B. and J. Kay. 1973. Zymogens of proteolytic enzymes. *Science* **180:**1022.

Kobayashi, R. and S. Ishi. 1974. The trypsin-catalyzed hydrolysis of some L-α-amino-lacking substrates. *J. Biochem.* **75:**825.

Koshland, D. E., Jr. 1958. Application of a theory of enzyme specificity to protein synthesis. *Proc. Nat. Acad. Sci.* **44**:98.

Kress, L. F. and M. Laskowski. 1967. The basic trypsin inhibitor of bovine pancreas. *J. Biol. Chem.* **242**:4925.

Krieger, M., L. M. Kay and R. M. Stroud. 1974. Structure and specific binding of trypsin: Comparison of inhibited derivatives and a model for substrate binding. *J. Mol. Biol.* **83**:209.

Kunitz, M. and J. H. Northrop. 1935. Crystalline chymo-trypsin and chymotrypsinogen. I. Isolation, crystallization, and general properties of a new proteolytic enzyme and its precursor. *J. Gen. Physiol.* **18**:433.

———. 1936. Isolation from beef pancreas of cystalline trypsinogen, trypsin, a trypsin inhibitor, and an inhibitor-trypsin compound. *J. Gen. Physiol.* **19**:991.

Leighton, T. J., R. H. Doi, R. A. J. Warren and R. A. Kelln. 1973. The relationship of serine protease activity to RNA polymerase modifications and sporulation in *Bacillus subtilis*. *J. Mol. Biol.* **76**:103.

Magnusson, S. 1971. Thrombin and prothrombin. In *The Enzymes* (ed. P. D. Boyer), vol. 3, p. 277. Academic Press, New York.

Mares-Guia, M. and E. Shaw. 1965. Studies on the active center of trypsin: The binding of amidines and guanidines as models of the substrate chain. *J. Biol. Chem.* **240**:1579.

Maroux, S., J. Baratti and P. Desnuelle. 1971. Purification and specificity of porcine enterokinase. *J. Biol. Chem.* **246**:5031.

Martinek, K., Y. V. Savin and I. V. Berezin. 1971. Kinetic manifestations of trypsin's active center during inhibition of its enzymatic activity by Ag^+ ions. *Biokhimiya* **36**:806.

Martinek, K., Kh. Vill', Z. A. Strel'tsova and I. V. Berezin. 1969. Kinetic manifestations of the active-center structure of α-chymotrypsin during inhibition of enzyme activity by Ag^+ ions. *Mol. Biol.* (U.S.S.R.) **3**:554.

Matthews, B. W., P. B. Sigler, R. Henderson and D. M. Blow. 1967. Three-dimensional structure of tosyl-α-chymotrypsin. *Nature* **214**:652.

Naughton, M. A. and F. Sanger. 1961. Purification and specificity of pancreatic elastase. *Biochem. J.* **78**:156.

Neurath, H. and G. H. Dixon. 1957. Structure and activation of trypsinogen and chymotrypsinogen. *Fed. Proc.* **16**:791.

Neurath, H., J. A. Rupley and W. J. Dreyer. 1956. Structural changes in the activation of chymotrypsinogen and trypsinogen. Effects of urea on chymotrypsinogen and delta-chymotrypsinogen. *Arch. Biochem. Biophys.* **65**:243.

Northrop, J. H., M. Kunitz and R. M. Herriot. 1948. *Crystalline Enzymes*, p. 96. Columbia University Press, New York.

O'Leary, M. H. and M. D. Kluetz. 1972. Nitrogen isotope effects on the chymotrypsin catalyzed hydrolysis of *N*-acetyl-L-tryptophanamide. *J. Amer. Chem. Soc.* **94**:3585.

Ong, E. B., E. Shaw and G. Schoellmann. 1964. An active center histidine peptide of α-chymotrypsin. *J. Amer. Chem. Soc.* **86**:1271.

Oppenheimer, H. L., B. Labouesse and G. P. Hess. 1966. Implication of an ionizing group in the control of conformation and activity of chymotrypsin. *J. Biol. Chem.* **241**:2720.

Owren, P. A. and H. Stormorken. 1973. The mechanism of blood coagulation. *Ergeb. Physiol. Biol. Chem. Exp. Pharmacol.* **68**:1.

Pauling, L. 1946. Molecular architecture and biological reactions. *Chem. Eng. News* **24**:1375.

Pollack, E., J. L. Hogg and R. L. Schowen. 1973. One-proton catalysis in the deacetylation of acetyl-α-chymotrypsin. *J. Amer. Chem. Soc.* **95**:968.

Robertus, J. D., J. Kraut, R. A. Alden and J. J. Birktoft. 1972. Subtilisin; a stereochemical mechanism involving transition-state stabilization. *Biochemistry* **11**:4293.

Ruhlmann, A., D. Kukla, P. Schwager, K. Bartels and R. Huber. 1973. Structure of the complex formed by bovine trypsin and bovine pancreatic trypsin inhibitor. *J. Mol. Biol.* **77**:417.

Sampath Narayanan, A. and R. A. Anwar. 1969. The specificity of purified porcine pancreatic elastase. *Biochem. J.* **114**:11.

Segal, D. M., J. C. Powers, G. H. Cohen, D. R. Davies and P. E. Wilcox, 1971. Substrate binding site in bovine chymotrypsin Aγ. A crystallographic study using peptide chloromethyl ketones as site-specific inhibitors. *Biochemistry* **10**:3728.

Shaw, E., M. Mares-Guia and W. Cohen. 1965. Evidence for an active-center histidine in trypsin through use of a specific reagent, 1-chloro-3-tosylamido-7-amino-2-heptanone, the chloromethyl ketone derived from N_a-tosyl-L-lysine. *Biochemistry* **4**:2219.

Shotton, D. M. and B. S. Hartley. 1970. Amino-acid sequence of porcine pancreatic elastase and its homologies with other serine proteases. *Nature* **225**:802.

Shotton, D. M. and H. C. Watson. 1970. The three-dimensional structure of crystalline porcine pancreatic elastase. *Phil. Trans. Roy. Soc. London* B **257**:111.

Sigler, P. W., D. M. Blow, B. W. Matthews and R. Henderson. 1968. Structure of crystalline α-chymotrypsin. II. A preliminary report including a hypothesis for the activation mechanism. *J. Mol. Biol.* **35**:143.

Spomer, W. E. and J. F. Wootton. 1971. The hydrolysis of a α-*N*-benzoyl-L-arginina-mide catalyzed by trypsin and acetyl trypsin. Dependence on pH. *Biochim. Biophys. Acta* **235**:164.

Stambaugh, R., B. Brackett and L. Mastroianni. 1969. Inhibition of *in vitro* fertilization of rabbit ova by trypsin inhibitors. *Biol. Reprod.* **1**:223.

Steitz, T. A., R. Henderson and D. M. Blow. 1969. Structure of crystalline α-chymotrypsin. III. Crystallographic studies of substrates and inhibitors. *J. Mol. Biol.* **46**:337.

Stroud, R. M. 1974. A family of protein-cutting proteins. *Sci. Amer.* **231**:74.

Stroud, R. M., L. M. Kay and R. E. Dickerson. 1971. The crystal and molecular structure of DIP-inhibited bovine trypsin at 2.7 Å resolution. *Cold Spring Harbor Symp. Quant. Biol.* **36**:125.

———. 1974. The structure of bovine trypsin: Electron density maps of the inhibited enzyme at 5 Å and 2.7 Å resolution. *J. Mol. Biol.* **83**:185.

Susi, H. 1972. The strength of hydrogen bonding: Infrared spectroscopy. In *Methods in Enzymology* (ed. S. P. Colowick and N. O. Kaplan), vol. 26, p. 381. Academic Press, New York.

Sweet, R. M., H. T. Wright, J. Janin, C. H. Chothia and D. M. Blow. 1974. Crystal structure of the complex of porcine trypsin with soybean trypsin inhibitor (Kunitz) at 2.6 Å resolution. *Biochemistry* **13**:4212.

Timasheff, S. N. and J. A. Rupley. 1972. Infrared titration of lysozyme carboxyls. *Arch. Biochem. Biophys.* **150**:318.

Tomkins, G. M., T. D. Gelehrter, D. Granner, D. Martin, Jr., H. H. Samuels and E. B. Thompson. 1969. Control of specific gene expression in higher organisms. *Science* **166**:1474.

Tschesche, H. 1974. Biochemistry of natural proteinase inhibitors. *Angew. Chem. Int. Ed. Eng.* **13**:10.

Wolfenden, R. 1972. Analog approaches to the structure of the transition state in enzyme reactions. *Acc't. Chem. Res.* **5**:10.

Wright, C. S., R. A. Alden and J. Kraut. 1969. Structure of subtilisin BPN′ at 2.5 Å resolution. *Nature* **221:**235.

Wright, H. T. 1973. Comparison of the crystal structures of chymotrypsinogen-A and α-chymotrypsin. *J. Mol. Biol.* **79:**1.

Zerner, B. and M. L. Bender. 1964. The kinetic consequences of the acyl-enzyme mechanism for the reactions of specific substrates with chymotrypsin. *J. Amer. Chem. Soc.* **86:**3669.

Zerner, B., R. P. M. Bond and M. L. Bender. 1964. Kinetic evidence for the formation of acyl-enzyme intermediates in the α-chymotrypsin-catalyzed hydrolysis of specific substrates. *J. Amer. Chem. Soc.* **86:**3674.

Appendix 4

Structure of Bovine Trypsinogen at 1.9 Å Resolution

[Reprinted from Biochemistry, (1977) 16, 654.]

Structure of Bovine Trypsinogen at 1.9 Å Resolution†

Anthony A. Kossiakoff,‡ John L. Chambers,§ Lois M. Kay, and Robert M. Stroud*,¶

ABSTRACT: The three-dimensional crystal structure of bovine trypsinogen at ~pH 7.5 was initially solved at 2.6 Å resolution using the multiple isomorphous replacement method. Preliminary refinement cycles of the atomic coordinates for trypsinogen have been carried out first to a resolution of 2.1 Å, and later to 1.9 Å, using constrained difference Fourier refinement. During the process, structure factors F_c and φ_c were calculated from the trypsinogen structure and final interpretation was based on an electron-density map computed with terms $(2|F_o| - |F_c|)$ and phases φ_c at a resolution of 1.9 Å. Crystals of trypsinogen grown from ethanol-water mixtures are trigonal, with space group $P3_121$, and cell dimensions a = 55.17 Å and c = 109.25 Å. The structure is compared with the bovine diisopropylphosphoryltrypsin structure at ~pH 7.2, originally determined from orthohombic crystals by Stroud et al. (Stroud, R. M., Kay, L. M., and Dickerson, R. E. (1971), *Cold Spring Harbor Symp. Quant. Biol. 36,* 125-140; Stroud, R. M., Kay, L. M., and Dickerson, R. E. (1974), *J. Mol. Biol. 83,* 185-208), and later refined at 1.5 Å resolution by Chambers and Stroud (Chambers, J. L., and Stroud, R. M. (1976), *Acta Crystallogr.* (in press)). At lower pH, 4.0-5.5, diisopropylphosphoryltrypsin forms crystals which are isomorphous with trypsinogen, with cell dimensions a = 55.05 Å and c = 109.45 Å. This finding was used in the solution of the six trypsinogen heavy-atom derivatives prior to isomorphous phase analysis, and as a further basis of comparison between trypsinogen and the low pH trypsin structure. There are small differences between the two diisopropylphosphoryltrypsin structures. Bovine trypsinogen has a large and accessible cavity at the site where the native enzyme binds specific side chains of a substrate. The conformation and stability of the binding site differ from that found in trypsin at ~pH 7.5, and from that in the low pH form of diisopropylphosphoryltrypsin. The catalytic site containing Asp-102, His-57, and Ser-195 is similar to that found in trypsin and contains a similar hydrogen-bonded network. The carboxyl group of Asp-194, which is salt bridged to the amino terminal of Ile-16 in native trypsin or other serine proteases, is apparently hydrogen bonded to internal solvent molecules in a loosely organized part of the zymogen structure. The unusually charged N-terminal hexapeptide of trypsinogen, whose removal leads to activation of the zymogen, lies on the outside surface of the molecule. There are significant structural changes which accompany activation in neighboring regions, which include residues 142-152, 215-220, 188A-195. The NH group of Gly-193, normally involved in stabilization of reaction intermediates (Steitz, T. A., Henderson, R., and Blow, D. M. (1969), *J. Mol. Biol. 46,* 337-348; Henderson, R. (1970), *J. Mol. Biol. 54,* 341-354; Robertus, J. D., Kraut, J., Alden, R. A., and Birkoft, J. J. (1972), *Biochemistry 11,* 4293-4303) in the enzyme, is moved 1.9 Å away from its position in trypsin. Alterations in the binding site for substrate side chains are prime candidates for explaining the relative inactivity of trypsinogen.

Tryptic activation of the family of pancreatic proenzymes or zymogens, which include trypsinogen, chymotrypsinogen, procarboxypeptidase, and proelastase, takes place in the duodenum by limited proteolysis (Davie and Neurath, 1955; Neurath, 1975). The primary activating cleavage for the serine proteases is hydrolysis of the bond between a basic residue 15,[1] and isoleucine (valine in elastase and plasmin). This cleavage is accompanied by a conformation change which generates, or at least greatly enhances, enzymatic activity (Neurath and Dixon, 1957; Sigler et al., 1968).

The conversion of trypsinogen to trypsin is the first step of the digestive cascaded-activation sequence, and it relies on the known high specificity of the activator (enterokinase) for the unusual N-terminal sequence Val-Asp-Asp-Asp-Asp-Lys unique to trypsinogens (Maroux et al., 1971). The activation of further trypsinogen by trypsin at the second-cascade step requires that the most favored tryptic cleavage of that zymogen be the activating split between residues 15 and 16. Yet, at the same time, it has been shown that the presence of four aspartic acids in the activation peptide (residues 10-15) has a markedly negative effect on this tryptic cleavage (Abita et al., 1969). In all species, the activation peptide must generate a good substrate quality for the activator, and a poor, but nonetheless most favorable, tryptic cleavage site on the entire trypsinogen molecule. In this light, it is not too surprising to find that the activation peptide sequence of trypsinogen, with its dual role, is so highly conserved throughout all species (De Haen et al., 1975).

It seems likely that the fundamental basis for inactivity of the proenzymes will be shared by all of the trypsin-like enzymes. The comparison between the structures of chymotrypsinogen (determined by Freer et al., 1970) and trypsinogen should serve to isolate characteristics common to both proenzymes, which will limit the primary reasons for inactivity, to the lowest common factor. In this respect, there are real and significant differences between the two proenzymes. Taking for granted that the enzymes themselves are catalytically active

† From the Norman W. Church Laboratory of Chemical Biology, California Institute of Technology, Pasadena, California 91125. *Received June 16, 1976.* Contribution No. 5342. Supported by National Institutes of Health Grant GM-19984 and National Science Foundation Grant No. BMS75-01405.

‡ Recipient of a NIH Postdoctorial Fellowship. Current address: Department of Biology, Brookhaven National Laboratories, Upton, Long Island, N.Y. 11973.

§ Recipient of a NIH Predoctorial Traineeship.

¶ Recipient of a NIH Career Development Award and a Sloan Foundation Fellow.

[1] The numbering referred to is that of chymotrypsinogen sequence (Hartley, 1970). The sequence for trypsinogen is that of Walsh and Neurath (1964), and Mikes et al. (1967).

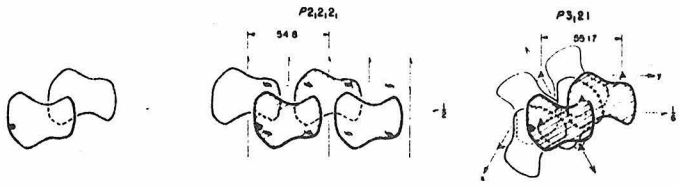

FIGURE 1: The packing diagram for trypsinogen (right) and trypsin (center) reveals a common intermolecular arrangement between molecules around a particular 2_1 axis.

(something which would not be obvious if the structures alone were viewed in the absence of such knowledge), we will compare the two proenzymes emphasizing the question as to why they should be relatively inactive. The answer to this question implies acceptance of the many well-established details of substrate binding and activity summarized, for example, by Blow (1974a).

Experimental Procedures

Crystallization and Derivative Preparation. Bovine trypsinogen (Worthington) was chromatographically purified using the procedure of Schroeder and Shaw (1968). Crystals were obtained by vapor diffusion of a 3% solution of protein against 30% ethanol-water. The crystals grew at 5 °C, as modified rhombohedra which generally averaged 0.25 mm across. A trypsin inhibitor, benzamidine, was added to the solution in a concentration of 2.5 mg/ml to prevent possible trypsin-mediated autolysis of the zymogen during the several weeks required for crystallization. It was essential to eliminate divalent cations from the crystallizing solutions, since they mimic the effects of Ca^{2+} and lead to autoactivation and autolysis of the trypsinogen in solution (Northrop et al., 1948). Crystals used for structure determination were grown from solutions adjusted to about pH 7.5, although isomorphous crystals were obtained throughout the pH range 5–8. Crystals grown this way are trigonal, space group $P3_121$ with cell parameters a = 55.17 Å and c = 109.25 Å. The unit cell volume is approximately 288 000 Å^3 and contains one molecule per asymmetric unit.

In view of the possible autolysis problem, the protein content of the crystals was checked by chromatography and by end-group amino acid analysis. Crystals were dissolved and found to contain pure trypsinogen by chromatography (Schroeder and Shaw, 1968). End-group analysis, using a modified Edman procedure, showed that the protein contained an N-terminal valine with no detectable alternative amino acid. This analysis rules out the possibility that any trypsinogen had been converted to trypsin during crystallization, since trypsin has an N-terminal isoleucine.

At low pH, DIP-trypsin[2] crystals were obtained which were isomorphous with the trypsinogen crystals. These crystals could be grown at pH 4.0–5.5 from either ethanol-water mixtures or from $MgSO_4$ solutions. At higher pH (5.7–8.5), trypsin crystallizes exclusively in the orthorhombic space group $P2_12_12_1$ (Stroud et al., 1971, 1974). At pH's between 4.0 and 5.5, the trigonal form of DIP-trypsin crystallized first. After several weeks, orthorhombic crystals grew from the same solution. The trigonal crystals were found to be unstable above pH 5.5, which suggests that there is some type of structural reorganization which occurs around pH 5.5.

In rare cases, DIP-trypsin crystals grew as trigonal-orthorhombic twins at about pH 5.5. These twins, in which the orthorhombic a axis was parallel to the trigonal a axis, suggested that the two crystal forms had some common symmetry element. The packing diagrams obtained from the structure solutions show that molecules are similarly disposed with respect to 2_1 screw axes in the two crystal forms. The 2_1 axes are parallel to the a axes in both the trigonal and orthorhombic crystals, as indicated in Figure 1. The unit-cell dimensions parallel to the 2_1 axes in the two crystal forms are 54.84 Å in orthorhombic DIP-trypsin and 55.17 Å in trigonal trypsinogen.

A vector parallel to the c axis of the orthorhombic cell in the trypsin molecule is tilted by a 13.49° rotation around the crystallographic 2_1 axis in the trigonal structure (eq 1, below).

Derivative Preparation. Isomorphous derivatives were prepared by placing the crystals into ethanol-water solutions containing heavy-atom salts. Optimum-diffusion conditions and soaking times were established by varying the pH from 6.0 to 8.0 and determining photographically the time necessary for a stable and reproducible diffraction pattern change to occur. Several of the derivatives showed a variation of pattern over an extended period of time.

The initial study of the HgI_4^{2-}, $Pt(NO_2)_4^{2-}$, and mersalyl derivatives showed that pattern stability had been reached after 1 to 2 weeks of crystal soaking. However, these same crystal soaks showed a further distinct change in diffraction pattern after 2 years. When the derivatives were solved, it was found that these changes were caused by appearance of several new minor sites, and fluctuation in the occupancies of several of the original sites. The overall differences between the short- and long-soak derivatives were large enough to allow them to be treated as independent derivatives in the phase refinement.

Data Collection. 1.8 Å data for native trypsinogen and 2.6 Å data for six derivatives were collected on a Syntex $P\bar{1}$ automated diffractometer using graphite-monochromatized Cu$K\alpha$ radiation. The detector was located 40.6 cm from the crystal, and a helium-filled tube was placed between the detector and the crystal to limit air absorption losses of the diffracted beam. Intensity data were collected using the Wyckoff step-scanning method (Wyckoff et al., 1970). An optimal scan width was chosen for each crystal separately, based on the criterion that the first steps outside of the usable peak should not be less than 95% of the peak step counts. Typically, the measurement of each reflection consisted of five steps centered on the diffrac-

[2] Abbreviations used are: DIP, diisopropylphosphoryl; DIPT, LpT, Tg, CT, and Cg refer to the crystallographically determined structures of diisopropylphosphoryl trypsin at ~pH 7.5 from orthorhombic crystals (Chambers and Stroud, 1976), low pH (~5.0) DIP-trypsin from trigonal crystals, trypsinogen (~pH 7.5) from trigonal crystals isomorphic with LpT crystals, tosyl-α-chymotrypsin (Birktoft and Blow, 1972), and chymotrypsinogen (Freer et al., 1970; Birktoft et al., 1976), respectively; NPGB, *p*-nitrophenyl-*p'*-guanidinobenzoate; BPTI, the basic pancreatic trypsin inhibitor.

tion maxima, taken over an omega range of 0.10°. The highest sum of three, or of four, adjacent steps was then treated as the integrated intensity. Scan rates ranged from 0.15° to 0.25°/min. In most cases, the native and derivative crystals were stable enough to collect a full 2.6 Å data set from a single crystal before any of the standard reflection intensities had changed by more than 10%.

The method used for data reduction and absorption correction was similar to that described by Stroud et al. (1974), but was altered for four-circle geometry. Individual background measurements were approximated by interpolation from empirical background curves, which were calculated as a function of 2θ, χ, and φ by the method of Krieger et al. (1974a).

Phase Analysis

Difference Patterson Methods. Initial phases for the trypsinogen $F_{(hkl)}$ were determined using the multiple-isomorphous-replacement method. Three-dimensional difference Patterson syntheses (Blow, 1958) were calculated for each one of the derivatives. However, of the ten derivatives examined, not one of the difference Patterson maps could be easily solved. The reasons for this difficulty became apparent only later when it was realized that there were no fewer than 12 sites per asymmetric unit in each one of the derivatives. A difference Patterson map for such a derivative contains in excess of 2500 vectors. Typically, the trypsinogen maps contained 800–1400 peaks of sufficient height to warrant investigation. Even with this large number of peaks, the ratio of the highest peaks on the map to the origin peak encouraged attempts to find at least the major sites by deconvolution of the Patterson map. Therefore, vector superposition methods were applied in attempts to solve the difference syntheses. In no case was an unambiguous solution to any derivative found. The primary source of difficulty was that a large number of cross vectors between nonequivalent "A–B" atom sites mimic the symmetry of "A–A" type vectors between symmetry-equivalent atoms around the threefold axes at $u = 1 - v = \frac{1}{3}, \frac{2}{3}$. As a result, they have double weight and so frustrate attempts at solution.

Solution of the Derivatives. At this stage, heavy-atom derivatives of the isomorphous low pH crystals of DIP-trypsin were investigated. A silver ion derivative was prepared, since a silver derivative of the neutral pH orthorhombic DIP-trypsin had previously shown a simple substitution pattern (Chambers et al., 1974). The trigonal trypsin derivative was unambiguously solved by the superposition programs and contained only two major sites and five minor sites. Since this form of trypsin is highly isomorphous with trypsinogen, an initial set of single isomorphous phases was obtained and they were used directly to determine the heavy atom positions in the trypsinogen derivatives.

Difference Electron Density Maps and Refinement. Three-dimensional single isomorphous replacement phases derived from the major Ag^+ site in the isomorphous DIP-trypsin derivative were used first to locate the major sites in the HgI_4^{2-} and mersalyl derivatives of trypsinogen. The maps were computed using $\Delta F = |F_{PH}| - |F_P|$ for each derivative, and phases from the Ag^+ (trypsin) site structure factors. Three HgI_4^{2-} sites and one mersalyl site were found using this procedure. Heavy-atom parameters were refined using a minicomputer (Data General Corp., NOVA 800), by the method of Dickerson et al. (1961, 1968) in alternating cycles of phase calculation and refinement of parameters. The positional parameters and occupancies of the two trypsinogen derivatives were refined along with those of the Ag^+ trypsin derivative. At a later stage of the refinement, the Ag^+ trypsin derivative was discarded to prevent bias in the phases towards a trypsin-like structure.

Phases from these derivatives were used to find the primary sites in the other trypsinogen derivatives. Secondary sites were located using a double-difference or error synthesis, which uses as structure factors the lack-of-closure error ϵ computed during phase refinement, with the calculated phases of the derivative data

$$(|F_{PH}| - |F_P + f_H|) \exp(i\varphi_{PH})$$

(Blake et al., 1963; Stroud et al., 1974), where f_H is the current value for the calculated heavy atom structure factor. In most derivatives, several minor sites were not included in the phasing calculations as their contributions were below the errors in measurement. Finally, anisotropic temperature factors for the sites of higher occupancy were included in the refinement. The correctness of each derivative solution was checked by permutation of pairs of derivatives which were corefined together, to generate phases which were then used to calculate difference maps for the other derivatives. Summary statistics for the six derivatives used are listed in Table I.

Electron-Density Maps. An electron density map was generated using multiple isomorphous replacement phases (MIR map) obtained from the derivatives listed in Table I. The first map was calculated using (hkl) data to a minimum interplanar spacing of 5 Å (figure of merit, FM = 0.88), and revealed the location and conformation of each molecule in the unit cell. The second MIR map was computed using data to 2.6 Å, and a model was built from Kendrew–Watson components to match the density map using an optical comparator (Richards, 1968). The mean figure of merit for all 5700 reflections with $F_{hkl} > 3\sigma$ from ∞ to 2.6 Å was FM = 0.71 (0.91 for centric reflections) when calculated according to Dickerson et al. (1968). A histogram shown in Figure 2 indicates the distribution of reflections according to their figures of merit.

The map was easily interpreted in most areas, although difficulties were encountered in the regions between residues 10–15, 143–151, and 186–188, all of which lie on the surface of the molecule.

Coordinates of all the reliably determined amino acid residues in trypsinogen were measured using an automated coordinate-measuring device which operates on the principle used by Salemme and Fehr (1972). Amplitudes F_{calcd} and phases φ_{calcd} were calculated from the measured coordinates, and a difference map was computed using terms:

$$\Delta F = |F_o| - |F_c|, \varphi_c$$

The well-determined parts of the molecule (90% of the structure) were adjusted using an automated procedure for constrained difference Fourier refinement and model building, which was developed to operate entirely on a minicomputer (Chambers and Stroud, 1976). Individual temperature factors were assigned to each heavy atom or ion (C, N, O, S, Ca^{2+}) based on electron density at atomic centers. No solvent molecules were included. Structure factors were calculated a second time and the procedure was repeated once more. At this stage, hkl data to 2.1 Å resolution were incorporated and an electron density map was calculated using terms $|2F_o - F_c|, \varphi_c$. Areas of structure which were ambiguous in the 2.6 Å MIR map were rebuilt using this map. Data were included to 1.9 Å resolution, and the molecule was subjected to several cycles of difference Fourier refinement. Isotropic temperature factors were refined so as to account for electron density at atomic centers in the

TABLE I: Statistical Analysis of Derivatives.

Derivative	No. of Sites	Occupancy[a]	$\langle\|\Delta F\|\rangle$[d]	ϵ[b]	R_c[c]	Resolution (Å)	No. of Reflections
HgI_4^{2-}	25	62	99	68	0.67	2.6	5450
		61	(242-81)	(93-61)	(0.37-0.84)		
		49					
		43					
$Pt(NO_2)_4^{2-}$	14	108	91	64	0.64	2.6	4213
		78	(211-64)	(87-53)	(0.35-0.91)		
		61					
		54					
Mersalyl 1	14	74	103	57	0.57	3.6	4908
		53	(195-84)	(87-55)	(0.41-0.65)		
		52					
		31					
Mersalyl 2	9	65	82	44	0.57	3.6	2184
		42	(130-70)	(57-42)	(0.43-0.61)		
		32					
		23					
Mersalyl 3	13	59	110	78	0.70	2.6	5043
		39	(217-98)	(74-79)	(0.33-0.72)		
		38					
		36					
Ag^+	15	76	98	61	0.60	2.6	5102
		49	(180-74)	(75-53)	(0.42-0.72)		
		45					
		22					

[a] Occupancy of the four most major sites. Scale is arbitrary (approximately 1.4 × absolute scale). [b] $\epsilon = \langle|F_{PH}| - |F_P + f_H|\rangle$ for all reflections. [c] $R_c = (\sum_{hkl}\epsilon_{hkl})/(\sum_{hkl}\Delta F_{hkl})$. [d] Numbers in parentheses give the average values of parameters at the lowest and highest values of the scattering angle 2θ used.

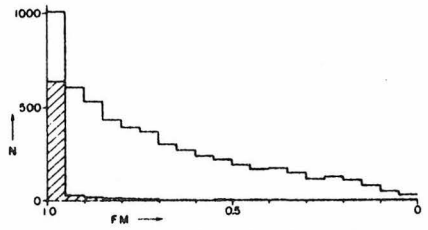

FIGURE 2: Histogram showing distribution of figures of merit for reflections. Histogram for the centrosymmetric reflections alone is shaded.

current $|F_o - F_c|$, φ_c synthesis. Therefore, large temperature factors for individual atoms give a measure of the possible error, or thermal motion of each group. The R_F value at this stage was 31% for all reflections from ∞ to 1.9 Å, where

$$R_F = \frac{\sum|F_o - F_c|}{\sum|F_o|}$$

While most of the molecule is well defined in the electron density (coordinates are probably defined to within about ±0.4 Å), there are small regions between residues 10-14, 143-150, and 186-194 where there is clearly a large degree of libration. These are external and solvent-accessible chains in the molecule. The electron density in the $2F_o - F_c$ synthesis is diffused and low in comparison with other regions, both when these residues were left out of the structure factor calculation and when included in the calculation. In addition, a density map for isomorphous trypsin, computed using trypsinogen phases, with amplitudes for trigonal trypsin was clearly interpretable for every residue in the region of residues 143-150 (10-14 is

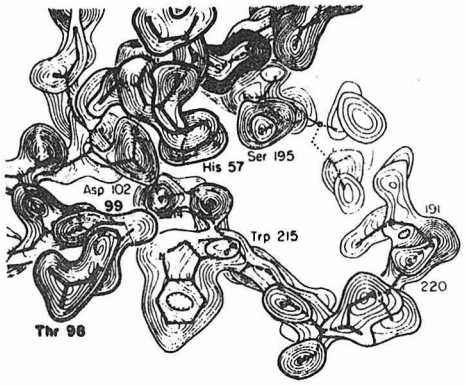

FIGURE 3: The structure around Asp-102, His-57, and Ser-195 in trypsinogen is shown superposed onto the electron-density map at 1.9 Å resolution.

no longer present), and at Ile-16-Val-17. Thus, there is clearly and unequivocally variability in the orientations of the trypsinogen residues 10-14, 143-150, and 186-194.

A region of the 1.9 Å electron density map around the active center is shown in Figure 3. The structure in this region is superposed on the density map. Most the carbonyl groups are clearly identified in the map and six-membered rings often have dimpled density in their centers, as, for example, does the side chain of Trp-215. The sulfur atoms in disulfide bridges are clearly resolved from each other. Some 10-20 ordered solvent molecules are contained within the molecular boundary, and, in cases where they exist as isolated molecules, these

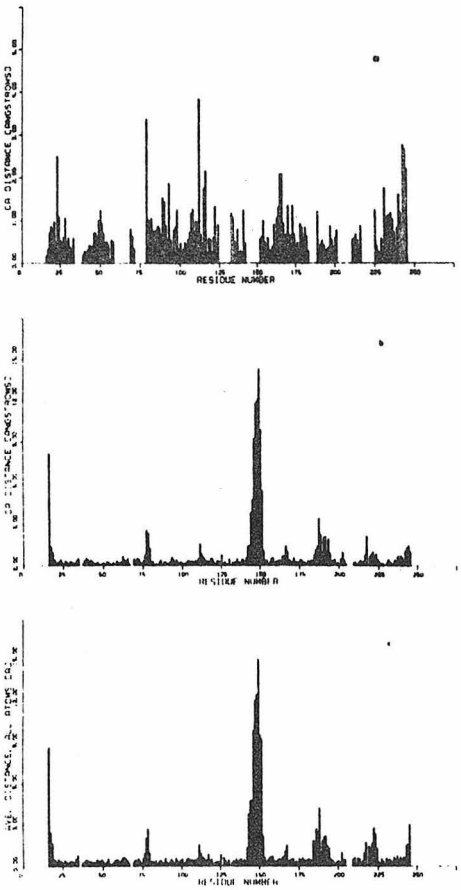

FIGURE 4: (a) Histogram showing the difference (Δd) between α-carbon positions in DIPT and CT. (b) Histogram showing the difference (Δd) between α-carbon positions of the Tg and DIPT structures after suitable rotation. Large differences in structure are seen around residues 16-19, 142-152, 186-194, and 215-220. (c) Histogram showing the mean difference (Δd) in position for all atoms in each residue between Tg and DIPT.

can usually be resolved. Solvent in the cavity which becomes occupied by Ile-16 upon activation was generally not resolved into discrete peaks.

Results and Discussion

The coordinates for trypsinogen are regarded as only preliminarily refined (R_1 = 31%). Typically, wire-model coordinates of a protein give rise to R_F values of ~40-45%, and can often contain occasional large errors of several angstroms. As refinement continues, the R_F value decreases and a value of <25% for a constrained structure often seems to represent convergence onto a respectable set of coordinates and isotropic temperature factors which account for thermal motion. Approximately, ten well-ordered solvent molecules were included in the later phase calculations. The model is clearly accurate for nearly all of the structure to within about 0.4 Å.

Comparison of Structures. The trypsinogen structure (Tg) was compared both with the orthorhombic DIP-trypsin structure (DIPT) and with the trigonal low-pH DIP-trypsin structure (LpT). The trypsinogen structure will be described in reference to the DIP-trypsin structure. The Tg and DIPT structures were determined and refined completely independently. The differences in structure between Tg and DIPT will, at the same time, be compared with the differences between the structures of chymotrypsinogen (Cg; Freer et al., 1970) and tosyl-α-chymotrypsin (CT; Birktoft and Blow, 1972).

Current Status of Trypsin Studies. The DIPT structure determined initially by Stroud et al. (1971, 1974) has since been refined using an automated procedure for constrained difference Fourier refinement (Chambers and Stroud, 1976). The agreement index was R = 23.5% for all reflections observable to a resolution of 1.5 Å at the time this comparison was made. The crystals were grown from 5.8% $MgSO_4$ solutions at about pH 7.5. X-ray data are observable to 1.1 Å resolution and, so far, recorded to 1.5 Å (22 117 observable reflections out of 35 566 independent reflections). There are well-defined and small conformational changes between this structure and that of benzamidine-trypsin (Krieger et al., 1974b). These changes have been shown by recomputing the maps with more recent phases not to be an artificial feature of the difference map, as suggested by Bode and Schwager (1975a), based on a comparison of their native trypsin structure with the 1.8 Å refined structure of benzamidine-inhibited trypsin.

The orthorhombic DIP-trypsin structure (Chambers and Stroud, 1976) is now among the most highly refined of any enzyme structure (R = 23.5% to 1.5 Å resolution), as is the more recently determined structure for benzamidine-trypsin of Bode and Schwager (1975a) (R = 22.9% to 1.8 Å resolution). No comparison between these two independently refined trypsin structures has yet been made. The comparison of Huber et al. (1974) was made between their refined structure and our initial unrefined wire-model coordinates for DIP-trypsin derived from the first 2.7 Å MIR density map. Wire-model coordinates such as these are inadequate for detailed comparison, even when the map is of the highest quality (Chambers and Stroud, 1976).

A comparison between our trypsin structure and α-chymotrypsin (Birktoft and Blow, 1972), similar to that made by Huber et al. (1974) between their trypsin structure and α-chymotrypsin, was carried out using a rigid-body least-squares computer program to superpose the two structures. Atoms compared in this manner included all α-carbon atoms, except in regions where amino acid deletions or insertions occur. The residue numbers included were thus the same as those used by Huber et al. (1974).

The average positional difference for α-carbon atoms of these residues was 0.80 Å, a value similar to that of 0.75 Å obtained by Huber et al. (1974) in their comparison of all main chain atoms for these residues (see Figure 4a). The similarity between this result and that of Huber et al. (1974) suggests that the DIP-trypsin refinement has resolved the discrepancies reported by those authors between the 2.7 Å unrefined DIP-trypsin structure and their 1.9 Å refined trypsin-PTI structure.

The LpT structure crystallizes preferentially below pH 5.5 and the crystals are isomorphous with those of Tg. This structure was compared directly with Tg by computing difference maps with amplitudes $\Delta F = |F_{Tg}| - |F_{LpT}|$, and phases for Tg to a resolution of 2.1 Å. This difference map is

a more sensitive test of small conformational changes than comparison of coordinates, and is correspondingly less prone to interpretative error. Such a map can clearly show changes which are smaller than the estimated error in the current set of atomic positions. Thus, "identical position" in the comparison of atomic positions between Tg and LpT probably implies identity within ±0.1 Å (which for a single carbon atom would result in a pair of peaks of 5σ above the noise level in the map), whereas the same phrase applied to the Tg/DIPT comparison implies equivalence to within about ±0.3 Å.

It must be noted that there is a strong possibility that the low-pH form of DIP-trypsin has a different structure from the neutral-pH form, as do low- and neutral-pH α-chymotrypsin (Tulinsky et al., 1973; Mavridis et al., 1974). Further, there is the possibility that the isomorphic low-pH trypsin structure is more like trypsinogen in some ways, and thus the difference map procedure would fail to identify any difference between the two proteins at such sites. In fact, the difference map is very clean in many areas where the neutral pH structures appear to be slightly different. However, the *activity* of the enzyme depends on only a single ionization between pH 2 and 8, and this has been identified as the ionization of Asp-102 at the active site (Koeppe and Stroud, 1976). Therefore, any pH-dependent structure change which does occur between pH 7 and 5 in trypsin is not a change which is reflected in the inherent activity of the enzyme, unless it can be associated directly with ionization of Asp-102. Thus, the changes between the isomorphous structures as seen in the difference Fourier are more likely to pick out the important differences for the change in catalytic activity in a direct way. This adds emphasis to this comparison as an assay for the important catalytic change.

Similarities in Structure. The atomic coordinates for DIPT were rotated to match those of Tg by least-squares minimization of the distances between equivalent atoms in the two molecules. Regions of major change in structure, i.e., residues 16–19, 143–152, 186–195, and 215–220, were left out of the rotation calculation, as were residues 76–80 where the differences are most probably due to errors in the model (see below).

The refined equation, which described rotation of the DIPT coordinates x, y, z (listed in angstroms with respect to the a, b, c axes) to match the trypsinogen set $(x', y', z')_{Tg}$ (listed in angstroms with respect to an orthogonal axial set, such that x' is perpendicular to the crystallographic b, c axes; y' and z' are parallel to the b and c axes, respectively), is:

$$\begin{pmatrix} x' \\ y' \\ z' \end{pmatrix} = \begin{pmatrix} -0.0017 & 0.9724 & -0.2333 \\ 1.0000 & 0.0028 & 0.0046 \\ 0.0052 & -0.2333 & -0.9724 \end{pmatrix} \begin{pmatrix} x \\ y \\ z \end{pmatrix} + \begin{pmatrix} 1.82 \\ -11.06 \\ -11.47 \end{pmatrix} \quad (1)$$

This rotation matrix closely approximates the form of a simple rotation of 13.5° about 2_1 axes in the two structures

$$\sim \begin{pmatrix} 0 & 1 & -0.23 \\ 1 & 0 & 0 \\ 0 & -0.23 & -1 \end{pmatrix}$$

It therefore explains the formation of the orthorhombic-trigonal twinned crystals and the congruence of the two a axial dimensions which are within 0.7% of each other (see Figure 1, and Experimental Section).

The histogram shown in Figure 4b indicates the distance between all α carbons for residues common to both structures after rotation, and clearly identifies the regions of greatest structural change. The mean deviation between equivalent α-carbon atoms in the two structures was calculated by leaving out the 32 residues with obviously different structure, and was $\Delta d_{C_\alpha} = 0.38$ Å. Thus, the difference in conformation of the main chain for all these residues is less than for the α carbons of the best region (the C-terminal α helix) of the Cg/CT comparison (Freer et al., 1970).

The mean deviation of position between all atoms in the main chain and side groups for the same residues was Δd = 0.45 Å (Figure 4c). Since the two structures are so similar in these regions, these distances presumably represent the sum of errors in the two coordinate sets, coupled with real differences in structure. The errors in the trypsinogen coordinates are clearly much greater than those of the more refined DIPT set. Real differences in structure could be due to (1) crystal packing forces, (2) different solvent or counterion effects, and (3) to genuine consequences of the difference in covalent structure of Tg and DIPT. Most of the differences in side-chain orientation for structurally homologous regions do occur on the surface of the protein.

It is notable that DIPT and Tg are much more homologous in structure than are CT and Cg. In a recent analysis, Birktoft et al. (1976) identified several regions of large difference between CT and Cg, associated with a relative movement of the two structural cylinders which are formed by the first and second halves of the chymotrypsin sequence. There is no corresponding difference between DIPT and Tg. However, it must be noted that the CT structure was determined at low pH, ~4.5, where the enzyme has different structure from the neutral-pH form (Tulinsky et al., 1973), and crystallized as a dimer, where the active center lay in the dimer interface.

The Active Center. The structure around the active center of Tg is shown in Figure 5a. Crystallographic studies of chymotrypsinogen (Freer et al., 1970) showed that the orientation and immediate environment of the active-site residues, Asp-102, His-57, and Ser-195, were very similar to that found in chymotrypsin. However, a small change in the orientation of Ile-99 permitted limited access of Asp-102 and His-57 to solvent in CT, and the hydroxyl of Ser-214 was not hydrogen bonded to Asp-102 in Cg, raising a question as to the importance of subtle changes in this region for zymogen activation. Similar features are not seen in Tg, where both Leu-99 ($\overline{\Delta d}_{99}$ = 0.5 Å) and the Oγ of Ser-214 (Δd = 0.2 Å) are in identical positions in the zymogen and enzyme; therefore, they cannot be common features of the mechanism of activation.

The α carbon of Ser-195 differs by only 0.4 Å between Tg and DIPT, and the Oγ of Ser-195 in Tg is hydrogen bonded to the ϵN of His-57 (Figure 5a) as it is in the benzamidine-trypsin structure (Kreiger et al., 1974b). The Tg-LpT difference map also indicates a small shift in the orientation of the imidazole of His-57 between the two structures. The presence of a DIP group at Ser-195 may be, in part, responsible for the observed shift of 0.3 Å in the ring. This movement of the imidazole ring is similar to the shift observed previously in a comparison of benzamidine-trypsin and DIP-trypsin (Krieger et al., 1974b). It is also clear from the latter comparison, and from more recently computed difference maps using improved phases, that there are several other small differences between these two structures. The fact that Bode and

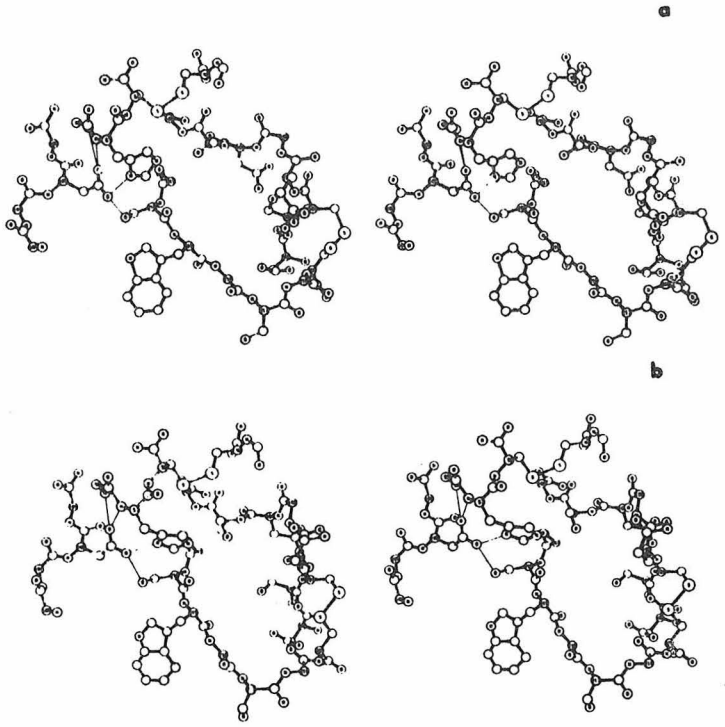

FIGURE 5: Structure of the active site in trypsinogen (a) is compared with structure for the same region of trypsin (b).

Schwager (1975a) did not find any such differences between benzamidine-trypsin and native trypsin suggests that the presence of the covalently bonded DIP group may be responsible for small differences in the DIP structure. Nevertheless, no significant movement of the α carbon of Ser-195 was observed in DIP-trypsin when compared with benzamidine-trypsin.

Birktoft et al. (1976) found that the hydrogen bond between the $N\epsilon_2$ of His-57 and the $O\gamma$ of Ser-195 was strained in CT, while it was relatively normal in Cg. Our present results with the trypsin system differ in that the $O\gamma$ of Ser-195 (even though attached to the DIP group) in DIP-trypsin is still only 1.15 Å from the ideal position (described by Birktoft et al., 1976) and only 0.67 Å from the ideal position in trypsinogen. This is to be compared with the corresponding values of about 2.5 Å for α-chymotrypsin and 0.7 Å for chymotrypsinogen.

Since the hydrogen-bond distances between His-57 and Ser-195 in trypsinogen are normal (2.5 Å) and can be made normal in trypsin without the DIP group (2.8 Å in DIP-trypsin), it does not seem that significant distortion at this site can be considered as a common feature of the activation mechanism of serine proteases.

The Side-Chain Binding Pocket. Freer et al. (1970) questioned whether the absence of a specific binding pocket could explain the inactivity of Cg. Trypsinogen has a large and accessible binding pocket, although the structure and stability of the cavity is different from that found in DIPT (or in benzamidine-trypsin (Krieger et al., 1974b)).

The region of chain between 186 and 194 is loosely organized and adopts several different conformations in Tg. The present structure for this chain was determined carefully. Evidence for this structure as the most predominant conformation depended on (1) the isomorphous-replacement density map; (2) $2F_o - F_c$ or $F_o - F_c$ electron-density syntheses using calculated phases for a model from which this region was omitted; (3) the LpT-Tg difference map, which gives the most direct measure of the loose organization of the 186–194 chain. This difference map shows unequivocally that the chain structure is variable and that the low density is not due to errors in the phases.

Two hydrogen bonds present in DIPT, between Val-17 NH and the main-chain carbonyl of Asp-189, and between the Val-17 C=O and Asp-189 NH, are absent in Tg. These may contribute relative stability to the chain in DIPT.

Benzamidine is a competitive inhibitor of trypsin ($K_i = 1.8 \times 10^{-5}$ M) (Mares-Guia and Shaw, 1965) which binds inside the side-chain specific binding pocket of the enzyme (Krieger et al., 1974b). Benzamidine was present at 20 mM concentration (at least 10^3 times the K_i for trypsin) in the trypsinogen-crystallizing solution; yet, there was no benzamidine bound to the proenzyme in the Tg structure. This emphasizes the fact that the structure for the binding site, as seen in the crystals, represents a functionally significant impediment to the binding capabilities of the site for benzamidine, which is an analogue

of the side chain of a substrate for trypsin. The binding constant for benzamidine binding to trypsinogen in solution was found to be about 10^5 times larger than for binding to trypsin (Gertler et al., 1974). The binding site seen in the Tg structure is large enough to accept a benzamidine molecule, and the fact that none was bound implies that the differences between zymogen and enzyme structures (as shown in Figure 5) are quite adequate to account for a large change in specificity.

A relatively large movement of the backbone chain from residues 187 to 194 in the Cg/CT comparison was correlated with the formation of the specific binding site for substrate side chains in CT, a cavity which was only partially formed in Cg (Freer et al., 1970). There are much smaller but significant changes between Tg and DIPT (or LpT) in the chain from residues 188A to 195 (Figure 5). The migration of Met-192 from a completely buried position (in the site occupied by the ion pair between Ile-16 and Asp-194) in Cg to the outside of the CT molecule also has no comparable counterpart in the Tg/LpT comparison. The α carbon of Gln-192 in Tg moves by ~1 Å on activation. The side chain of Asp-189 inside the specific binding pocket of trypsin and responsible for the substrate specificity of trypsin lies within ~1 Å of the position found in Tg, $\Delta d_{C_\alpha,189} = 0.9$ Å. Thus, it would seem that modification, rather than generation of the specific cavity, must be considered as a possible reason for zymogen inactivity in general.

Studies of the residual activity of trypsinogen have generally been carried out on simple esters where hydrogen bonds to the main chain of 214–219 are not made. For NPGB hydrolysis by Tg, the binding constant was found to be at least 10^3 times worse than for trypsin (Robinson et al., 1973). Changes in the binding-pocket structure could well be responsible for some or all of this poorer binding.

Residues 214–220. In Cg, changes occurred in the main chain between Ser-214 and Cys-220, a region known to be involved in hydrogen bonding to a peptide substrate (Segal et al., 1971; Sweet et al., 1974; Huber et al., 1974; Blow, 1974b). In Tg, the chain structure differs slightly from trypsin as shown in Figure 5. The C=O of Ser-214 ($\Delta d = 0.3$ Å), and the NH ($\Delta d = 0.5$ Å) and C=O ($\Delta d = 1.4$ Å) of Gly-216 still point in the same direction. The peptide bond between Gly-219 and Cys-220 is apparently rotated by 180° with respect to trypsin at neutral pH (DIPT). There is a difference in residues 214–217 of Cg in that the NH and C=O of Gly-216 would be unable to participate in substrate binding (Freer et al., 1970). This and the other differences in binding-site structure between Cg and Tg are not inconsistent with the fact that the basic pancreatic trypsin inhibitor (BPTI) will form a stoichiometric 1:1 complex with trypsinogen and with trypsin or chymotrypsin, but will not so complex with chymotrypsinogen (Dlouha and Keil, 1969).

There was an error in the original placement of the side chain of Trp-215 in DIPT (Figure 8 of Krieger et al., 1974b). Refinement of that structure revealed that the indole ring is reversed, such that ϵN points in toward the center of the molecule (Chambers and Stroud, 1976). The same configuration is found in Tg. This orientation is now the same as that found in CT (Birktoft and Blow, 1972). Modification of Trp-215 in trypsinogen blocks the binding of BPTI by trypsinogen (Keil-Dlouha and Keil, 1972).

Asp-194. The side chain of Asp-194 forms a salt bridge with Ile-16 in trypsin. The N terminal of Ile-16 is not available in Tg, since it lies in the zymogen-activation peptide. Asp-194 is in a similar orientation inside the trypsinogen molecule, although the α carbon is moved by $\Delta d = 0.9$ Å. The side chain is surrounded by internal solvent molecules. There appears to be only one intramolecular hydrogen bond to Asp-194 in Tg between the Oδ-1 of Asp-194 and the Oγ of Ser-190. The side chain of Asn-143 (in Tg) points in toward the solvent cavity around Asp-194.

Freer et al. (1970) postulated that interaction between Arg-145 and Asp-194 could contribute to charge stabilization of the carboxyl group of Asp-194 in Cg possibly through water molecules. In a more detailed analysis, Wright (1973a,b) found that the guanidine group of Arg-145 was too far from Asp-194 to participate directly in this role, but could neutralize the charged carbonyl via water molecules hydrogen bonded to the δ nitrogen of His-40. The ϵ nitrogen of His-40 was found to be 3.5 Å from the carboxyl group of Asp-194, and so was indirectly implicated as providing a possible pathway for proton transfer from the surface of the molecule to the buried carboxyl group.

In Tg, neither Lys-145 nor His-40 lies close to the side chain of Asp-194 (see Figure 6), and, therefore, cannot be involved in stabilizing Asp-194. The side chain of Lys-145 is on the outside of the molecule and the ζN of Lys-145 is about 10 Å from Asp-194. Indeed, there are no basic side chains close enough to contribute directly to charge neutralization of Asp-194. His-40 is found in the same orientation in Tg as in LpT, and almost exactly the same as in DIPT ($\Delta d_{C_\alpha} = 0.4$ Å). The Nδ-1 of His-40 is hydrogen bonded to the Oγ of Ser-32 in both Tg and DIPT (and CT, but not Cg). Nϵ-2 of His-40 is hydrogen bonded to the C=O of Gly-193 in DIPT and CT, but is hydrogen bonded to an external solvent molecule in Tg. This change corresponds to the movement of the Cα of 194 (Δd = 0.9 Å) and 193 ($\Delta d = 2.0$ Å) toward the solvent-filled cavity around Asp-194. Wright (1973b) emphasized the apparent conservation of a basic group at residue 145 of the trypsin-like enzymes, although there are now exceptions in the sequences of dogfish trypsin (where the residue is methionine), and in all the bacterial enzymes (Bradshaw et al., 1970; De Haen et al., 1975). His-40 is also not a conserved residue among trypsin-like enzymes, and is Leu in bovine thrombin, Gly in blood-clotting factor X, and Met, Arg, or Leu in bacterial trypsin sequences (De Haen et al., 1975).

The "Autolysis Loop" (Residues 142–151). The largest conformational difference between Tg and DIPT or LpT occurs between residues 142 and 151. This sequence was referred to as the "autolysis loop" by Blow et al. (1969), since it contains a region where two amino acids are excised in α-chymotrypsin. The difference map between Tg and LpT (Tg–LpT) showed clear negative density, which picked out the conformation of the autolysis loop in LpT. There was much less (~50%) positive density in the map for this part of the chain, establishing that the chain is flexible in Tg and adopts a quite different conformation there. (The LpT structure was identical to that of DIPT in this region.) A further change in the structure of this loop or of Lys-15–Ile-16 would be required if an activating enzyme was to approach the Lys-15–Ile-16 bond in the Tg conformation.

Trp-141 is in essentially the same orientation in Tg as found in DIPT ($\Delta d_{C_\alpha} = 0.6$ Å). The side chain of Asn-143, which was solvent accessible in DIPT, points in toward the cavity around Asp-194 in Tg ($\Delta d_{C_\alpha} = 1.4$ Å). The side chain of Thr-144 (Tg) is moved by several angstroms toward the disulfide Cys-191–Cys-220 ($\Delta d_{C_\alpha} \simeq 4.0$ Å), and residues 145–151 are in quite different conformation in the two structures. They are all solvent accessible in both Tg and DIPT. There may be a functional correlation between the loose structure of this chain in the zymogen, and the necessity for

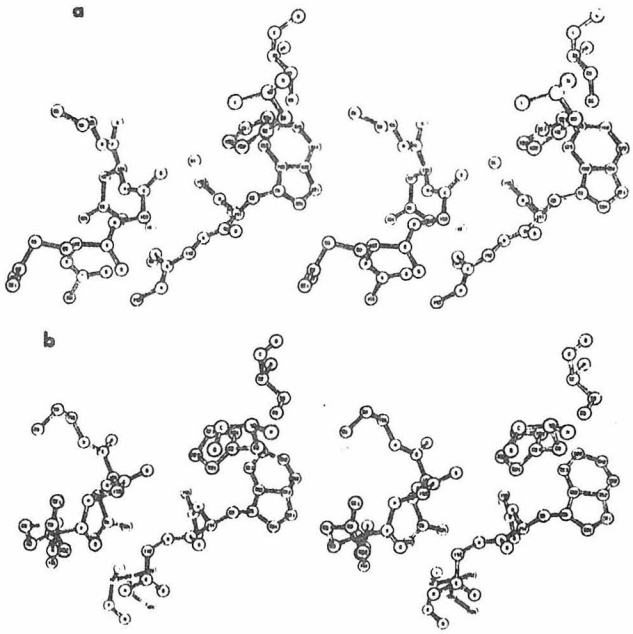

FIGURE 6: (a) Structure around Asp-194 and His-40 in Tg. (b) Structure around Asp-194 and His-40 in DIPT.

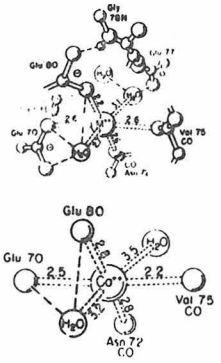

FIGURE 7: A schematic of the coordination of ions at the primary Ca^{2+} ion binding site in trypsin (top) and trypsinogen (bottom). Distances between the ion and chelating ligands are indicated in angstroms.

access of the activating enzyme to the Lys-15-Ile-16 bond. The sequences for residues 146-154 are extremely variable in related enzymes (De Haen et al., 1975), and no specific roles can be assigned to any of the side chains of these residues in trypsinogen, as judged from the Tg structure.

The Primary Calcium Ion Binding Site. There are two calcium ion binding sites in trypsinogen. The primary site, with higher affinity for calcium ion ($K_D \sim 10^{-3.2}$ M, Abita et al., 1969), is common to both trypsinogen and trypsin. Occupancy of this site stabilizes the protein toward thermal denaturation or autolysis (Northrop et al., 1948). Figure 7 shows a schematic of the primary Ca^{2+} ion site in trypsinogen and in trypsin (Chambers and Stroud, 1976). Coordination of the ion in both models is approximately octahedral and the ligands are identical in the two structures, although there are differences of up to 0.7 Å in the absolute positions of the ligands involved ($\Delta d_{Ca^{2+}} = 0.15$ Å).

It seems likely that these differences may be due to error rather than to any real structure change, since there were no peaks in the Tg-LpT difference map around the ion. The peak of electron density assigned to the Ca^{2+} ion in trypsinogen was the highest peak on the entire Fourier map, even during the first stages of Fourier refinement at 2.1 Å resolution and site occupancy refined to 18 electrons.

The primary Ca^{2+} binding site in trypsin was first identified and described in detail by Bode and Schwager (1975b) based on analysis of an independently refined trypsin structure seen at 1.8 Å and the Ca^{2+} content of their crystals. No comparison of their coordinates with ours has been made, although the structures for the Ca^{2+} site in all three determinations seem to be essentially the same. In our case, no Ca^{2+} was added to any of the crystallizing solutions and no attempt has been made to determine the Ca^{2+} content in the crystals.

The ion found at the primary site in DIPT is probably a magnesium ion present in the crystallizing liquor (5.8% $MgSO_4$). The electron density at this site refined to that expected for a water molecule (10 electrons) or a magnesium ion (Chambers and Stroud, 1976). Since Ca^{2+} accelerates autoactivation of trypsinogen to trypsin, reasonable care was taken to exclude it from the trypsinogen-crystallizing solution. Ca^{2+} was present in the buffer (0.02 M in $CaCl_2$) used during the chromatographic purification, although the solution was

later dialyzed using large volumes of 10^{-3} M HCl. Thus, it was surprising to find that the bound ion at the primary ion site in Tg refined to an occupancy of 18 electrons. We presume this to be a single site, fully occupied by a single, tightly-bound, Ca^{2+} ion, which remained as an integral component of the zymogen throughout.

The difference map calculated between the isomorphous crystals of Tg and LpT showed no electron density in the Ca^{2+} region. Therefore, the primary calcium ion binding sites in trypsinogen, low-pH trypsin, or DIP-trypsin at about pH 7.5, are similar to one another and to the structure described by Bode and Schwager (1975b) in benzamidine-trypsin.

The Second Ca^{2+} Binding Site and the N-terminal Sequence. A secondary Ca^{2+} ion binding site of $K_D \sim 10^{-1.8}$ M exists only on the zymogen. Binding of Ca^{2+} at this site is essential for complete and efficient activation of trypsinogen (Northrop et al., 1948). The effect of binding is to improve the substrate character of the activation peptide, so, favoring tryptic hydrolysis of the Lys-15–Ile-16 peptide bond. (K_m decreases by a factor of three, while k_{cat} remains unchanged (Abita et al., 1969).) Tryptic hydrolyses of the nonapeptide Val-$(Asp)_4$-Lys-Ile-Val-Gly and of the hexapeptide Val-$(Asp)_3$-Lys-Ile-Val have been shown to be Ca^{2+} dependent in a very similar way, while hydrolyses of peptides containing only one aspartate do not depend on Ca^{2+} (Delaage et al., 1967; Abita et al., 1969). Thus, Ca^{2+} ion binding to Asp-13 and Asp-14 together is sufficient to explain the zymogen Ca^{2+} ion effect (Abita et al., 1969). There is no corroborative crystallographic evidence as yet, since Ca^{2+} was excluded from the crystallizing solution.

The overall weak electron density for much of the N-terminal hexapeptide of trypsinogen must be attributed to local disorder or loosely organized structure, rather than to phasing error. This conclusion is implied by the (Tg–LpT) difference map computed using phases for trypsinogen. In regions where there is difference in structure, this map should show a positive-density image for trypsinogen, and a somewhat weaker negative image for trypsin. Yet, the positive density for trypsinogen residues 10–15 was consistently much lower in amplitude than the negative images for trypsin structure.

The loose arrangement of this hexapeptide on the surface of the proenzyme is consistent with the finding that the synthetic nonapeptide Val-$(Asp)_4$-Lys-Ile-Val-Gly is hydrolyzed by trypsin at almost the same rate ($k_{cat} \sim 10^{-3}$ s^{-1}) as the Lys–Ile bond on the same sequence in Tg for which $k_{cat} = 2.5 \times 10^{-3}$ s^{-1} (Abita et al., 1969). Thus, it is clear that the slow hydrolysis of the Lys–Ile bond by trypsin does not depend on any unique tertiary structure of these residues. The four aspartates are all available to modification by carbodiimides, and such modification does not destroy activatibility of trypsinogen (Radhakrishnan et al., 1967). This is in agreement with our finding that the Val-10–Asp-14 sequence is not a determinant of tertiary structure. Thus, the binding of Ca^{2+} to Asp-13 and Asp-14 is probably independent of the protein structure as an ion-specific conformer, and is adequately explained by an induced structural change in the peptide (10–15) alone, or by neutralization of charge at Asp-13 and Asp-14.

There is a clear necessity for trypsinogen among all pancreatic zymogens to develop immunity to autolysis or activation by its own residual activity, since trypsin activates other zymogens. The loosely structured hexapeptide is presumably protected against trypsin more by its negative charge than by tertiary structure. The Lys-15–Ile-16 is not inaccessible, although some reorientation of this chain or of the autolysis loop must accompany enzyme binding to this bond. The fact that this bond is still the most readily hydrolyzed is consistent with the fact that compact native structures are generally more resistant to degradation than are denatured ones. The φ and ψ angles on either side of Lys-15 are not dissimilar to those found for the susceptible Lys-15 bond on the trypsin inhibitor (a good substrate model). Since it is clearly proven that both this chain and the neighboring autolysis loop have little to restrain their configuration, the reorientation necessary for access by the activating enzyme should be energetically easy to accomplish.

Because of disorder, no real density for the side chains of Asp-11 or Asp-12 exists.

The Reasons for Zymogen Inactivity. Freer et al. (1970) and later Wright (1973b) identified four possible factors which might be responsible for inactivity of chymotrypsinogen. We now see that two of them do not seem to be shared by trypsinogen, since (1) the potential source of a hydrogen bond from Gly-216 NH is not excluded, although this group is moved by 0.5 Å from its "substrate-binding" position in the free enzyme, and (2) the side chain of Gln-192 occupies a fairly innocuous position outside the trypsinogen molecule, whereas the corresponding Met-192 of chymotrypsinogen was shown to undergo a complete reorganization upon activation.

The third factor, an incompletely formed binding site in Cg, does have a counterpart in Tg, although the binding pocket is open and accessible in Tg, whereas it was less so in Cg. Nevertheless, alterations in the binding site are sufficient to alter or remove specificity.

The remaining factor was the lack of an important hydrogen-bonding group in the NH of Gly-193. Steitz et al. (1969), Henderson (1970), and later Robertus et al. (1972) postulated that the NH groups of Gly-193 and of Ser-195 could play an important catalytic role in stabilization of reaction intermediates. In chymotrypsinogen, the NH of Gly-193 points away from the position for the carbonyl oxygen of the substrate (Freer et al., 1970). In trypsinogen, the NH of Gly-193 and of Ser-195 both point toward a site not dissimilar to that found in trypsin and chymotrypsin. Nevertheless, this site, termed "the oxyanion hole" by Robertus et al. (1972), is removed by 1.9 Å away from the position of the site in trypsin. Thus, oxyanion stabilization is possible in trypsinogen, but not at the ideal site. Peaks in the (Tg–LpT) difference map for this region are further testimony to the differences between these two molecules and also indicate a shift of about 2.0 Å. Loss of this component of the catalytic apparatus may well account for the slower reaction rate of the zymogen. There is a plausible connection between the movement of this site away from the cavity around Asp-194 and the formation of the salt bridge to Ile-16 upon activation. There is also plausible connection between the small changes in the binding pocket and the relocation of Ile-16. Similar changes in the structure of the binding site could account for the poorer binding of substrate by the zymogens in general.

Conclusion

The structure of trypsinogen is generally much closer to that of trypsin than in chymotrypsinogen to chymotrypsin. The structure of trypsinogen does not exclude the possibility of substrate binding in a mode similar to that found for trypsin, although changes in the structure of this region contribute to an impaired or altered substrate binding mode—certainly for benzamidine and, most probably, for a substrate side chain. If the proenzyme is considered to be rigid, then the general base catalyst (the ϵN of His-57) and the oxyanion-binding site formed by the NH groups of Gly-193 and Ser-195 are too far

apart to cooperate in substrate hydrolysis. Even if the proenzyme structure was to change on substrate binding, as seems likely, nonproductive binding may provide another important component for zymogen inactivity. Such binding might still leave too great a distance, or an unfavorable interaction between the substrate and elements of the catalytic center. The altered position of the chain between Lys-188A and Ser-195 and the main chain between Trp-215 and Ser-217 could be responsible for competitive, yet nonproductive, substrate binding, as could the NH group of Gly-193, since they are normally involved in orienting the substrate. These possibilities remain as prime candidates in a universal scheme for inactivity of the trypsinogen-like zymogens.

Acknowledgments

We thank M. O. Jones and R. Price for assistance with calculations for the comparisons of structures.

References

Abita, J. P., Delaage, M., Lazdunski, M., and Savrda, J. (1969), *Eur. J. Biochem. 8,* 314–324.

Birktoft, J. J., and Blow, D. M. (1972), *J. Mol. Biol. 68,* 187–240.

Birktoft, J. J., Kraut, J., and Freer, S. T. (1976), *Biochemistry, 16,* 4481.

Blake, C. C. F., Fenn, R. H., North, A. C. T., Phillips, D. C., and Poljak, R. J. (1963), *Acta Crystallogr. 16,* A77.

Blow, D. M. (1958), *Proc. R. Soc. London, Ser. A 247,* 302–336.

Blow, D. M. (1974a), *Isr. J. Chem. 12,* 483–494.

Blow, D. M. (1974b), *Bayer-Symp. 5,* 473–483.

Blow, D. M., Birktoft, J. J., and Hartley, B. S. (1969), *Nature (London) 221,* 337–340.

Bode, W., and Schwager, P. (1975a), *J. Mol. Biol. 98,* 693–717.

Bode, W., and Schwager, P. (1975b), *FEBS Lett. 56,* 139–143.

Bradshaw, R. A., Neurath, H., Tye, R. W., Walsh, K. A., and Winter, W. P. (1970), *Nature (London) 226,* 237–239.

Chambers, J. L., Christoph, G. G., Krieger, M., Kay, L., and Stroud, R. M. (1974), *Biochem. Biophys. Res. Commun. 59,* 70–74.

Chambers, J. L., and Stroud, R. M. (1976), *Acta Crystallogr.* (in press).

Davie, E. W., and Neurath, H. (1955), *J. Biol. Chem. 212,* 515–529.

De Haen, C., Neurath, H., and Teller, D. C. (1975), *J. Mol. Biol. 92,* 225–259.

Delaage, M., Desnuelle, P., Lazdunski, M., Bricas, E., and Savrda, J. (1967), *Biochem. Biophys. Res. Commun. 29,* 235–240.

Dickerson, R. E., Kendrew, J. C., and Strandberg, B. E. (1961), *Acta Crystallogr. 14,* 1188–1195.

Dickerson, R. E., Weinzierl, J. E., and Palmer, R. A. (1968), *Acta Crystallogr., Sect. B 24,* 997–1003.

Dlouha, V., and Keil, B. (1969), *FEBS Lett. 3,* 137–140.

Freer, S. T., Kraut, J., Robertus, J. D., Wright, H. T., and Xuong, Ng. H. (1970), *Biochemistry 9,* 1997–2009.

Gertler, A., Walsh, K. A., and Neurath, H. (1974), *Biochemistry 13,* 1302–1310.

Hartley, B. S. (1970), *Philos. Trans. R. Soc. London, Ser. B 257,* 77–87.

Henderson, R. (1970), *J. Mol. Biol. 54,* 341–354.

Huber, R., Kukla, D., Bode, W., Schwager, P., Bartels, K., Deisenhofer, J., and Steigemann, W. (1974), *J. Mol. Biol. 89,* 73–101.

Keil-Dlouha, V., and Keil, B. (1972), *J. Mol. Biol. 67,* 495–505.

Koeppe, R. E., II, and Stroud, R. M. (1976), *Biochemistry 15,* 3450–3458.

Krieger, M., Chambers, J. L., Christoph, G. G., Stroud, R. M., and Trus, B. L. (1974a), *Acta Crystallogr. Sect. A 30,* 740–748.

Krieger, M., Kay, L. M., and Stroud, R. M. (1974b), *J. Mol. Biol. 83,* 209–230.

Mares-Guia, M., and Shaw, E. (1965), *J. Biol. Chem. 240,* 1579–1585.

Maroux, S., Baratti, J., and Desnuelle, P. (1971), *J. Biol. Chem. 246,* 5031–5039.

Mavridis, A., Tulinsky, A., Liebman, M. N. (1974), *Biochemistry 13,* 3661–3666.

Mikes, O., Tomasek, V., Holeysovsky, V., and Sorm, F. (1967), *Collect. Czech. Chem. Commun. 32,* 655–677.

Neurath, H. (1975), in Cold Spring Harbor Symposium on Proteases and Biological Control, *1975,* Reich, E., Rifkin, D. B., and Shaw, E., Ed., Cold Spring Harbor, N.Y., Cold Spring Harbor Laboratory, pp 51–64.

Neurath, H., and Dixon, G. H. (1957), *Fed. Proc., Fed. Am. Soc. Exp. Biol. 16,* 791–801.

Northrop, J. H., Kunitz, M., and Herriot, R. M. (1948), Crystalline Enzymes, New York, N.Y., Columbia University Press, pp 133–136.

Radhakrishnan, T. M., Walsh, K. A., and Neurath, H. (1967), *J. Am. Chem. Soc. 89,* 3059–3061.

Richards, F. M. (1968), *J. Mol. Biol. 37,* 225–230.

Robertus, J. D., Kraut, J., Alden, R. A., and Birktoft, J. J. (1972), *Biochemistry 11,* 4293–4303.

Robinson, N. C., Neurath, H., and Walsh, K. A. (1973), *Biochemistry 12,* 420–425.

Salemme, F. R., and Fehr, D. G. (1972), *J. Mol. Biol. 70,* 697–700.

Schroeder, D. D., and Shaw, E. (1968), *J. Biol. Chem. 243,* 2943–2949.

Segal, D. M., Powers, J. C., Cohen, G. H., Davies, D. R., and Wilcox, P. E. (1971), *Biochemistry 10,* 3728–3738.

Sigler, P. B., Blow, D. M., Matthews, B. W., and Henderson, R. (1968), *J. Mol. Biol. 35,* 143–164.

Steitz, T. A., Henderson, R., and Blow, D. M. (1969), *J. Mol. Biol. 46,* 337–348.

Stroud, R. M., Kay, L. M., and Dickerson, R. E. (1971), *Cold Spring Harbor Symp. Quant. Biol. 36,* 125–140.

Stroud, R. M., Kay, L. M., and Dickerson, R. E. (1974), *J. Mol. Biol. 83,* 185–208.

Sweet, R. M., Wright, H. T., Janin, J., Chothia, C. H., and Blow, D. M. (1974), *Biochemistry 13,* 4212–4228.

Tulinsky, A., Vandlen, R. L., Morimoto, C. N., Mani, N. V., and Wright, L. H. (1973), *Biochemistry 12,* 4185–4192.

Walsh, K. A., and Neurath, H. (1964), *Proc. Natl. Acad. Sci. U.S.A. 52,* 884–889.

Wright, H. T. (1973a), *J. Mol. Biol. 79,* 1–11.

Wright, H. T. (1973b), *J. Mol. Biol. 79,* 13–23.

Wyckoff, H. W., Tsernoglou, D., Hanson, A. W., Knox, J. R., Lee, B., and Richards, F. M. (1970), *J. Biol. Chem. 245,* 305–328.

Appendix 5

Mechanisms of Zymogen Activation

MECHANISMS OF ZYMOGEN ACTIVATION

Robert M. Stroud, Anthony A. Kossiakoff[1], and John L. Chambers

Norman W. Church Laboratory of Chemical Biology

California Institute of Technology

Pasadena, California 91125, U.S.A.

(Ann. Rev. Biophys. Bioeng.--in press)

---

[1]Present address: Brookhaven National Laboratory

Upton, Long Island, New York 11973, U.S.A.

Introduction

It is now well recognized that proteolytic enzymes play key roles in the regulation of or control over the action of other proteins (1,2,3). Such enzymes can be found in all species from bacteria to man, and in control of diverse systems which include hormone production, bacteriophage assembly (4), development, fertilization (5), digestion, defense against invading organisms (6), and tissue repair (7,8). In most cases the proteolytic enzymes are known to be synthesized as inactive precursor proenzymes, or zymogens (9). They are activated by proteolytic cleavage of a single peptide bond in the proenzyme, and so become catalytically active. Further control over the degree of specificity for a target molecule or molecules is determined by the degree of specificity inherent to the enzyme. Further control over the time and location of action is often carried out by protein inhibitors of the requisite specificity.

There are several different classes of proteolytic enzymes which were first classified according to their susceptibility toward different inhibitors (10), and later according to their homologous amino acid sequences or structures within each class (11). There are many excellent papers and reviews which deal with all aspects of the collected information of the proenzymes of proteases (for example 1,2,3, 9,11). Therefore in this review we shall consider the single question of why the zymogens of the serine proteases--the enzyme class about which most is known--are relatively inactive. We consider this in the

light of most information about the known structures of two proenzymes, chymotrypsinogen (12) and trypsinogen (13), and their activated counterparts, α-chymotrypsin (14) and trypsin (15).

Inactivity of the Proenzyme

Several reasons have been proposed for the relative inactivity of these proenzymes. The question became particularly intriguing when it was found that the active site in chymotrypsinogen appeared to be preformed and accessible, much as it is in chymotrypsin (12; and Figures 1 and 2). The finding of similar structures at the active center would suggest that the ubiquitous basis for the unusual reactivity of the catalytic groups in the enzyme should be present in the proenzyme; that the proenzyme should be catalytically active. Indeed, some reactivity does exist in the proenzyme (9,16), although the catalytic rates for hydrolysis of simple esters are at least 10^4 - 10^7 times lower than for the enzyme. Attention was focused (12) on the substrate binding site, which appeared to be incompletely formed in chymotrypsinogen, although in trypsinogen the binding site for substrate side chains is open and quite large enough to accept the side chain of a normal substrate of trypsin (13; and Figures 3 and 4). It is not at all obvious why a trypsin substrate should not bind to trypsinogen in a mode similar to that found for trypsin, although it is clear that substrate binding is impaired.

Birktoft, Kraut & Freer (17), as the result of a closer look at the comparison between active center structure in the chymotrypsinogen/chymotrypsin pair, proposed that the development of a high degree of strain in the hydrogen bond between His 57 and Ser 195[1] in the enzyme (Figure 2) but not in the proenzyme (Figure 1) may be a further contributor to the reactivity of the enzyme. Yet in the trypsin/trypsinogen comparison such differences are certainly much less apparent if they are present at all (13; and Figures 3 and 4). There are two hydrogen bond donors in the enzyme which may stabilize the high energy transition states during substrate hydrolysis. These are the N—H groups of Gly 193 and Ser 195 (18). The N—H group of Gly 193 is not available for this role in chymotrypsinogen, while in trypsinogen the N—H of Gly 193 still points in the same direction as in trypsin but is moved by 1.9 Å from its site in the enzyme.

Together, it seems that (i) the contribution of correct substrate binding, and (ii) the ability to stabilize the intermediates in catalysis are implicated most strongly as prerequisites for the enzyme to work efficiently. This leaves open the question of how much, if any, small changes in or around the groups that participate most directly in covalent catalysis do contribute to the difference in reactivity of proenzyme and enzyme.

Since there is no clear answer to the question of the basis for such a significant change in the reactivity of proenzyme upon activation (a change which is crucial to the function of the many related serine proteases in a general sense), the status of the structures

and their accuracy and the conditions under which the structures for comparison were determined become particularly important. A summary of these factors is included in Table I. At this stage the trypsin and trypsinogen structures have been subjected to more complete refinement and at a higher resolution than have the corresponding chymotrypsin pair. Indeed, the trypsin structure is probably the best determined of any enzyme structure (15,19). A portion of the most recent electron density map around the active center of DIP-trypsin, obtained by Chambers & Stroud (15), is shown in Figure 5.

The pH-optimum of the enzymes lies between pH 7 and pH 9. The trypsin pair were determined at pH $\sim$ 7, while α-chymotrypsin was initially determined at pH $\sim$ 4.5 where the molecule has low activity and exists mainly as a dimer (20). However, the α-chymotrypsin structure has since been studied up to pH $\sim$ 8.6 by Mavridis, Tulinsky & Liebman (21) who reported a number of significant pH-dependent changes which occur between pH $\sim$ 4.5 and pH 7.5. The fact that the α-chymotrypsin structure crystallized as a dimer is a further factor which must be taken into account in a detailed structure comparison since Tulinsky *et al*. (22) also found the two molecules which form the dimer to be of somewhat different structure within the dimer interface. This is a critical region for this analysis, since it includes the reactive center of α-chymotrypsin.

We therefore consider the trypsin/trypsinogen pair of structures most suitable as the primary basis of comparison between enzyme and proenzyme for the purpose of this review. Further, the comparison

between chymotrypsinogen and trypsinogen should serve to isolate characteristics common to both proenzymes, which will limit the primary reasons for inactivity to the lowest common factor. In this respect, there are real and significant differences between the structures of the two proenzymes. Taking for granted that the enzymes themselves are catalytically active (something which would not be obvious if the structures alone were viewed in the absence of such knowledge), we will compare the two proenzymes emphasizing the question as to why they should be relatively inactive. The answer to this question implies acceptance of the many well-established details of substrate binding and activity summarized, for example, by Blow (23).

This question cannot yet be answered simply. Some of the smallest alterations in structure may be crucial for the answer, while others may be merely consequences of crystal packing forces, etc. Therefore, we first describe the conditions under which the trypsinogen and trypsin structures were determined. It must be noted that both trypsin and α-chymotrypsin were crystallized from high salt solutions, while trypsinogen and chymotrypsinogen were crystallized from ethanol solutions. Trypsin can also be crystallized from ethanol solution.

Trypsinogen structure--Crystals of bovine trypsinogen were obtained by vapor diffusion of a 3% solution of protein against 30% ethanol/water (13). Benzamidine was added to the solution in a

concentration of 2.5 mg/ml to prevent possible trypsin-mediated autolysis of the zymogen during the several weeks required for crystallization. It was essential to eliminate divalent cations from the crystallizing solutions, since they mimic the effects of Ca^{++} and lead to autoactivation and autolysis of the trypsinogen in solution (24). Crystals used for structure determination were grown from solutions adjusted to about pH 7.5, although isomorphous crystals were obtained throughout the pH range 5 - 8. Crystals grown this way were trigonal, space group $P3_121$ with cell parameters $\underline{a}$ = 55.17 Å and $\underline{c}$ = 109.25 Å. The unit cell contains one molecule per asymmetric unit (13).

Trypsin structure--At low pH, DIP-trypsin[2] crystals which were isomorphous with the trypsinogen crystals were obtained. These crystals could be grown at pH 4 - 5.5 from either ethanol/water mixtures or from $MgSO_4$ solutions. At higher pH (5.7 - 8.5) trypsin crystallizes exclusively in the orthorhombic space group $P2_12_12_1$ (15,25,26). The trigonal crystals were found to be unstable above pH 5.5, which suggests that there is some type of structural reorganization which occurs around pH 5.5.

Thus there are three trypsin-related structures used as the basis for comparison between proenzyme and enzyme. The neutral pH, or orthorhombic form of DIP-trypsin--the most highly refined structure--is compared with the neutral pH, trigonal form of trypsinogen. The fact that DIP-trypsin crystallizes at low pH, in a form isomorphous with trypsinogen, is useful in that it provides an accurate means of

assay for structure change between the two molecules by difference Fourier map techniques. These methods can pinpoint differences in structure which are on the same scale or smaller than the average expected errors in atomic coordinates of the refined structures from different crystal forms. Thus, there is an independent means of assay for structure change which is almost independent of the absolute accuracy of the orientation of, for example, a single side chain which may not be accurately placed by the constrained difference Fourier refinement procedures in either structure alone.

There is a further complexity to this comparison, which may be used to advantage. There is a strong possibility that the low pH form of DIP-trypsin has a different structure from the neutral pH form, as does chymotrypsin (21,22). Further, there is the possibility that the low pH trypsin structure is more like trypsinogen in some ways, and thus the difference map procedure would fail to identify any difference between the two proteins at such sites. In fact, the difference map is very clean in many areas where the neutral pH structures appear to be slightly different. However, the activity of the enzyme depends on only a single ionization between pH 2 and pH 8, and this has been identified as the ionization of Asp 102 at the active site (27). Therefore, any pH-dependent structure change which does occur between pH 7 and pH 5 in trypsin is not a change which is reflected in the inherent activity of the enzyme, unless it can be associated directly with Asp 102. Thus, the changes between the isomorphous structures are more likely to pick out the important changes for the change in

catalytic activity, the subject of this review, in a direct way.

Similarities in Structure--The atomic coordinates for DIPT were rotated to match those of Tg by least-squares minimization of the distances between equivalent atoms in the two molecules. Regions of major change in structure, i.e., residues 16-19, 143-152, 186-195, and 215-220, were left out of the rotation calculation, as were residues 76-80 where the differences may be due to errors in the model (13). The histogram shown in Figure 6a points up the distance between all alpha carbons for residues common to both structures after rotation, and clearly identifies the regions of greatest structural change. The mean deviation between equivalent alpha-carbon atoms in the two structures was calculated by leaving out the 32 residues with obviously different structure, and was $\Delta d_{C\alpha} = 0.4$ Å. The difference in conformation of the main chain for all these residues is about the same as for the alpha carbons of the best region (the C-terminal alpha helix) of the Cg/CT comparison (12). The mean deviation of position between all atoms in the main chain and side groups for the same residues of Tg and DIPT was $\Delta d = 0.45$ Å.

Since the two structures are so similar in these regions, the distances presumably represent the sum of errors in the two coordinate sets, coupled with real differences in structure. Most of the differences in side chain orientation for structurally homologous regions occur on the surface of the protein, and are probably not of primary importance for our purpose here.

The Active Center--The structure around the active center of Tg is shown in Figure 3. Crystallographic studies of chymotrypsinogen (12) showed that the orientation and immediate environment of the active site residues, Asp 102, His 57, and Ser 195, were very similar to those found in chymotrypsin. However, a small change in the orientation of Ile 99 permitted limited access of Asp 102 and His 57 to solvent, and the hydroxyl of Ser 214 was not hydrogen bonded to Asp 102 in Cg, raising a question as to the importance of subtle changes in this region for zymogen activation. Similar features are not seen in Tg, where both Leu 99 and Ser 214 ($\Delta d_{C\alpha}$ = 0.27 Å, $\Delta d_{C\alpha}$ = 0.3 Å, respectively) are in identical positions in the zymogen and enzyme, therefore they cannot be common features of the mechanism of activation.

The alpha carbon of Ser 195 differs by only 0.4 Å between Tg and DIPT, although the $O\gamma$ of Ser 195 is still hydrogen bonded to the εN of His 57 (Figure 3) as it is in the benzamidine trypsin structure (28). The Tg/LpT difference map also indicates a small shift in the orientation of the imidazole of His 57 between the two structures. The presence of a DIP group at Ser 195 may be in part responsible for the observed shift of 0.3 Å in the ring. This movement of the imidazole ring is similar to the shift observed previously in a comparison of benzamidine trypsin and DIP-trypsin (28). The fact that Bode and Schwager (19) did not find any such differences between benzamidine trypsin and native trypsin suggests that the presence of the covalently bonded DIP group may be responsible for small differences in

the DIP structure. Nevertheless, no significant movement of the alpha carbon of Ser 195 was observed in DIP-trypsin when compared with benzamidine trypsin.

The change in position of Cα Ser 195 seen in Tg may be of some importance for the relative inactivity of trypsinogen. It lies at the end of the sequence of residues 186-195, which all occupy different positions in Tg and DIPT as they do in the comparison of Cg with CT.

Birktoft, Kraut & Freer (17) observed a striking difference between the structures of CT and Cg in the active center. They defined an "ideal" site for the Oγ of Ser 195 relative to the side chain of His 57. This was chosen to lie 2.8 Å away from the εN of His 57 and in the direction of the $\underline{sp}^2$ orbital of the εN. While they found that the Oγ of Ser 195 was within 0.7 Å of this site in Cg, it could not be brought closer than about 2.5 Å to this site in CT by any manipulation of these side chain orientations (17). They raised the question of whether a strained hydrogen bond at this site in the enzyme could contribute to enhanced catalytic efficiency. The Oγ of Ser 195 in Tg and in DIPT (where the Oγ is covalently bonded to the DIP group) are not so dramatically different. Although the actual position of the Oγ differs by almost 1 Å between these structures, the Oγ lies at 0.7 and 1.1 Å, respectively, away from the "ideal" position, and it is not clear that this difference is enough to account for any significant contribution of distortion at this site to the catalytic mechanism. Birktoft, Kraut & Freer (17) have also identified other quite large differences between CT and Cg in this region of interface between the

two "structural cylinders" (14) of CT. We see no corresponding difference in the Tg-DIPT comparison. Perhaps the fact that the CT structure existed as a dimer is in part responsible for alteration in the structure of α-chymotrypsin, relative to the neutral pH form of the enzyme?

This does not rule out the possibility that even a small change in the active center structure could contribute to the generation of enzyme activity, but at present there is no common factor which can be identified.

The Side Chain Binding Pocket--Freer et al. (12) questioned whether the absence of a specific binding pocket could explain the inactivity of Cg. Trypsinogen has a large and accessible binding pocket (see Figure 3), although the structure of the cavity is different from that found in DIPT or in benzamidine trypsin (see Figure 4).

Benzamidine is a competitive inhibitor of trypsin (K_i = 1.8 x 10^{-5} M) (29), which binds inside the side-chain specific binding pocket of the enzyme (19,28). Benzamidine was present at 20 mM concentration (at least 10^3 times the K_i for trypsin) in the trypsinogen crystallizing solution, yet there was no benzamidine bound to the proenzyme in the Tg structure. This emphasizes the fact that the structure for the binding site, as seen in the crystals, represents a functionally significant impediment to the binding capabilities of the site for benzamidine, which is an analog of the side chain of a substrate for trypsin. The binding constant for benzamidine binding

to trypsinogen in solution was found to be about 10^5 times larger than for binding to trypsin (30). The binding site seen in the Tg structure is large enough to accept a benzamidine molecule, and the fact that none was found implies that the differences between zymogen and enzyme structures (as shown in Figures 3 and 4) are quite adequate to account for a large change in specificity.

A relatively large movement of the backbone chain from residues 187 to 194 in the Cg/CT comparison was correlated with the formation of the specific binding site for substrate side chains in CT, a cavity which was only partially formed in Cg (12). There are much smaller but significant changes between Tg and DIPT (or LpT) in the chain from residues 188A - 195. The migration of Met 192 from a completely buried position (in the site occupied by the ion pair between Ile 16 and Asp 194) in Cg to the outside of the CT molecule also has no comparable counterpart in the Tg/LpT comparison. The alpha carbon of Gln 192 in Tg moves by 0.9 Å on activation. The side chain of Gln 192 moves by about 4 Å. The side chain of Asp 189 inside the specific binding pocket of trypsin and responsible for the substrate specificity of trypsin lies within 0.9 Å of the position found in Tg, $\Delta d_{c\alpha 189}$ = 0.9 Å. Thus, it would seem that modification rather than generation of the specific cavity must be considered as a possible reason for zymogen inactivity in general.

Studies of the residual activity of trypsinogen have generally been carried out on simple esters where hydrogen bonds to the main chain of 214 - 219 are not made. For NPGB hydrolysis by Tg the

binding constant was found to be at least 10^3 times worse than for trypsin (31). Changes in the binding pocket structure could well be responsible for some or all of this poorer binding.

Residues 214-220--In Cg changes occurred in the main chain between Ser 214 and Cys 220, a region known to be involved in hydrogen bonding to a peptide substrate (32-35). In Tg the chain structure differs slightly from trypsin as shown in Figure 3. The C=O of Ser 214 (Δd = 0.3 Å) and the N—H (Δd = 0.5 Å) and C=O (Δd = 1.4 Å) of Gly 216 still point in the same direction. The peptide bond between Gly 219 and Cys 220 is apparently rotated by 180° with respect to trypsin at neutral pH (DIPT). There is a difference in residues 214 - 217 of Cg in that the N—H and C=O of Gly 216 would be unable to participate in substrate binding (12). This and the other differences in binding site structure between Cg and Tg are not inconsistent with the fact that the basic pancreatic trypsin inhibitor (BPTI) will form a stoichiometric, 1:1 complex with trypsinogen and with trypsin or chymotrypsin, but will not so complex with chymotrypsinogen (36).

There was an error in the original placement of the side chain of Trp 215 in DIPT (Figure 8 of reference 28). Refinement of that structure revealed that the indole ring is reversed, such that εN points in toward the center of the molecule (15). The same configuration is found in Tg. This orientation is the same as that found in CT (14). Modification of Trp 215 in trypsinogen blocks the binding of BPTI by trypsinogen (37).

Asp 194--The side chain of Asp 194 forms a salt bridge with Ile 16 in trypsin. The N-terminal of Ile 16 is not available in Tg, since it lies in the zymogen activation peptide. Asp 194 is in a similar orientation inside the trypsinogen molecule, although the alpha carbon is moved by $\Delta d = 0.9$ Å. The side chain is surrounded by internal solvent molecules. There appears to be only one intramolecular hydrogen bond to Asp 194 in Tg between the $O\delta$-1 of Asp 194 and the $O\gamma$ of Ser 190. The side chain of Asn 143 (in Tg) points in toward the solvent cavity around Asp 194 (see Figures 7 and 8).

Freer et al. (12) postulated that interaction between Arg 145 and Asp 194 could contribute to charge stabilization of the carboxyl group of Asp 194 in Cg--possibly through water molecules. In a more detailed analysis Wright (38,39) found that the guanidine group of Arg 145 was too far from Asp 194 to participate directly in this role, but could neutralize the charged carboxyl via water molecules hydrogen bonded to the δN of His 40. The εN of His 40 was found to be 3.5 Å from the carboxyl group of Asp 194, and so was indirectly implicated as providing a possible pathway for proton transfer from the surface of the molecule to the buried carboxyl group (see Figure 9).

In Tg neither Lys 145 nor His 40 lies close to the side chain of Asp 194, and therefore cannot be involved in stabilizing Asp 194. The side chain of Lys 145 is on the outside of the molecule and the ζN of Lys 145 is about 10 Å from Asp 194. Indeed, there is no basic side chain close enough to contribute directly to charge neutralization of Asp 194. His 40 is found in the same orientation in Tg as in LpT, and

almost exactly the same as in DIPT ($\Delta d_{C\alpha}$ = 0.4 Å). The Nδ-1 of His 40 is hydrogen bonded to the Oγ of Ser 32 in both Tg and DIPT (and CT, but not in Cg). Nε-2 of His 40 is hydrogen bonded to the C=O of Gly 193 in DIPT and CT, but is hydrogen bonded to an external solvent molecule in Tg. This change corresponds to the movement of the Cα of 194 (Δd = 0.9 Å) and 193 (Δd = 2.0 Å) toward the solvent-filled cavity around Asp 194. Wright (39) emphasized the apparent conservation of a basic group at residue 145 of the trypsin-like enzymes, although there are now exceptions in the sequences of dogfish trypsin (where the residue is methionine), and in all the bacterial enzymes (40,41). His 40 is also not a conserved residue among trypsin-like enzymes, and is Leu in bovine thrombin, Gly in blood-clotting factor X, and Met, Arg or Leu in bacterial trypsin sequences (41).

The "Autolysis Loop" (Residues 142-151)--The largest conformational difference between Tg and DIPT or LpT occurs between residues 142 - 151. This sequence was referred to as the "autolysis loop" (42) since it contains a region where two amino acids are excised in α-chymotrypsin. The difference map between Tg and LpT (Tg-LpT) showed clear negative density which picked out the conformation of the autolysis loop in LpT. There was much less (∿ 50%) positive density in the map for this part of the chain, establishing that the chain is flexible in Tg and adopts a quite different conformation there. (The LpT structure was identical to that of DIPT in this region.) A further change in the structure of this loop or of Lys 15 - Ile 16 would be

required if an activating enzyme were to approach the Lys 15 - Ile 16 bond in the Tg conformation.

Trp 141 is essentially in the same orientation in Tg as found in DIPT ($\Delta d_{C\alpha}$ = 0.6 Å). The side chain of Asn 143, which was solvent accessible in DIPT, points in toward the cavity around Asp 194 in Tg ($\Delta d_{C\alpha}$ = 1.4 Å). The side chain of Thr 144 (Tg) is moved by several angstroms toward the disulfide Cys 191 - Cys 220 ($\Delta d_{C\alpha} \simeq 4.0$ Å), and residues 145 - 151 are in quite different conformation in the two structures. They are all solvent accessible in both Tg and DIPT. There may be a functional correlation between the loose structure of this chain in the zymogen, and the necessity for access of the activating enzyme to the Lys 15 - Ile 16 bond. The sequences for residues 146 - 154 are extremely variable in related enzymes (41), and no specific roles can be assigned to any of the side chains of these residues in trypsinogen, as judged from the Tg structure.

The Effect of Divalent Cations on Trypsinogen--There are two calcium ion binding sites in trypsinogen. The primary site, with higher affinity for calcium ion ($K_D \sim 10^{-3.2}$ M, (43)), is common to both trypsinogen and trypsin. Occupancy of this site stabilizes the protein toward thermal denaturation or autolysis (24). The primary Ca^{++} binding site in trypsin was first identified and described in detail by Bode and Schwager (44) based on analysis of an independently refined trypsin structure seen at 1.8 Å, and the Ca^{++} content of their crystals. The difference map calculated between the isomorphous

crystals of Tg and LpT showed no electron density in the Ca^{++} region. Therefore, the primary calcium ion binding site in trypsinogen and low pH trypsin are identical. There are small differences between this Ca^{++} site in Tg and DIPT (13).

A secondary Ca^{++} ion binding site of $K_D \sim 10^{-1.8}$ M exists only on the zymogen. Binding of Ca^{++} at this site is essential for complete and efficient activation of trypsinogen (24), and this site is more pertinent to the subject of this review. The effect of binding is to improve the substrate character of the activation peptide, so favoring tryptic hydrolysis of the Lys 15 - Ile 16 peptide bond. (K_m decreases by a factor of three while k_{cat} remains unchanged (43).) Tryptic hydrolysis of the nonapeptide Val-$(Asp)_4$-Lys-Ile-Val-Gly, and of the hexapeptide Val-$(Asp)_2$-Lys-Ile-Val, have been shown to be Ca^{++} dependent in a very similar way, while hydrolyses of peptides containing only one aspartate do not depend on Ca^{++} (43,45). Ca^{++} ion binding to Asp 13 and Asp 14 together is thus sufficient to explain the zymogen Ca^{++} ion effect (43). There is as yet no corroborative crystallographic evidence for binding at this site since Ca^{++} was excluded from the trypsinogen solution.

The overall weak electron density for much of the N-terminal hexapeptide of trypsinogen must be attributed to local disorder of loosely organized structure rather than to phasing error. This conclusion is implied by the trypsinogen/DIP-trypsin difference map computed using phases for trypsinogen. In regions where there is difference in structure, this map should show a positive density image

for trypsinogen, and a somewhat weaker negative image for trypsin. Yet, the positive density for trypsinogen residues 10 - 15 was consistently much lower in amplitude than the negative images for trypsin structure.

The loose arrangement of this hexapeptide on the surface of the proenzyme is consistent with the finding that the synthetic nonapeptide Val-$(Asp)_4$-Lys-Ile-Val-Gly is hydrolyzed by trypsin at almost the same rate ($k_{cat} \sim 10^{-3}$ sec^{-1}) as the Lys - Ile bond on the same sequence in Tg for which $k_{cat} = 2.5 \times 10^{-3}$ sec^{-1} (43). Thus, it is clear that the slow hydrolysis of the Lys - Ile bond by trypsin, a factor which is important in preventing premature activation of all trypsinogens, does not depend on any unique tertiary structure of these residues. The four aspartates are all available to modification by carbodiimides, and such modification does not destroy activatibility of trypsinogen (46). This is in agreement with our finding that the Val 10 - Asp 14 sequence is not a determinant of tertiary structure (13). The binding of Ca^{++} to Asp 13 and Asp 14 is probably independent of the protein structure as an ion specific conformer, and is adequately explained by an induced structural change in the peptide (10 - 15) alone, or by neutralization of charge at Asp 13 and Asp 14.

There is a clear necessity for trypsinogen among all pancreatic zymogens to develop immunity to autolysis or activation by its own residual activity, since it activates other zymogens. The loosely structured hexapeptide is presumably protected against trypsin more

by its negative charge than by tertiary structure. The hexapeptide sequence also provides a good substrate character for the physiological activator, enterokinase (47). The hexapeptide, with its dual role as most favored substrate for enterokinase, and a poor but still most favored substrate site for activation by trypsin, is highly conserved throughout all species (41). The Lys 15 - Ile 16 bond is not inaccessible, although some reorientation of this chain or of the autolysis loop must accompany enzyme binding to this site. The fact that this bond is still the most readily hydrolyzed by trypsin in the presence of Ca^{++} ions is consistent with the fact that compact native structures are generally more resistant to degradation than are denatured ones. The ϕ and ψ angles on either side of Lys 15 are not dissimilar to those found for the susceptible Lys 15 bond on the trypsin inhibitor (a good substrate model). Since it is clearly proven that both this chain and the neighboring autolysis loop have little to restrain their configuration, the reorientation necessary for access by the activating enzyme should be energetically easy to accomplish.

In many of the trypsin-like enzymes involved in biological control mechanisms, the primary activating cleavage occurs at a site analogous to the Lys 15 - Ile 16 bond with respect to the catalytic component of the protein. This split may be far from the N-terminal of the whole protein since the activation peptides, or proteins released, often have separate functions (11). In prothrombin, for example, the activating cleavage occurs between residues Arg 323 and

Ile 324 in the sequence. The B-chain (residues 324 - 582) is highly homologous with trypsin, while the A-chain, which remains attached to the B-chain via a disulfide bridge, is thought to have an important role in the blood-clotting mechanism (48).

The Reasons for Zymogen Inactivity--Freer et al. (12) and later Wright (39) identified four possible factors which might be responsible for inactivity of chymotrypsinogen. We now see that three of them do not seem to be shared by trypsinogen, since (in Wright's notation): (i) the binding site of trypsinogen is open and accessible while it is not quite so open in chymotrypsinogen; (ii) the potential source of a hydrogen bond from Gly 216 NH is not excluded, although this group is moved by 0.5 Å from its "substrate binding" position in the free enzyme; and (iii) the side chain of Gln 192 occupies a fairly innocuous position outside the trypsinogen molecule, whereas the corresponding Met 192 of chymotrypsinogen was shown to undergo a complete reorganization upon activation. The remaining reason was the lack of an important hydrogen-bonding group in the N—H of Gly 193. It has been pointed out that the N—H groups of Gly 193 and of Ser 195 could play an important catalytic role in stabilization of reaction intermediates (18,49,50). In chymotrypsinogen the N—H of Gly 193 points away from the position for the carbonyl oxygen of the substrate (12). In trypsinogen the N—H of Gly 193 and of Ser 195 both point toward a site not dissimilar to that found in trypsin and chymotrypsin. Nevertheless, this site termed the "oxyanion hole" by Robertus et al.

(18) is removed by 1.9 Å from the position of the site in trypsin. Thus, oxyanion stabilization is possible in trypsinogen, but not at the ideal site. The loss of this component of the catalytic apparatus may well account for the slower reaction rate of the zymogen. There is a plausible connection between the movement of this site away from the cavity which is subsequently occupied by Ile 16 upon activation, when Ile 16 forms the salt bridge to Asp 194. There is also plausible connection between the small changes in the binding pocket, and the location of Ile 16. Similar change in the structure of the binding site could account for the poorer binding of substrate by the zymogens in general.

Conclusion

The structure of trypsinogen is generally much closer to that of trypsin than is chymotrypsinogen to chymotrypsin. The structure of trypsinogen does not exclude the possibility of substrate binding in a mode similar to that found for trypsin, although changes in the structure of this region contribute to an impaired or altered substrate binding mode--certainly for benzamidine, and most probably for a substrate side chain. If the proenzyme is considered to be rigid, then the general base catalyst (the εN of His 57) and the oxyanion binding site formed by the N—H groups of Gly 193 and Ser 195 are too far apart to cooperate in substrate hydrolysis. Even if the proenzyme structure were to change on substrate binding, as seems likely,

nonproductive binding may provide another important component for zymogen inactivity. Such binding might still leave too great a distance, or an unfavorable interaction, between the substrate and elements of the catalytic center. The altered position of the chain between Lys 188A and Ser 195, and the main chain between Trp 215 and Ser 217, could be responsible for competitive yet nonproductive substrate binding, as could the N—H group of Gly 193, since they are normally involved in orienting the substrate. These possibilities remain as prime candidates in a universal scheme for inactivity of the trypsinogen-like zymogens.

Acknowledgments

We thank Melvin Jones and Rebecca Price for assistance with calculations used in the comparison of structures. We gratefully acknowledge the support received from research grants from the National Institutes of Health and the National Science Foundation. One of us (RMS) is the recipient of a National Institutes of Health Career Development Award, another (AAK) was the recipient of a National Institues of Health Postdoctoral Fellowship, and another (JLC) holds a National Institutes of Health Predoctoral Traineeship.

This is contribution #5445 from the Norman W. Church Laboratory of Chemical Biology, California Institute of Technology.

References

1. Neurath, H. 1957. Adv. Protein Chem. 12:320-86.
2. Ottesen, M. 1967. Ann. Rev. Biochem. 36:55-76.
3. Neurath, H. 1975. In Cold Spring Harbor Symposium on Proteases and Biological Control, eds. E. Reich, D.B. Rifkin, E. Shaw, pp. 51-64. New York: Cold Spring Harbor Laboratory. 1021 pp.
4. Leighton, T.J., Doi, R.E., Warren, R.A.J., Kelln, R.A. 1973. J. Mol. Biol. 76:103-22.
5. Stambaugh, R., Brackett, B., Mastroianni, L. 1969. Biol. Reprod. 1:223-27.
6. Muller-Eberhard, H.J. 1969. Ann. Rev. Biochem. 38:389-414.
7. Owren, P.A., Stormorken, H. 1973. Ergeb. Physiol. Biol. Chem. Exp. Pharmakol. 68:1-53.
8. Magnusson, S. 1971. In The Enzymes, ed. P.D. Boyer, 3:277-321. New York: Academic Press. 886 pp.
9. Kay, J., Kassell, B. 1971. J. Biol. Chem. 246:6661-65.
10. Hartley, B.S. 1960. Ann. Rev. Biochem. 29:45-72.
11. Walsh, K.A. 1975. In Cold Spring Harbor Symposium on Proteases and Biological Control, eds. E. Reich, D.B. Rifkin, E. Shaw, pp. 1-11. New York: Cold Spring Harbor Laboratory. 1021 pp.
12. Freer, S.T., Kraut, J., Robertus, J.D., Wright, H.T., Xuong, Ng. H. 1970. Biochemistry 9:1997-2009.
13. Kossiakoff, A.A., Chambers, J.L., Kay, L.M., Stroud, R.M. 1976. Biochemistry 16:654-64.

14. Birktoft, J.J., Blow, D.M. 1972. J. Mol. Biol. 68:187-240.

15. Chambers, J.L., Stroud, R.M. 1976. Acta Crystallogr.--in press.

16. Morgan, P.H., Robinson, N.C., Walsh, K.A., Neurath, H. 1972. Proc. Nat. Acad. Sci. USA 69:3312-16.

17. Birktoft, J.J., Kraut, J., Freer, S.T. 197 . Biochemistry 15:4481-85.

18. Robertus, J.D., Kraut, J., Alden, R.A., Birktoft, J.J. 1972. Biochemistry 11:4293-4303.

19. Bode, W., Schwager, P. 1975. J. Mol. Biol. 98:693-717.

20. Sigler, P.B., Blow, D.M., Matthews, B.W., Henderson, R. 1968. J. Mol. Biol. 35:143-64.

21. Mavridis, A., Tulinsky, A., Liebman, M.N. 1974. Biochemistry 13:3661-66.

22. Tulinsky, A., Vandlen, R.L., Morimoto, C.N., Mani, N.V., Wright, L.H. 1973. Biochemistry 12:4185-92.

23. Blow, D.M. 1974. Israel J. Chem. 12:483-94.

24. Northrop, J.H., Kunitz, M., Herriot, R.M. 1948. Crystalline Enzymes, pp. 133-6. New York: Columbia University Press. 352 pp.

25. Stroud, R.M., Kay, L.M., Dickerson, R.E. 1971. Cold Spring Harbor Symposium on Quantitative Biology 36:125-40.

26. Stroud, R.M., Kay, L.M., Dickerson, R.E. 1974. J. Mol. Biol. 83:185-208.

27. Koeppe, R.E., Stroud, R.M. 1976. Biochemistry 15:3450-57.

28. Krieger, M., Kay, L.M., Stroud, R.M. 1974. J. Mol. Biol. 83:209-30.

29. Mares-Guia, M., Shaw, E. 1965. J. Biol. Chem. 240:1579-85.

30. Gertler, A., Walsh, K.A., Neurath, H. 1974. Biochemistry 13:1302-10.

31. Robinson, N.C., Neurath, H., Walsh, K.A. 1973. Biochemistry 12:420-5.

32. Segal, D.M., Powers, J.C., Cohen, G.H., Davies, D.R., Wilcox, P. E. 1971. Biochemistry 10:3728-38.

33. Sweet, R.M., Wright, H.T., Janin, J., Chothia, C.H., Blow, D.M. 1974. Biochemistry 13:4212-28.

34. Huber, R., Kukla, D., Bode, W., Schwager, P., Bartels, K., Deisenhofer, J., Steigemann, W. 1974. J. Mol. Biol. 89:73-101.

35. Blow, D.M. 1974. In Bayer-Symposium V "Proteinase Inhibitors", eds. H. Fritz, H. Tschesche, L.J. Greene, E. Truscheit, pp. 473-483. New York: Springer-Verlag. 751 pp.

36. Dlouha, V., Keil, B. 1969. FEBS Letters 3:137-40.

37. Keil-Dlouha, V., Keil, B. 1972. J. Mol. Biol. 67:495-505.

38. Wright, H.T. 1973a. J. Mol. Biol. 79:1-11.

39. Wright, H.T. 1973b. J. Mol. Biol. 79:13-23.

40. Bradshaw, R.A., Neurath, H., Tye, R.W., Walsh, K.A., Winter, W.P. 1970. Nature 226:237-9.

41. DeHaen, C., Neurath, H., Teller, D.C. 1975. J. Mol. Biol. 92:225-59.

42. Blow, D.M., Birktoft, J.J., Hartley, B.S. 1969. Nature 221:337-40.

43. Abita, J.P., Delaage, M., Lazdunski, M., Savrda, J. 1969. Eur. J. Biochem. 8:314-24.

44. Bode, W., Schwager, P. 1975. FEBS Letters 56:139-43.

45. Delaage, M., Desnuelle, P., Lazdunski, M., Bricas, E., Savrda, J. 1967. Biochem. Biophys. Res. Commun. 29:235-40.

46. Radhakrishnan, T.M., Walsh, K.A., Neurath, H. 1967. J. Amer. Chem. Soc. 89:3059-61.

47. Maroux, S., Baratti, J., Desnuelle, P. 1971. J. Biol. Chem. 246:5031-39.

48. Magnusson, S.L. 1975. In Cold Spring Harbor Symposium on Proteases and Biological Control, eds. E. Reich, D.B. Rifkin, E. Shaw, pp. 123-49. New York: Cold Spring Harbor Laboratory. 1021 pp.

49. Steitz, T.A., Henderson, R., Blow, D.M. 1969. J. Mol. Biol. 46:337-48.

50. Henderson, R. 1970. J. Mol. Biol. 54:341-54.

Footnotes

[1]Numbering scheme used will be that of chymotrypsinogen throughout the manuscript.

[2]Abbreviations used: DIP-trypsin, diisopropylphosphoryl trypsin; NPGB, p-nitrophenyl-p'-guanidinobenzoate; Tg, trypsinogen; DIPT, DIP-trypsin; LpT, low pH DIP-trypsin; CT, chymotrypsin; Cg, chymotrypsinogen; BPTI, basic pancreatic trypsin inhibitor.

TABLE I. Summary of corresponding zymogen and enzyme structures used for comparison in the text.

Structures	Resolution (Å)	State of Refinement[1]
α-Chymotrypsin[2,3] tosyl-, pH 4.2	2.0	R 43%
Chymotrypsinogen[4,5], pH 6.3	2.5	R 43%
Trypsin		
DIP-[4,6,7], pH 5.0	2.1	
DIP-[6,8], pH 7.5	1.5	R = 23%
Benzamidine[2,9], pH 7.0	1.8	R = 23%
Trypsinogen[4,10], pH 7.5	1.9	R = 31%

[1]State of refinement is indicated as the value of $R = \Sigma|F_o-F_c|/\Sigma F_o$, representing the agreement between observed and calculated structure factors to the resolution indicated.

[2]Crystallized from ammonium sulphate.

[3]Model building; real space and energy refinement (14).

[4]Crystallized from ethanol.

[5]Calculated phases; rebuilt model (12,17).

[6]Crystallized from magnesium sulphate.

[7]Difference Fourier versus trypsinogen (13).

[8]Constrained difference Fourier refinement (15).

[9]Constrained difference Fourier refinement (19).

[10]Constrained difference Fourier refinement (13).

Figure Legends

FIGURE 1. The structure around the active center in chymotrypsinogen. Coordinates were those obtained from the Brookhaven Protein Data Bank (12). The orientation of this view differs from that in succeeding figures.

FIGURE 2. Structure around the active center in α-chymotrypsin (14).

FIGURE 3. The structure around the active center in trypsinogen (13).

FIGURE 4. Structure around the active center in DIP-trypsin (15). The DIP group has been omitted for clarity.

FIGURE 5. A portion of the electron density map for DIP-trypsin in the region of the active center (15).

FIGURE 6. (a) Histogram showing the distance Δd (Å) between equivalent alpha-carbon atoms in Tg and DIPT after the two coordinate sets have been rotated and translated to achieve optimum superposition of the two coordinate sets. (b) Histogram showing the average positional difference of all atoms within each residue of the Tg/DIPT comparison.

FIGURE 7. Structure of trypsinogen in the region of His 40. The Nδ-1 of His 40 is hydrogen bonded to the Oγ of Ser 32 as it is in trypsin. The C=O of Gly 193 is moved from its position in trypsin. Asp 194 adopts a similar conformation to that seen in trypsin (13).

FIGURE 8. The structure of trypsin in the region of His 40 shows the hydrogen bond formed between Nδ-1 of His 40 and the Oγ of Ser 32, and the hydrogen bond between the Nε-2 of His 40 and the C=O of Gly 193. Asp 194 is salt bridged to the amino terminal of Ile 16 (15).

FIGURE 9. The chymotrypsinogen structure around His 40 and Asp 194 shows a closer interaction between these two groups, which are in quite different orientation than that seen in trypsin or trypsinogen. Coordinates were obtained from the Brookhaven Protein Data Bank (12).

Figure 1

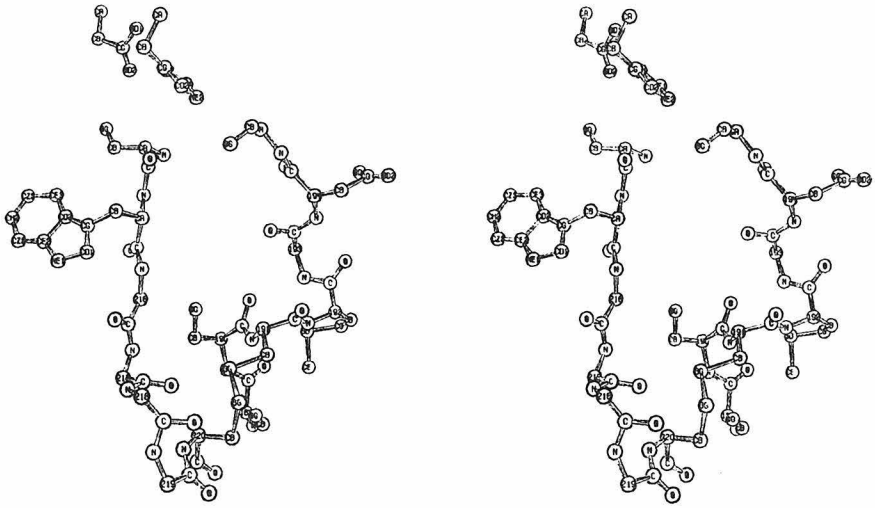

Figure 2

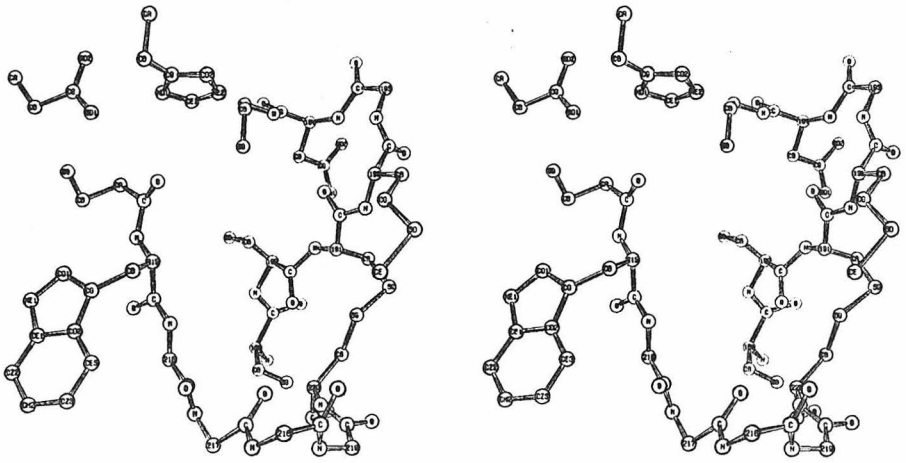

Figure 3

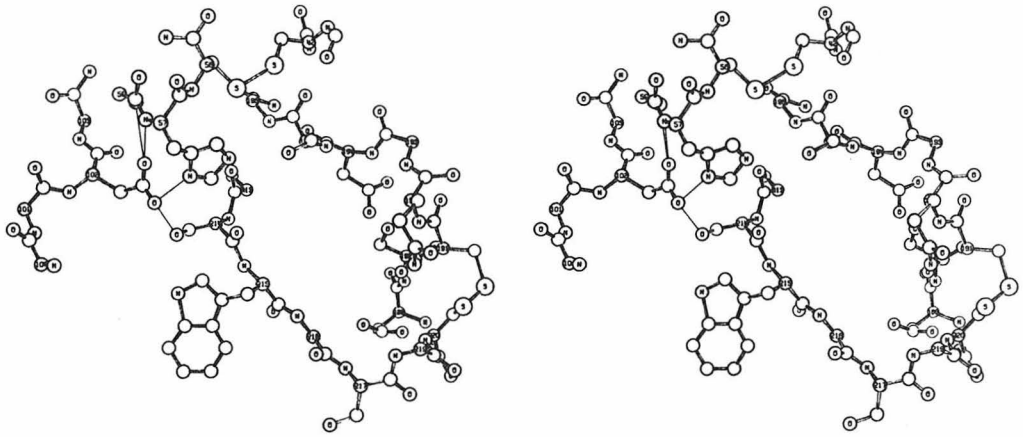

Figure 4

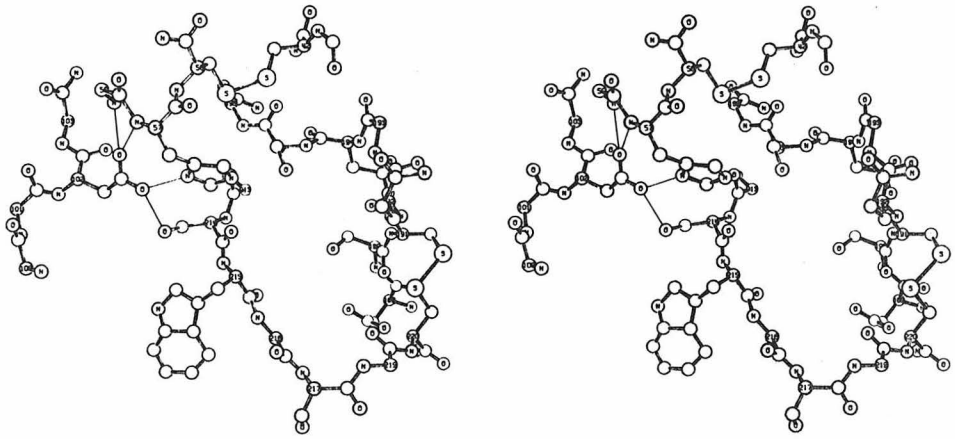

Figure 5

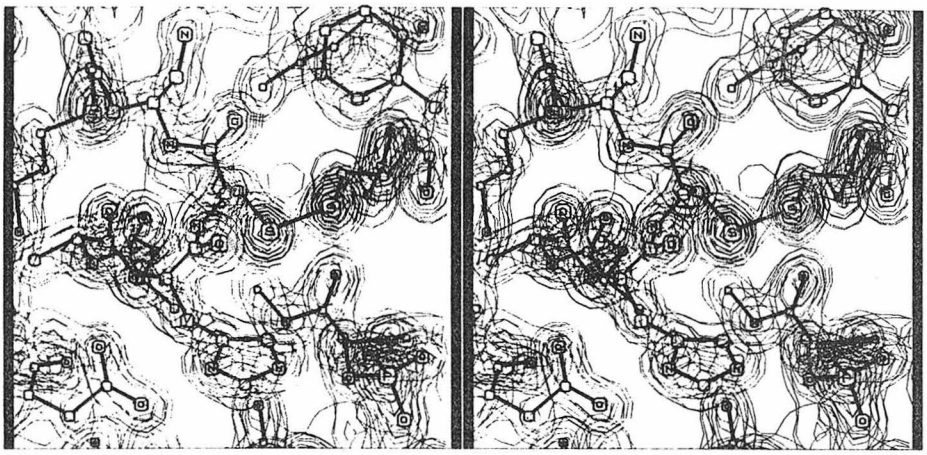

Figure 6a

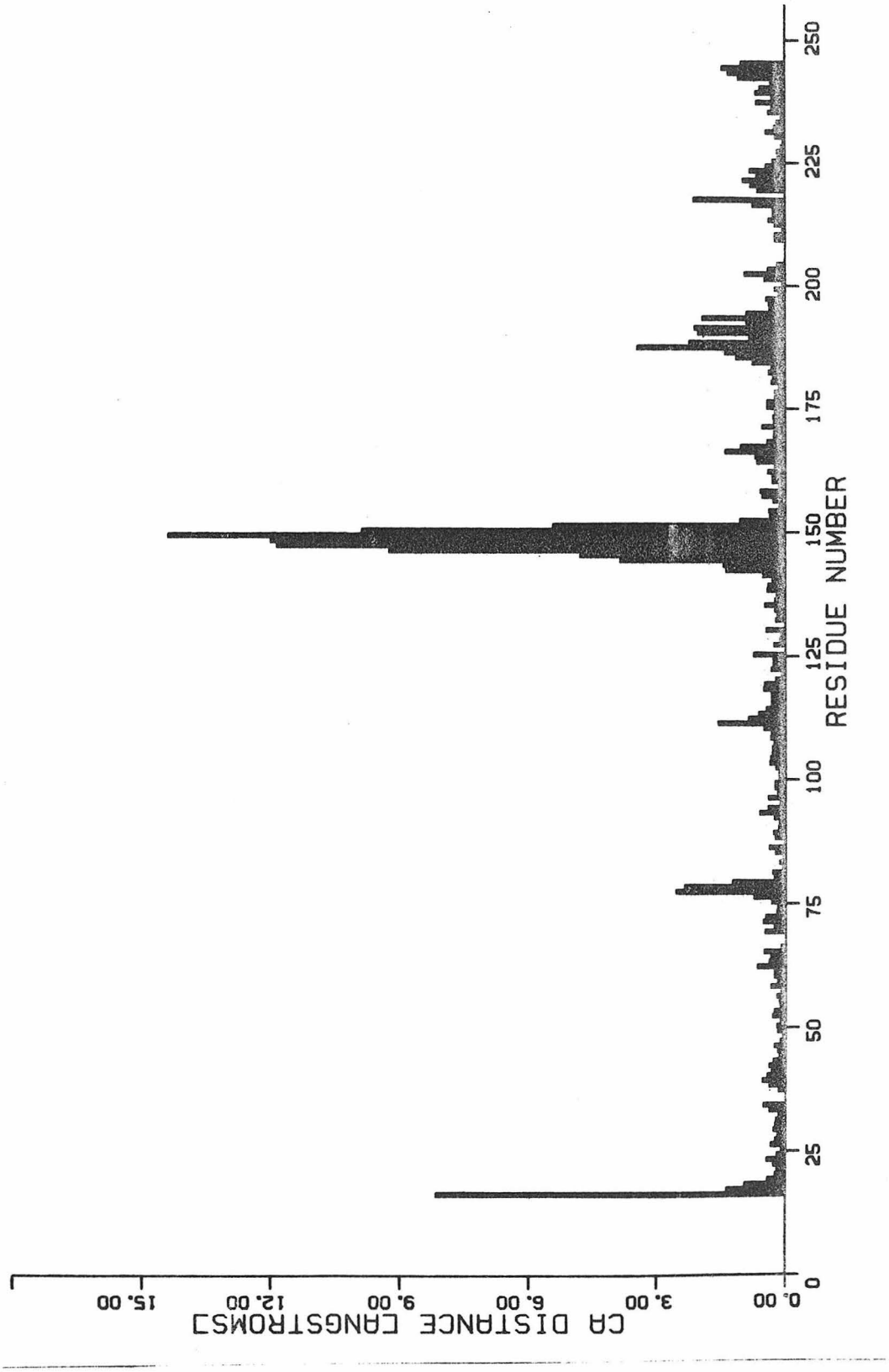
CA DISTANCE (ANGSTROMS)
0.00
3.00
6.00
9.00
12.00
15.00
0
25
50
75
100
125
150
175
200
225
250
RESIDUE NUMBER

Figure 6b

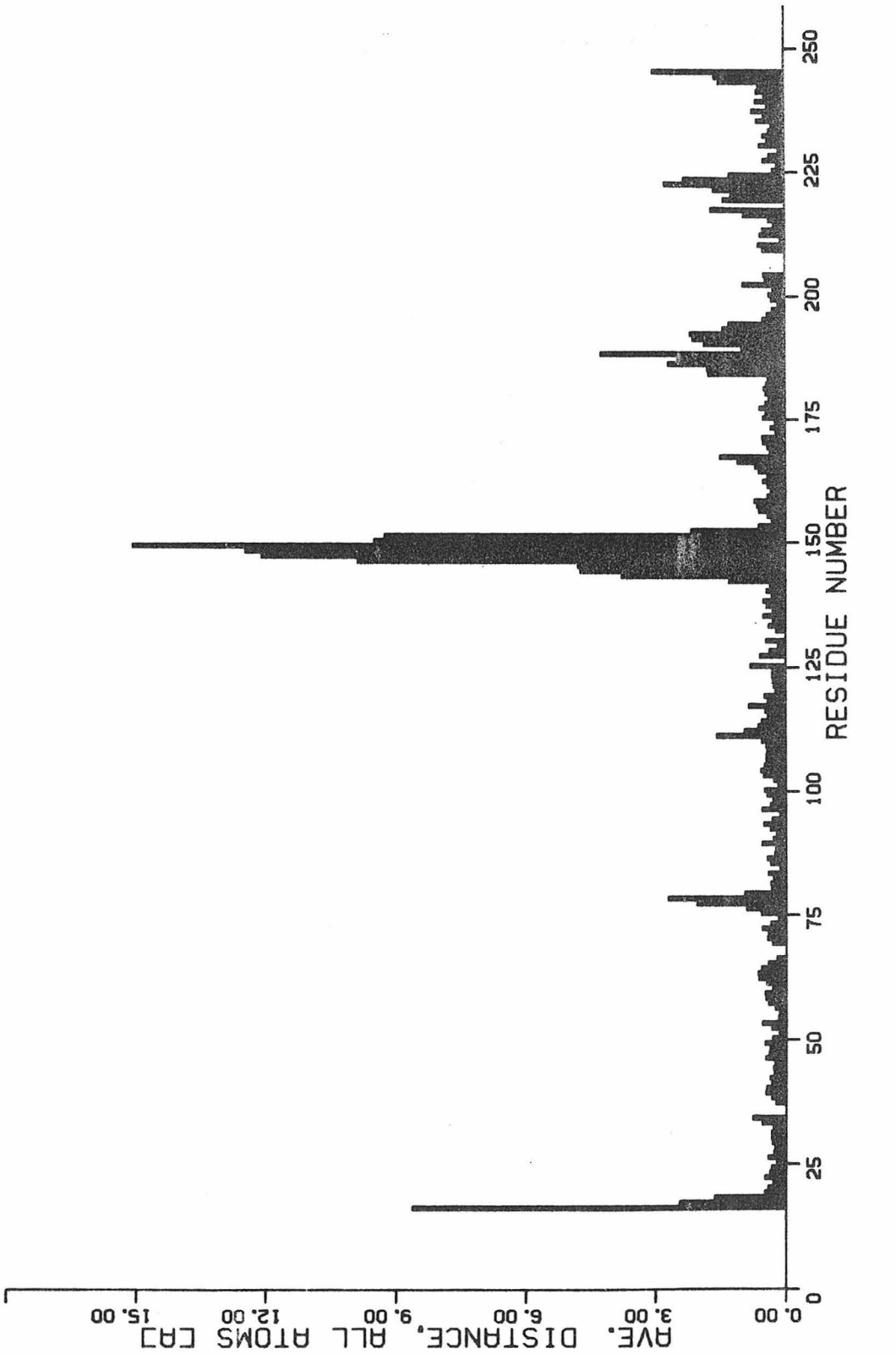
AVE. DISTANCE, ALL ATOMS CAJ
0.00
3.00
6.00
9.00
12.00
15.00
0
25
50
75
100
125
150
175
200
225
250
RESIDUE NUMBER

Figure 7

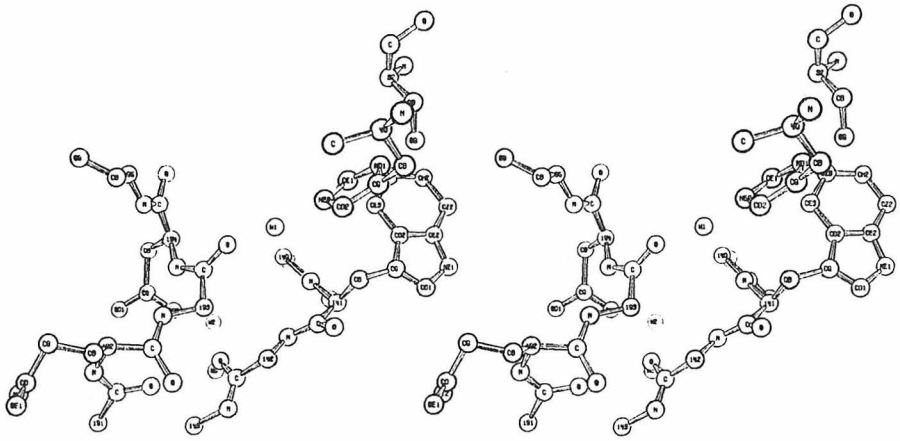

Figure 8

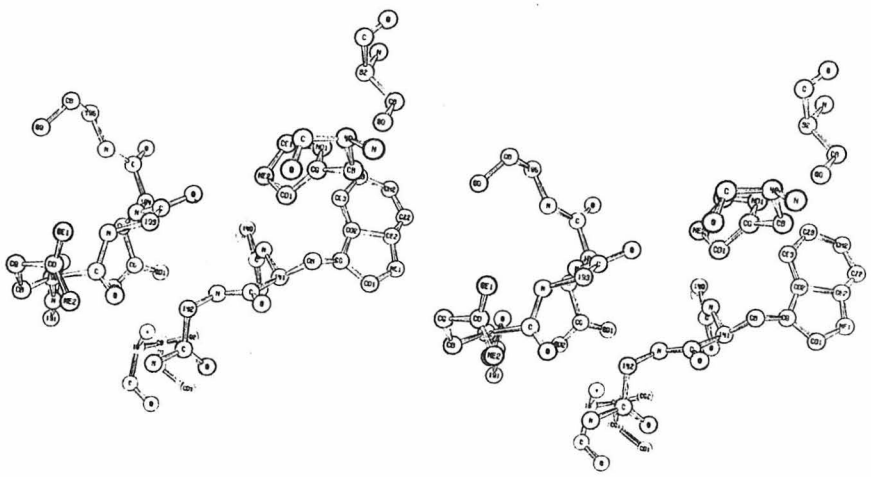

Figure 9

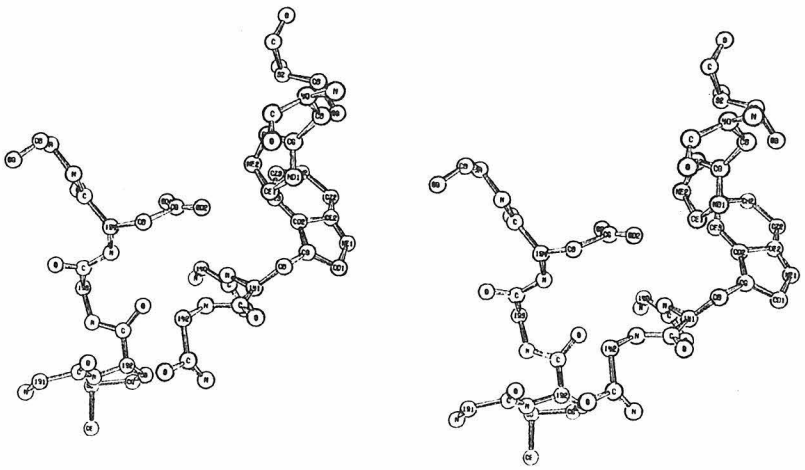

Appendix 6

Difference Fourier Refinement of the Structure of DIP-Trypsin at 1.5 Å With a Minicomputer Technique

Difference Fourier Refinement of the Structure of DIP-Trypsin at 1.5 Å With a Minicomputer Technique*

JOHN L. CHAMBERS† AND ROBERT M. STROUD‡

Norman W. Church Laboratory of Chemical Biology
California Institute of Technology
Pasadena, California 91125, U.S.A.

(Acta Crystallogr.---in press)

Running Title: 1.5 Å Refinement of DIP-Trypsin.

---

*Contribution #5352. Supported by National Institutes of Health grant GM-19984 and National Science Foundation grant BMS75-01405.

†National Institutes of Health Predoctoral Trainee.

‡National Institutes of Health Career Development Awardee, U.S. Public Health Service Grant GM-70469.

ABSTRACT

The x-ray crystal structure of diisopropylfluorophosphate-inhibited bovine trypsin has been refined to a resolution of 1.5 Å with the use of a constrained difference Fourier technique. The refinement was carried out almost entirely on a minicomputer with a set of programs written for this study to largely automate the refinement procedure. Use of the minicomputer has allowed the refinement to progress efficiently at an extremely low cost, from a starting R-factor of 47.2% at 2.7 Å resolution to 27.7% at 1.5 Å resolution. Two cycles of a least-squares refinement procedure using a first-order gradient minimization have since reduced R to 23.5% at 1.5 Å resolution. The refined model and electron density maps are substantially improved over the starting ones. The methods described may be very attractive when computing funds or access to a large computer are limited.

INTRODUCTION

During the past few years a number of protein structures determined by x-ray crystallography have been refined to 2 Å or better resolution using a variety of techniques (Watenpaugh, Sieker, Herriot, and Jensen, 1973; Sayre, 1974; Diamond, 1974; Huber, Kukla, Bode, Schwager, Bartels, Deisenhofer, and Steigemann, 1974; Freer, Alden, Carter, and Kraut, 1975; Moews and Kretsinger, 1975; Deisenhofer and

Steigemann, 1975; Bode and Schwager, 1975a). The refinement programs written by Diamond (1966, 1971) are particularly effective and are used extensively. However, the programs are large and require significant amounts of storage and central processing unit (CPU) time on a large computer. Several of these workers have successfully employed difference Fourier (ΔF) refinement techniques, both alone and in conjunction with Diamond's programs. The ΔF method is economical in terms of programming complexity and cost, and is readily adaptable for use on a small computer.

This paper describes the methods developed and used for ΔF refinement of the structure of diisopropylfluorophosphate (DFP)-inhibited bovine trypsin originally determined by Stroud, Kay, and Dickerson (1971, 1974). A set of refinement programs has been written and implemented almost entirely on a Data General NOVA 800 minicomputer. Use of the minicomputer has enabled the refinement to progress efficiently at a very low cost, and the methods described here may therefore be attractive when large amounts of time and a very low rate of cost on a large computer cannot be obtained.

The refinement has resulted in a model which is greatly improved over the starting one, with substantial (i.e., several angstroms) changes in some areas. This study thus indicates, as do those cited earlier, that the improvement to be gained by refinement warrants the routine use of some refinement procedure in the determination of protein crystal structures.

The refined model is described only as much as necessary to illustrate the application of the methods. A detailed description of this structure will be presented in a future paper. The methods described here have also been used successfully in a preliminary refinement of the bovine trypsinogen structure (Kossiakoff, Chambers, Kay, and Stroud, 1977).

METHODS

DIP-trypsin crystals

The conditions for crystallization of diisopropylphosphoryl (DIP)-trypsin are described by Stroud *et al.* (1974). The crystals are orthorhombic, space group $P2_12_12_1$, with unit cell dimensions *a* = 54.84 Å, *b* = 58.61 Å, *c* = 67.47 Å, and one molecule per asymmetric unit. Crystals of a size approximately 0.6 mm x 0.5 mm x 0.5 mm were used for recording the high (1.5 Å) resolution data; those used for data to 2 Å were slightly smaller. Although these crystals contain about 40% α-trypsin (cleaved between Lys 145 and Ser 146) and 60% β-trypsin (uncleaved), they do not appear to be significantly less well ordered than the crystals of benzamidine-inhibited trypsin described by Fehlhammer and Bode (1975), which contain about 80% β-trypsin. The diffraction pattern from the DIP-trypsin crystals extends to at least 1.1 Å resolution.

Data collection and reduction

Diffracted intensities from DIP-trypsin crystals were measured with a Syntex $P\bar{1}$ diffractometer equipped with a graphite monochromator and a helium-filled tube between the crystal and detector. The tube voltage and current for the x-ray source were 40 KV and 20 ma, respectively. Background corrections were made with an interpolation technique which accounts for variations in the background with the setting angles, ϕ, χ, and 2θ (Krieger, Chambers, Christoph, Stroud, and Trus, 1974a). The remaining data reduction and scaling together of data collected from different crystals were accomplished according to the procedure of Stroud et al. (1974). In all, eight crystals were required to provide a full set of intensities to 1.5 Å resolution ($2\theta = 62°$).

A total of 4072 intensities to 1.5 Å were measured from different crystals for scaling purposes. The average value of $R = \Sigma|F_1-F_2|/\Sigma F_1$ (where F_1 is the current value of the structure factor in the master data set, and F_2 is the value for the crystal data to be merged into the master set) was 4.6% for these multiply-measured reflections. Of the 35566 independent reflections in the 1.5 Å sphere, those 22117 reflections having structure factors greater than three times their standard deviation were included in the final data set. To 2.1 Å, 88.5% of the 13,261 possible data were observed. Between 2.1 and 1.76 Å the number observed was 4784 of a possible 8979, or 53.3%, and between 1.76 and 1.5 Å, 5602 of 13,326 possible reflections were observed, or 42%.

Starting model

The starting coordinates for the refinement were measured from a wire model constructed in an optical comparator (Richards, 1968) with reference to a 2.7 Å MIR-phased map. This map was more recent than that described by Stroud et al. (1974), differing in that the 2.7 Å data from the Ag^+ derivative (Chambers, Christoph, Krieger, Kay, and Stroud, 1974) had been incorporated into the phase refinement. Atomic coordinates from the model were measured using an electronically operated device, similar in principle to the one described by Salemme and Fehr (1972).

Minicomputer system

The components of the minicomputer system used in this study are listed in Table I, along with typical execution times for certain types of operations and function evaluations. All computations except calculation and plotting of electron density maps were carried out using this system. An IBM 370/158 computer was employed for the electron density syntheses.

Difference Fourier method

Detailed descriptions of the difference Fourier method have been given elsewhere (Cochran, 1951; Stout and Jensen, 1968). The method is based on the principle that an electron density map computed using coefficients $(F_o - F_c)e^{i\phi c}$ (where F_o is the observed structure factor amplitude, and F_c and ϕ_c are the structure factor amplitude and phase

computed from the current model) contains positive peaks in positions where additional electron density should be added to the model, and negative peaks in positions where it should be subtracted, in order to produce better agreement between the model and the observed data. The position of an atom can thus generally be improved by computing the density gradient in the ΔF map at the atomic center and moving the atom toward higher density along this gradient. For an atom which is correctly positioned, the density at the atomic center gives an indication of the shift in the temperature factor for that atom. The density at atomic centers is also strongly influenced by the overall scale and temperature factor between the observed and calculated structure factors.

The course of a typical cycle of ΔF refinement performed in this study is schematized in Figure 1. Each cycle was begun with calculation of structure factors based on the current model of the structure. The calculated structure factors were then scaled to the observed ones, which in turn had been placed on an absolute scale early in the refinement, and were then used to generate a new electron density map. This map was either a difference map (computed using coefficients $\Delta F = F_o - F_c$ and phases ϕ_c), which shows the differences between the current model and an improved one, or a map computed with terms $(nF_o - [n - 1]F_c)e^{i\phi c}$ which superposes n difference maps on the current structure, showing the improved structure in its entirety. Because peaks resulting from a difference synthesis are about half their theoretical height (Henderson and Moffat, 1971), n = 2 was used for

most of these maps. Empirically, n = 2 usually produced the best compromise between freedom from noise and appearance of new information.

Following generation of the density map, the indicated corrections to atomic positions were derived and applied to the structure. Three techniques were used to determine atomic shifts (Figure 1). The simplest and most accurate procedure was to estimate shifts from the difference maps automatically, using a program written for the NOVA 800 (the middle path in the flow chart of Figure 1). The automated technique was most useful where relatively small movements from the input structure were required. If the map indicated that gross structural changes were needed, one of the other two branches was taken. The branch to the left in Figure 1, which was the simpler of the two, involved manual adjustment of atomic positions as indicated by a map made from twelve-inch square Plexiglas ® sections upon which were drawn both density contours and the atomic positions. It was very difficult to preserve accurate bond lengths and angles when making shifts in these small scale maps, and incorporation of shifts derived in this manner was relatively tedious. Using this technique, atomic shifts could be made at a rate of about 1800 atoms in two days.

Once during the refinement the wire model was rebuilt and the coordinates remeasured (the branch to the right in Figure 1). Although this procedure was useful for interpreting interactions involving long regions of secondary structure and hydrogen bonding possibilities, making changes in this manner was very tedious and the resulting coordinates were not typically of very good quality.

An automated constraints procedure was used to restore bond lengths and angles to physically reasonable values after the shifts in atomic positions had been applied. Occasionally, additional rounds of atomic shifts and constraints carried out before computing a new map resulted in further improvement, especially when $nF_o - (n - 1)F_c$ syntheses were used. The best results with difference syntheses were obtained when a new map was computed after each round.

If indicated in the calculated maps, new solvent molecules were added to the structure, or old ones deleted based on their occupancy and close approach distances to other atoms in the structure. A new refinement cycle was then initiated.

Refinement software

The refinement software and algorithms employed in the individual steps mentioned above are described below. Except where noted, all programs were written in FORTRAN IV, and execution times refer to execution on the NOVA 800.

a) Structure factor calculation

Structure factors were calculated by conventional Fourier transformation of atomic coordinates, using expressions specific for space group $P2_12_12_1$. The assembly language code output by the FORTRAN compiler for the inner loops in the program was optimized to increase execution speed. The contribution from each atom was added into every reflection before proceeding with the next atom, enabling the use of

recursive multiple-angle relationships for rapid evaluation of the trigonometric functions. Scattering factors for the individual atoms were approximated by the five-parameter analytical expressions of Forsyth and Wells (1959). Atoms within the coordinate list were sorted into groups which contained identical scattering factors and individual isotropic temperature factors, requiring only one evaluation of these parameters per group for each reflection. A provision was made in the program for deleting small groups of atoms from, or adding them to, the current set of computed structure factors. Such an option is essential if the entire set of F's is not to be recalculated whenever changes are made over a relatively small portion of the structure.

Execution time for this program was 6.75×10^{-4} seconds per atom-reflection. For the DIP-trypsin coordinate file, containing about 1800 atoms per asymmetric unit, total execution time was approximately four hours at 2.1 Å (11713 reflections), seven and a half hours at 1.76 Å (22309 reflections), and twelve hours at 1.5 Å (35566 reflections).

b) Scaling and R-factor calculations

A number of authors have noted that at low diffraction angles the average intensities observed from protein crystals are significantly reduced from their expected values (Watenpaugh et al. 1973; Moews et al. 1975). This effect has been attributed to the relatively large amount of disordered solvent present in protein crystals. Such

an effect is seen in the scaling plot for DIP-trypsin shown in Figure 2. This behavior was accounted for by least-squares refinement of a four-parameter function to the scaling plot. The function was chosen to represent a linear fit at high angles with an exponential falloff at low angles:

$$y = A_1 \exp(-A_2 x) + A_3 x + A_4$$

This procedure is similar to one described by Moews and Kretsinger (1975). The least-squares fits for both the linear and nonlinear function are shown in Figure 2. The linear fit for reflections at small values of $\sin^2\theta/\lambda^2$ was totally inadequate, and inclusion of these reflections scaled in this manner caused large low-frequency ripples in the resulting electron density maps.

The improvement in agreement between F_o and F_c for these reflections is shown in Figure 3. For the linear fit, the residual, R ($R = \Sigma|F_o - F_c|/\Sigma F_o$), increased sharply at low angles, reaching over 75%; however, when properly scaled, using the nonlinear expression, the agreement for these reflections was up to three times better. It should be emphasized that, while the technique accounts well for the difference in scale of the low-angle data, the expression used is an empirical one and is not meant to be a mathematical description of a physical phenomenon. The actual function used, as long as it conforms well to the shape of the scaling plot, does not appear to be critical to either the appearance of the density maps, or the value of R.

Reflections for which

$$\frac{F_o - F_c}{0.5\ (F_o + F_c)} > 120\%$$

were left out of the calculation of the residual (about 700 reflections to 1.5 Å). These reflections were also omitted from the calculation of density maps, since the ΔF term which results from the case where $F_o >> F_c$ is likely to be poorly phased. Difference terms for those reflections where $F_c >> F_o$ are probably correctly phased and were included in the R-factor and Fourier map calculations (Stout and Jensen, 1968). Unobserved reflections were included in the scaling with F's equal to twice the average standard deviation for unobserved F's in the appropriate zone of $\sin\theta$. They were not included in the Fourier or R-factor calculations.

Absolute scaling was accomplished with the use of a standard Wilson plot technique, neglecting the reflections inside 5 Å resolution. The overall temperature factor thus obtained was 14 $Å^2$ for the 1.5 Å data. All atoms included in the structure factor calculation (i.e., protein and ordered solvent) were included in the absolute scaling.

c) Fourier map calculation

Generation of electron density maps was the only step of the refinement carried out on the IBM 370/158, with a Fourier program

originally written by G. N. Reeke. CPU time required to generate a map of approximately 100,000 grid points from 22117 reflections to 1.5 Å resolution was 6.5 minutes. A grid spacing of approximately 1.25 Å along each of the crystallographic axes was used throughout most of the refinement. The coarse grid produced satisfactory results with 2.7 and 2.1 Å data, and was economical in terms of computing cost and map storage requirements. The fact that the grid size exceeded the interval corresponding to the Nyquist frequency (i.e., was greater than half the resolution of the data) at 2.1 Å did not appear to affect the course of the refinement adversely. At 1.76 Å and higher resolution, better results were obtained with a finer grid, and an interval of 0.75 Å was therefore used in later stages.

d) Atomic shifts

Because of the iterative nature of the refinement procedure, small errors introduced by making approximations in order to simplify programming or computation can be corrected in subsequent cycles. A number of such approximations were made in the atomic shifts program.

Electron density at an atomic position, ρ, was interpolated from a three-dimensional array of either 8 or 27 grid points (depending on the coarseness of the map grid) surrounding the atom, according to the scheme

$$\rho = \frac{\sum_i \rho_i w_i}{\sum_i w_i}$$

where ρ_i are densities at each of the grid points, and w_i are weights for each grid point in the sum, which fall off exponentially ($w_i = e^{-ad_i^2}$) as the distance, d_i, between the grid point and the atom increases. Values for the constant, a, were in the range 0.25-1.0 $Å^{-2}$. Gradients were computed by evaluation of the density 0.1 Å on either side of the atom along each coordinate axis. In more recent cycles, the electron density was approximated using a three-dimensional polynomial, with coefficients (a_1—a_7) determined from seven grid points around the atom center.

$$\rho = a_1\Delta x^2 + a_2\Delta y^2 + a_3\Delta z^2 + a_4\Delta x + a_5\Delta y + a_6\Delta z + a_7$$

This expression allows analytical evaluation of the gradients, resulting in faster execution. Both schemes produced satisfactory shifts.

The correction to an atomic position indicated in a ΔF map for noncentrosymmetric structures is: $\vec{\Delta x} = -2\vec{g}/C$, where $\vec{\Delta x}$ is the change in position, $\vec{g}$ is the difference density gradient at the atomic site, and C is the curvature at that site in the corresponding F_o synthesis Cochran, 1951; Stout and Jensen, 1968). In practice the curvature has been approximated with empirically determined values for each type of atom or ion (Watenpaugh et al. 1973; Freer et al. 1975; Moews and Kretsinger, 1975).

A number of factors in addition to the atom type influence the actual values to be used, including resolution of the data, the overall scale and temperature factors, and the scale of the densities written at the grid points of the map. To account for variations in

these parameters over the course of the refinement, and to give the program greater flexibility, the curvature was taken to be proportional to the atomic number, Z, and shifts were scaled by a specified constant, K, chosen to produce reasonable values for the shifts:

$$\vec{\Delta x} = \frac{K\vec{g}}{Z}$$

A value of K was used which produced positional changes approximately equal in magnitude to those estimated from $2F_o-F_c$ maps (averaging about 0.4 Å in early cycles and 0.1 Å in later stages). After a shift was computed, the density at the prospective new atomic site in the map used to derive the shift was evaluated to make certain that the atom had moved into more positive density. If not, the program repeatedly cut the size of the shift by half until this criterion was met. In addition, any shift exceeding a specified maximum Δx_{max} (usually 0.4 Å) was reset to this value, maintaining the original direction. The above expression enabled shifts to be readily evaluated from MIR maps and $nF_o-(n-1)F_c$ maps, as well as from difference Fourier syntheses.

The electron density for an atom (ρ) can be approximated by a spherical Gaussian of the form

$$\rho \simeq (B/4\pi)^{-3/2} Z \exp[-\pi r^2/(B/4\pi)],$$

where r is the distance from the atomic center, Z is the number of electrons, and B is the individual isotropic temperature factor for the atom (see Diamond, 1971). From this expression, the expected

change in temperature factor (ΔB) corresponding to a small change in electron density at the center of the atom ($\Delta\rho_o$) is,

$$\Delta B = \frac{-\Delta\rho_o}{12\pi^{3/2} Z} \cdot B^{5/2}$$

This expression is in practice effective only for atoms which are correctly positioned, and is also affected by scaling errors. The equation was therefore modified empirically to provide more satisfactory results, and the expression used to compute corrections to the individual isotropic temperature factors was,

$$\Delta B = \frac{-K_2 \, (\rho_\Delta - \overline{\rho_\Delta})}{Z} \sqrt{B} \cdot e^{-\Delta x/\Delta x_{max}}$$

where ΔB is the shift, ρ_Δ is the difference electron density at the atomic site, $\overline{\rho_\Delta}$ is the expected average difference electron density for all atomic sites, and K_2 is a scaling constant similar to the one for positional shifts.

Because atoms at the beginning of the refinement tend to reside in negative difference density due to the fact that they are not correctly positioned, there is a tendency for the temperature factors to become too large in early cycles, providing they are allowed to vary. The terms involving $\overline{\rho_\Delta}$ and $e^{-\Delta x/\Delta x_{max}}$ enable this interaction between positions and temperature factors to be partially decoupled. The former term also compensates for errors in scaling of calculated F's to the observed ones, which can also greatly influence ΔB. The latter

term reduces the shift in the temperature factor according to the size of the gradient at the atomic site; thus, the full shift is applied only when an atom is close to its correct position. The equation used produced satisfactory values for ΔB, which resulted in rapid improvement in flatness of the ΔF maps at atomic centers, and reasonable values for the temperature factors themselves (values of 10, 12, 14, 16, 18, 23, 28, 38, and 58 $Å^2$ were used). Larger B factors were generally associated with external side chains. Execution time for this program for a coordinate list of about 1800 atoms was approximately 30 minutes.

e) Constraints

Constraints were applied to the coordinates by minimization of a residual composed of sums of squares of the deviations of the atoms from "ideal" relative positions. Four types of differences contributed to the residual. The first was the difference between the positions of the atoms in the starting structure and those in the constrained structure. This term was given unit weight throughout the constraints procedure. The other three terms contained deviations from standard values of the bond lengths, bond angles, and dihedral angles to be constrained. Each of these three terms was given a relative weight which was increased on each pass through the atom list, allowing greater movements from the starting structure and a closer approach to standard constraints in each subsequent pass. The procedure was terminated either after a fixed number of passes, or when

rms deviations of bond lengths and angles had fallen below selected values. Similar procedures have been described by Hermans and McQueen (1974) and Freer et al. (1975). More recently similar techniques have been independently developed for constraining bond lengths, angles, and dihedral angles by minimization of deviations from standard interatomic distances only (Dodson, Isaacs, and Rollet, 1976; Ten Eyck, Weaver, and Matthews, 1976).

Standard values for bond lengths and angles were obtained from Marsh and Donohue (1967), and the references cited therein. Standard values for the dihedral angles constrained were chosen in order to make the peptide amide groups trans- and planar. In later stages, planarity of rings and side chain amide, carboxyl, and guanidino groups was enforced by constraining dihedral angles, since bond length and bond angle constraints alone were not in practice sufficient to make these groups planar. In the case of side chain amide and carboxyl groups, dummy dihedral angles were constrained (e.g., θ (C_β, C_γ, O_{δ_1}, O_{δ_2}) in Asp).

Constraints were applied to a zone of one to five residues. A small portion of the peptide chain on either side of the zone was used as a fixed boundary, which was necessary for convergence of the procedure at the interface between zones. A simple steepest-descent gradient minimization technique was used, and was very reliable in its ability to produce converging shifts even when atomic coordinates were far removed from ideality; it was also fast and satisfactory in its rate of convergence. (This was in contrast to the gradient-curvature

techniques, e.g., Newton-Raphson minimization tried in early versions of the program, which converged rapidly in the neighborhood of the minimum, but often produced unreasonable shifts for regions which were poorly constrained in the starting structure, and required substantially more computing time per cycle.)

Since the molecular parameters in real proteins, particularly the planarity of peptide amides (Ramachandran, Lakshminarayanan, and Kolaskar, 1973; Huber et al. 1974), may deviate significantly from "ideal" values, the fact that the constraints can be given any desired degree of flexibility using this procedure is highly advantageous. It is moreover helpful to keep the constraints rather flexible when performing alternate cycles of atomic shifts and constraints in order to prevent oscillation between a constrained and an unconstrained structure.

Four passes through the coordinate file were generally run after atomic shifts had been applied in order to achieve the desired rigidity in the constraints. Weights for the contributions to the residual of bond lengths, angles, and dihedral angles were initially set at 5, 1, and 1 for lengths in angstroms and angles in radians, and were multiplied by 3, 6, and 6, respectively, at the beginning of each new pass. Resulting overall rms deviations from ideality were typically 0.07 Å in bond lengths, 3.5° in bond angles, and 4.5° in dihedral angles. Maximum deviations were usually about four times the overall rms deviations. Execution time was about 30 minutes for each pass through the coordinate file containing 223 residues.

f) Peak search and close contacts

The peak search and close contacts programs were used primarily for selection of solvent molecules from difference maps. The peak search program locates prospective solvent straightforwardly from one asymmetric unit of the map, and runs in about five minutes for 100,000 grid points.

Close contacts between nonbonded atoms were tabulated by first sorting the atoms based on their position in the asymmetric unit, requiring comparison between a relatively small number of atoms and their symmetry equivalents to find all distances less than a specified value. Approximately twenty minutes were required to tabulate all close contacts between atoms in an 1800-atom-coordinate file. Prospective solvent molecules which were closer than 2.5 Å to atoms already present in the structure, or solvent which had moved within this distance of other atoms in the protein, were generally removed from the data set. In a few cases, particularly when close contacts existed between groups of the protein itself, corrections were made manually. The current structure contains 174 solvent molecules, most of them hydrogen-bonded to groups on the surface of the protein and to other solvent. About 30 of them can be considered internal.

RESULTS

Progress of the refinement

The graph in Figure 4 indicates the progress of the refinement to date. The R-factor at 2.7 Å computed for the starting structure (Revision 1) was 47%, rising to 50% upon incorporation of the 2.1 Å data. Manual adjustment of atomic positions with the use of small scale $2F_o-F_c$ maps reduced the residual to 40.2%.

The automated atomic shifts program was written at this stage. The improvement in R was very rapid, and after three cycles of shifts determined from ΔF maps, R was 34%. The resulting rms deviations from standard bond lengths and angles were, however, very poor--0.5 Å and 22°, respectively. Moreover, 33 α-carbon atoms and 10 Ile and Thr β-carbons had adopted the wrong sense. The constraints program was subsequently implemented, and several cycles of automated shifts using a $2F_o-F_c$ map followed by constraints were performed. A number of the wrong-handed asymmetric carbon atoms were corrected manually using small scale maps. The resulting overall rms deviations from ideality for bond lengths and angles were 0.15 Å and 6.5°; at the same time, there was only a small decrease in the average value of electron density at atomic centers. The R-factor for this constrained structure was 38.8% at 2.1 Å.

Alternate cycles of shifts and constraints were then applied nine times, using seven difference Fourier maps (Revisions 6-12 in Figure 4). During these cycles, solvent atoms were added and deleted where

indicated. At Revision 12 of the coordinates (see Figure 4), the atom file contained 220 solvent molecules. Deviations from ideal bond lengths, angles, and dihedral angles were 0.1 Å, 2.4°, and 3.8°, respectively. The sense of all asymmetric atoms had been corrected and the residual had been reduced to 26.6% at 2.1 Å. The 1.76 Å data were included, and two refinement cycles produced a 1.76 Å R-factor of 28.8% (231 solvent molecules).

Since it appeared that additional automated cycles would produce little further improvement in R, it was felt that a large-scale visual inspection of the structure in its current state was warranted, and the wire model was rebuilt to a $2F_o-F_c$ map. A number of substantial changes from the starting wire model had taken place, and will be briefly described later. Some additional improvements were made at this step, including major reorientation of six amide planes and addition of seven ordered solvent molecules. Approximately 70% of the coordinates were replaced with coordinates measured from the rebuilt model. The 1.76 Å R-factor rose sharply to 35%.

Examination of the new coordinates in a small-scale map showed that, while the atoms were not far from their intended positions, large pieces of the structure appeared randomly translated by about 0.5 Å from the center of the density, particularly in that direction perpendicular to the plane of the map sections in the Richards' box. Five difference Fourier refinement cycles rapidly corrected these translations, the R-factor at 1.76 Å dropping to 26.9%. During these cycles a number of chemically unreasonable and low-occupancy solvent

molecules were removed, leaving a total of 174. Following these cycles, 1.5 Å data were added, and one subsequent refinement cycle reduced the 1.5 Å R-factor to 27.7% for the constrained structure containing 174 ordered solvent molecules (rms deviations from ideality for bond lengths, angles, and dihedral angles were 0.07 Å, 3.2°, and 4.6°, respectively).

Changes from the starting model

A histogram indicating the movement of α-carbon atoms between the starting and current models is shown in Figure 5. The average positional change for α-carbons was 0.9 Å, and for all atoms was 1.2 Å. The largest movements were in the regions of residues 60-63, 74-80 (the primary calcium binding site, first identified and described in detail by Bode and Schwager, 1975a,b), 110-121, 144-147 (the α-, β-trypsin autolysis site), 186-187, and particularly in the C-terminal α-helix. All of these residues are on the surface of the enzyme, and were not unambiguously defined in the MIR map. The problem with the terminal α-helix was largely a translational one, since it was the region farthest from the mirror of the Richards' box when building the wire model, and was therefore most prone to errors in depth perception.

One type of error commonly encountered over the course of the refinement was the 180° misorientation of an amide plane. At a resolution of 2.7 Å the MIR map did not allow unambiguous assignment in a number of cases; however, the errors were clearly identified in the high resolution ΔF maps. The regions where these misinterpretations

occurred were again all on the surface of the molecule: the amide planes between residues 22-23, 24-25, 34-37, 39-40, 75-76, 84-85, 110-111, 117-118, 144-145, 187-188, and 222-223 all required reorientation. The region of the molecule around His 40 in one of the early 2.1 Å ΔF maps, showing the misorientation particularly of the Tyr 39-His 40 amide, is pictured in Figure 6a. Figure 6b is a drawing of the 2.7 Å MIR map and starting model in the same region. At this resolution, an unambiguous assignment cannot be made for the Asn34-Ser 37 and Tyr 39-His 40 peptides. Figures 6c and 6d are respectively pictures of the current model and 1.5 Å refined map, and the 1.5 Å difference map in this region. The difference map is much flatter since the required corrections have been made.

Although large structural changes did occur in some parts of the molecule, the chemically important residues of the active site and binding pocket did not move greatly upon refinement. Positional changes for these residues resulted from limitations in resolution and clarity of the MIR map, rather than from misinterpretation. The most significant change involving the active site is the tilting of the Asp 102 carboxyl group and the His 57 imidazole into positions where the interaction between them is no longer symmetrical as previously suggested (Stroud et al. 1974; Krieger, Kay, and Stroud, 1974b). The δ-nitrogen of His 57 points more toward the lower oxygen, $O\delta_2$, of the Asp 102 carboxyl, as shown in Figure 7, forming a 2.7 Å hydrogen bond. The distance between the upper oxygen atom, $O\delta_1$, and His 57 Nδ is too great for favorable hydrogen bond formation, 3.9 Å. However, this

atom does form hydrogen bonds with the main chain nitrogen atoms of Ala 56 and His 57 of 2.7 Å and 3.2 Å, respectively. As can be seen from Figure 7, the positions of these groups are well defined in the refined map.

Refinement of the structure from residues 72 - 81 indicated a tightly bound positive ion and several well-ordered solvent molecules, which were previously not resolved in the 2.7 Å MIR map. Bode and Schwager (1975a,b) in their independent refinement of the structure of benzamidine-inhibited bovine trypsin recognized this area as the primary calcium ion binding site. While the refined structure of DIP-trypsin arrived at from the present study is nearly identical in this area to that reported by Bode and Schwager, the density for the positive ion in the present study is about half of that expected for a fully occupied calcium ion. It is possible that this site is partially occupied by Ca^{2+}; however, the ligands do not appear disordered as expected for such a situation. Since the crystallizing solution contained a high concentration of Mg^{2+} (5.8 % $MgSO_4$), occupancy by a magnesium ion is another possibility in spite of the difference in atomic radius between Ca^{2+} and Mg^{2+}. Occupancy by a water molecule is not as likely, because of the high density of negative charge surrounding this site.

DISCUSSION

There are a number of criteria which indicate that the refinement has indeed resulted in an improved structure. First, the refined structure fits the observed data better than did the starting structure. The most commonly quoted index of this agreement is the standard crystallographic R-factor, which decreased from 50% at 2.1 Å to 27.7% at 1.5 Å, as just described. This decrease is derived, however, from a number of sources in addition to improvement of atomic positions, including the use of individual temperature factors, inclusion of solvent, use of the four-parameter scaling procedure, and omission of the approximately 700 reflections with $F_o >> F_c$ from the data set. The contribution of each of these factors to the decrease in R can be estimated by computing the R-factor for the refined model without its benefit. The respective contributions to the R-factor at 2.1 Å are 3%, 3%, 2%, and 1.5%. The R values for the starting and current model at this resolution are 50% and 25%, respectively, leaving about 15% of the 25% decrease attributable to improvement in atomic positions of the atoms originally in the starting model.

Although the R-factor is a useful indicator of the overall progress of the refinement, it was noted in this study as well as by Huber et al. (1974) that small changes in isolated portions of the structure, such as a flipped amide plane, are not strongly reflected in the value of R. A much more sensitive device for the detection of these local errors is the ΔF map. The average unsigned difference electron

density dropped from 0.31 electrons/Å^3 for the 2.1 Å ΔF map at the start of the refinement to 0.08 electrons/Å^3 for the 1.5 Å refined ΔF map, where the integration was performed over an entire asymmetric unit. The present 1.5 Å difference map contains few interpretable features, with no density above 0.54 electrons/Å^3 in magnitude. These numbers can be compared with 2.6 electrons/Å^3 for a well-defined carbonyl oxygen in the refined $2F_o-F_c$ map.

The correctness of the refined structure is also indicated by the representative result shown in Figure 8, which is a picture of the 1.5 Å $2F_o-F_c$ map in the same area as that of Figure 6. In this case, however, all the atoms shown (N34 C=O, S37, G38, Y39 main chain, H40, F41, C42, and G43) have been omitted from the structure factor calculation. The density for these atoms is nevertheless very clear and, although the resolution suffers somewhat, the structural information is clearly contained in the observed F's. This result serves to emphasize that the $2F_o-F_c$ map is not merely a reflection of the atoms included in the phase calculation.

The second criterion indicating the improvement of the refined model is that it has become chemically more reasonable. Larger regions of the protein fit into classical patterns of secondary structure. In a number of regions formerly lacking good hydrogen bonding, new hydrogen bonds were formed, many of them through solvent molecules. Forty-nine close contacts between nonbonded atoms, shorter than the extreme limits of Ramachandran and Sasisekharan (1968) have been eliminated. The wire model rebuilt from the 1.76 Å refined map contains

no large empty regions within the interior (except the specific binding pocket), whereas several of these areas were present in the starting model.

The MIR map also serves as a check on the correctness of the refined model, and was a very useful aid in regions where the calculated maps were noisy. The major changes made in the structure resulted primarily from difficulties in interpretation of the MIR map (except in the terminal α helix); however, these changes have not generally resulted in contradictions with this map. The refined coordinates fit the MIR electron density considerably better than did the starting ones.

The mean change in phase angle, $\Delta\phi$, between the "best" MIR and refined phases was 62°, and between the phases calculated from the starting model and refined phases was 58°, for all reflections to 2.7 Å. These are large average changes, but are similar to those reported for other protein structures (Watenpaugh et al. 1973; Huber et al. 1974; Moews and Kretsinger, 1975; Deisenhofer and Steigemann, 1975). However, the appearance of the Fourier map is ultimately determined by contributions from a large number of reflections and, because $\Delta\phi$ contains no information concerning the interrelationships between the various reflections, it is not a very meaningful number when considering how different the MIR and refined maps really are.

In order to visualize the kinds of differences involved between the MIR and refined maps, a difference synthesis was computed with

coefficients $F_o e^{i\phi_{MIR}} - F_o e^{i\phi_c}$. While substantial difference density ($\Delta\rho$) was present over most of the map, this density was considerably smaller at atomic positions than the corresponding density (ρ_o) in an $F_o e^{i\phi_c}$ map computed at the same resolution. This result reflects the strong similarity between the MIR and 2.7 Å refined maps. An index of the disagreement between these maps can be computed from the rms densities in the difference and F_o syntheses:

$$R_\phi = \frac{\langle \Delta\rho \rangle_{rms}}{\langle \rho_o \rangle_{rms}}$$

Averaged over the entire asymmetric unit, R_ϕ was 86%. This number is smaller than the R_ϕ of 106% estimated from the 62° value of $\Delta\phi$, indicating that the differences between the MIR and refined phases tend to be smaller for the larger reflections. Averaged over only those grid points surrounding the atoms in the refined structure, R_ϕ fell to 28%.

The average change of 1.2 Å between the starting wire model coordinates and the current set is quite substantial, and arises from two major sources of error. The first source involves errors in interpretation caused primarily by the lack of resolution and clarity, and phase errors in the MIR map. These changes result in movements of up to several angstroms, but occur over relatively small portions of the molecule. The other major source of error is in the actual construction of the wire model, particularly due to inaccurate depth perception, irregularities in the mirror, and mechanical difficulties in

fitting residues together, placement of supports, and bent parts. These errors are comparatively small, but are distributed over the entire molecule. Errors arising from measurement of wire model coordinates were very small--within 0.5 mm, or 0.025 Å.

A reasonable estimate of the size of the noninterpretative errors in the wire model coordinates can be derived from the positional differences between the coordinates of the wire model rebuilt at 1.76 Å (Revision 16 in Figure 5) and those obtained from the five cycles of refinement following this rebuilding, since no gross reinterpretations were involved during these cycles. The mean change in atomic positions between these two sets was 0.6 Å. There were no overall systematic translations between the data sets compared. Correction of these errors led to a substantial decrease in R--from 35% to 27% at 1.76 Å, the R-factor being sensitive to small translations of large pieces of the structure. Similar types of errors, although considerably smaller in magnitude (and dependent upon the coarseness of the map grid), appeared when performing shifts manually in the small-scale maps. For this reason it is felt that these approaches are inadequate to provide an optimal fit to the electron density: some type of computerized scheme for atomic shifts is essential for an optimal fit with a correspondingly lower value of R.

Several early problems resulted from the high content of ordered and disordered solvent. In retrospect, the presence of ordered solvent was one of the greatest factors in misinterpretation of the MIR map. At 2.7 Å resolution few of the ordered solvent were separated from

neighboring residues, leading to inaccurate placement of these residues in the model.

Although it was found that inclusion of ordered solvent and use of individual temperature factors could produce significant reduction in the R-factor in early stages, it is felt that their application in the initial stages of refinement is a mistake. Difference Fourier maps at the start were relatively noisy, making selection of peaks corresponding to real solvent difficult. Solvent added in these early stages tended to move toward the atoms of the protein, influencing the gradients and corresponding atomic shifts. In these stages it is best to add solvent only at a very high confidence level (the MIR map can be very helpful), and preferably not until the ΔF maps have become easily interpretable. Because of the strong coupling between the atomic positions and the shifts indicated for individual temperature factors, individual temperature factors should also be left largely untouched at the beginning of the refinement.

Unfortunately, the fact that the ΔF maps were very noisy in early cycles made location of parts of the structure which had been omitted from the phasing, or which were very far from the correct position, very difficult. The technique which produced the best result in this situation was to perform several cycles of refinement in order to optimize the fit for the known parts of the structure. This improved the phases to the point where the missing features could often be recognized, and made the ΔF maps considerably less noisy. One method which was not employed in this study but may be very useful in cases

where the early calculated maps are very noisy is the use of a weighting factor such as the one described by Sim (1959) to reduce the contribution of terms which are likely to be poorly phased.

Although the R-factor and the flatness of the ΔF map indicate that the refined structure is generally correct, there are a few regions which would benefit from further refinement. The first is the area around Lys 145, where the α/β-trypsin autolytic cleavage occurs. There is some disorder in this region arising from the fact that the crystals used contain about 40% α-trypsin, and that this region forms an external loop, with some thermal motion probably present. Bode and Schwager (1975a) in their refinement of the benzamidine-trypsin structure, which was analyzed as 80% β-trypsin, also suggest that there is some mobility in this region. Another area requiring further work is the C-terminal α helix between residues 238-244. The slowness of convergence in this region is primarily a result of the large errors in the starting model.

There are several improvements which can be made in the present refinement system. Although a refinement cycle can presently be carried out in a single day, it would be advantageous to shorten the time required. The rate-limiting step is presently the calculation of structure factors. It may be possible to greatly shorten this step by use of a three-dimensional fast Fourier transform (FFT) program such as that described by Ten Eyck (1973). Generation of sampled electron density from a list of atomic coordinates, suitable for transformation to obtain 1.5 $\mathring{A}$ structure factors (i.e., one asymmetric unit of the

structure on a 0.75 Å grid) currently requires about twenty minutes on the minicomputer. A three-dimensional FFT program would also be useful for generating electron density maps, and implementation on the NOVA 800 would eliminate the need for use of a large computer for any step in the cycle. The fast Fourier algorithm would be essential for minicomputer refinement of a much larger structure, or for extending the resolution of the present structure to the limits imposed by the diffraction pattern.

The treatment of low-angle reflections, currently accomplished through use of the nonlinear scaling expression, might be improved by including some physically reasonable model for the disordered solvent continuum in the structure factor calculation.

An improvement which is expected to facilitate convergence of the refinement is the incorporation of information from the electron density map into the residual minimized in the constraints program, to yield a constrained real-space refinement program. The modifications required are very simple, and the results obtained to date in tests of this program indicate that it is considerably more efficient than alternate cycles of atomic shifts and constraints. This program can also be readily adapted for energy minimization of the type described by Levitt (1974), as suggested by Hermans and McQueen (1974). Konnert (1976) has used a similar technique in reciprocal space to perform constrained structure factor least-squares refinement. One further capability which can be added to the constraints program involves the configuration at asymmetric atoms. Currently, any inversion of

configuration brought about by allowing atomic shifts to become too large between applications of constraints must be corrected manually. Nevertheless, it seems likely that inclusion of information about the configuration, such as the scalar triple-product of the bonds to the atom, could prevent or correct these errors.

The computing cost of the DIP-trypsin refinement to date has been approximately $650, almost entirely for calculation and plotting of Fourier maps on the IBM 370/158. About 320 hours of CPU time on the NOVA 800 have been required over the course of the refinement for programs in which computation is rate limiting, excluding program development. Considering the sevenfold decrease in CPU time that we have generally observed for compute-bound programs on the IBM 370/158, this translates into about $25,000 for equivalent time on the large machine at the current overall average rate of $540/CPU hour (including use of peripherals, etc.). It must be kept in mind that, had the refinement been carried out on a large machine, the programs would have been written to take advantage of the greater core storage available with a corresponding significant decrease in execution time. However, since the figure above is exclusive of program development and neglects the very large number of smaller programs executed during the refinement, it is felt that this figure represents a realistic estimate of the equivalent cost on the IBM 370. The savings in computing costs with the use of the minicomputer have therefore been substantial, and considering the potential cost for refinement of a protein structure, these savings can rapidly begin to offset the initial investment for

the smaller machine.

Since this paper was first submitted for publication, two cycles of a least-squares refinement procedure using a first-order gradient minimization reduced the 1.5 Å R-factor to 23.5%. The mean change in atomic position was small--about 0.07 Å during each cycle. Details will be described in a later paper.

ACKNOWLEDGMENTS

We wish to thank Drs. Monty Krieger and Anthony Kossiakoff for valuable discussions.

REFERENCES

Bode, W. and Schwager, P. (1975a). J. Mol. Biol. 98, 693-717.

Bode, W. and Schwager, P. (1975b). FEBS Letters 56, 139-143.

Chambers, J.L., Christoph, G.G., Krieger, M., Kay, L.M., and Stroud, R.M. (1974). Biochem. Biophys. Res. Commun. 59, 70-74.

Cochran, W. (1951). Acta Crystallogr. 4, 408-411.

Deisenhofer, J. and Steigemann, W. (1975). Acta Crystallogr. B31, 238-250.

Diamond, R. (1966). Acta Crystallogr. 21, 253-266.

Diamond, R. (1971). Acta Crystallogr. A27, 436-452.

Diamond, R. (1974). J. Mol. Biol. 82, 371-391.

Dodson, E.J., Isaacs, N.W., and Rollet, J.S. (1976). Acta Crystallogr. A32, 311-315.

Fehlhammer, H. and Bode, W. (1975). J. Mol. Biol. 98, 683-692.

Forsyth, J.B. and Wells, M. (1959). Acta Crystallogr. 12, 412-415.

Freer, S.T., Alden, R.A., Carter, C.W. Jr., and Kraut, J. (1975). J. Biol. Chem. 250, 46-54.

Henderson, R. and Moffat, J.K. (1971). Acta Crystallogr. B27, 1414-1420.

Hermans, J. Jr. and McQueen, J.E. Jr. (1974). Acta Crystallogr. A30, 730-739.

Huber, R., Kukla, D., Bode, W., Schwager, P., Bartels, K., Deisenhofer, J., and Steigemann, W. (1974). J. Mol. Biol. 89, 73-101.

Konnert, J.H. (1976). Acta Crystallogr. A32, 614-617.

Kossiakoff, A.A., Chambers, J.L., Kay, L.M., and Stroud, R.M. (1977). Biochemistry 16, 654-664.

Krieger, M., Chambers, J.L., Christoph, G.G., Stroud, R.M., and Trus, B.L. (1974a). Acta Crystallogr. A30, 740-748.

Krieger, M., Kay, L.M., and Stroud, R.M. (1974b). J. Mol. Biol. 83, 209-230.

Levitt, M. (1974). J. Mol. Biol. 82, 393-420.

Marsh, R.E. and Donohue, J. (1967). Adv. Prot. Chem. 22, 235-256.

Moews, P.C. and Kretsinger, R.H. (1975). J. Mol. Biol. 91, 201-228.

Ramachandran, G.N., Lakshminarayanan, A.V., and Kolaskar, A.S. (1973). Biochem. Biophys. Acta 303, 8-13.

Ramachandran, G.N. and Sasisekharan, V. (1968). Adv. Prot. Chem. 23, 284-438.

Richards, F.M. (1968). J. Mol. Biol. 37, 225-230.

Salemme, F.R. and Fehr, D.G. (1972). J. Mol. Biol. 70, 697-700.

Sayre, D. (1974). Acta Crystallogr. A30, 180-184.

Sim, G.A. (1959). Acta Crystallogr. 12, 813-815.

Stout, G.H. and Jensen, L.H. X-ray Structure Determination: A Practical Guide. Macmillan, New York, 1968, pp. 356-385.

Stroud, R.M., Kay, L.M., and Dickerson, R.E. (1971). Cold Spring Harbor Symposium on Quantitative Biology 36, 125-140.

Stroud, R.M., Kay, L.M., and Dickerson, R.E. (1974). J. Mol. Biol. 83, 185-208.

Ten Eyck, L.F. (1973). Acta Crystallogr. A29, 183-191.

Ten Eyck, L.F., Weaver, L.H., and Matthews, B.W. (1976). Acta Crystallogr. A32, 349-350.

Watenpaugh, K.D., Sieker, L.C., Herriot, J.R., and Jensen, L.H. (1973). Acta Crystallogr. B29, 943-956.

TABLE I

Computing System Configuration

NOVA 800 (Data General Corporation)

32 K (16 bit) Words Core

Floating Point Hardware*

12-1/2 ips Magnetic Tape Drive

25 ips Magnetic Tape Drive

2.5 M byte Moving Head Disk

Keyboard Printer

Matrix Line Printer/Plotter

Typical Execution Times for FORTRAN Coded Instructions

OPERATION	TIME (μsec)
Integer Add	2
Integer Multiply	80
Floating Point Add	20
Floating Point Multiply	25
Floating Point Divide	50
SIN(X)	400

*Syntex Analytical Instruments

FIGURE CAPTIONS

FIGURE 1. This flow chart outlines the major steps involved in a single refinement cycle, using the technique described in the text. Alternate branches are indicated in the center of the figure. The main sequence was through automated shifts in difference maps. The branch toward small-scale maps was used for major reorientation of parts of the structure. The wire model was rebuilt once during the refinement as an additional check on its progress, as described in the text.

FIGURE 2. The observed F's for DIP-trypsin fall off rapidly with respect to the calculated F's at low angles, as shown in this scaling plot for the 1.5 Å data. $\Sigma F_o/\Sigma F_c$ was computed for 100 zones in $\sin^2\theta/\lambda^2$. The solid line drawn through these computed points (O) represents the four-parameter fit. Points calculated from the linear fit are symbolized by (+). Unit weights were used in this case. For the linear fit, points inside 5 Å resolution were neglected.

FIGURE 3. The improvement in agreement between F_o and the scaled F_c for low-angle reflections when using the four-parameter scale is shown in this graph of overall R-factor vs. resolution. The R-factor was computed for each point using all reflections to the indicated resolution. (+) = linear fit; (O) = four-parameter fit.

FIGURE 4. Summary of DIP-trypsin refinement using the scheme outlined in Figure 1, indicating the improvement in agreement between F_o and F_c. The decrease in R-factor over the course of the refinement was from 47.2% at 2.7 Å to 27.7% at 1.5 Å. The sharp increase in R at Revision 16, after rebuilding the wire model to a 1.76 Å refined map, resulted from errors in the wire model coordinates, as described in the text.

FIGURE 5. The distances between α-carbon atoms in the starting and refined structures are shown in this histogram. The largest changes all occurred on the surface of the molecule, especially in the C-terminal α helix.

FIGURE 6. The fit of the model to the electron density at different stages of refinement in the region around His 40, viewed down the crystallographic b axis, is pictured in these stereo drawings generated using the minicomputer. The portion of the sequence shown is L33, N34, S37, G38, Y39 (the entire ring is not shown), H40, F41, C42 (plus the Sγ of C58), and G43:

a) The misorientation of the Y39-H40 (and to a lesser extent the N34-S37) amide is reflected in an early 2.1 Å ΔF map. Contours are from 0.3 $e^-/Å^3$ in increments of 0.15 $e^-/Å^3$. The dotted contours represent negative density.

b) The orientation of these amides is ambiguous in the 2.7 Å MIR map, contoured from 0.375 $e^-/Å^3$ in steps of 0.25 $e^-/Å^3$.

c) The reorientation of these amides allows an excellent fit to the 1.5 Å refined ($F_o e^{i\phi_c}$) map, where the ambiguity no longer exists. Contours are from 0.5 $e^-/Å^3$ in steps of 0.35 $e^-/Å^3$.

d) The 1.5 Å ΔF map is correspondingly clean since the required corrections have been made. Contours are from 0.2 $e^-/Å^3$ in 0.1 $e^-/Å^3$ steps.

FIGURE 7. A view down the b axis of the area around the catalytic site residues Asp 102, His 57, and Ser 195, shows the fit of the refined coordinates to the 1.5 Å refined ($[2F_o-F_c]e^{i\phi_c}$) density. The sulfur atoms in the 42-58 disulfide bridge are well resolved. The very large peak at the lower right arises from the phosphorus and oxygen atoms of the DIP-group. Contours start at 0.5 $e^-/Å^3$ in 0.5 $e^-/Å^3$ steps.

FIGURE 8. View of the same area as shown in Figure 6 of a 1.5 Å $(2F_o-F_c)e^{i\phi_c}$ map. All the atoms shown in this drawing were omitted from the phasing, indicating that the structural information is indeed present in the observed F's. Contours are from 0.5 $e^-/Å^3$ in 0.4 $e^-/Å^3$ steps.

Figure 1

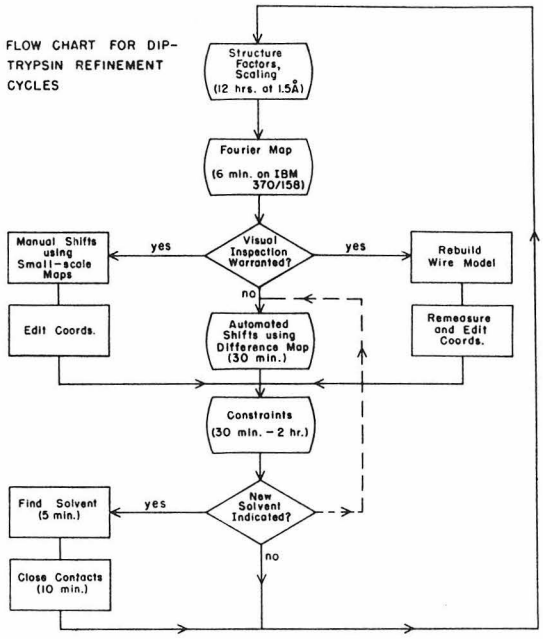
FLOW CHART FOR DIP-TRYPSIN REFINEMENT CYCLES
Structure Factors, Scaling (12 hrs. at 1.5Å)
Fourier Map (6 min. on IBM 370/158)
Visual Inspection Warranted?
yes
Manual Shifts using Small-scale Maps
Edit Coords.
yes
Rebuild Wire Model
Remeasure and Edit Coords.
no
Automated Shifts using Difference Map (30 min.)
Constraints (30 min. - 2 hr.)
New Solvent Indicated?
yes
Find Solvent (5 min.)
Close Contacts (10 min.)
no

Figure 2

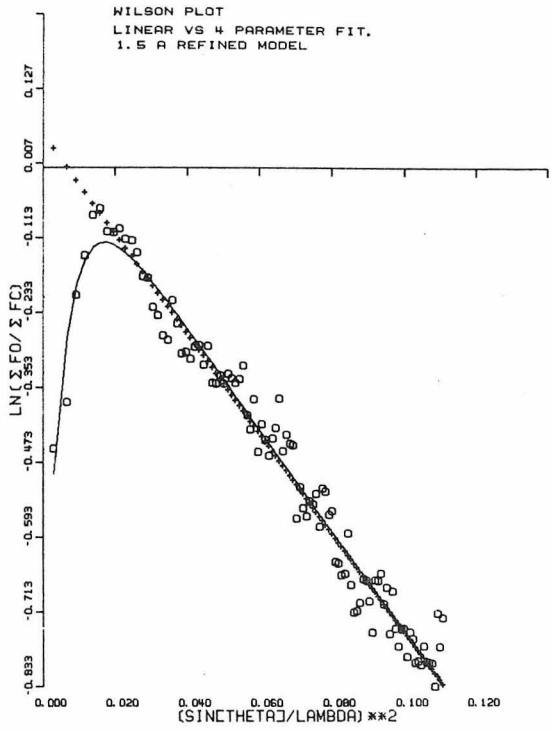
WILSON PLOT
LINEAR VS 4 PARAMETER FIT.
1.5 A REFINED MODEL
LN(ΣFO/ΣFC)
0.127
0.007
-0.113
-0.233
-0.353
-0.473
-0.593
-0.713
-0.833
0.000
0.020
0.040
0.060
0.080
0.100
0.120
(SINCTHETA)/LAMBDA)**2

Figure 3

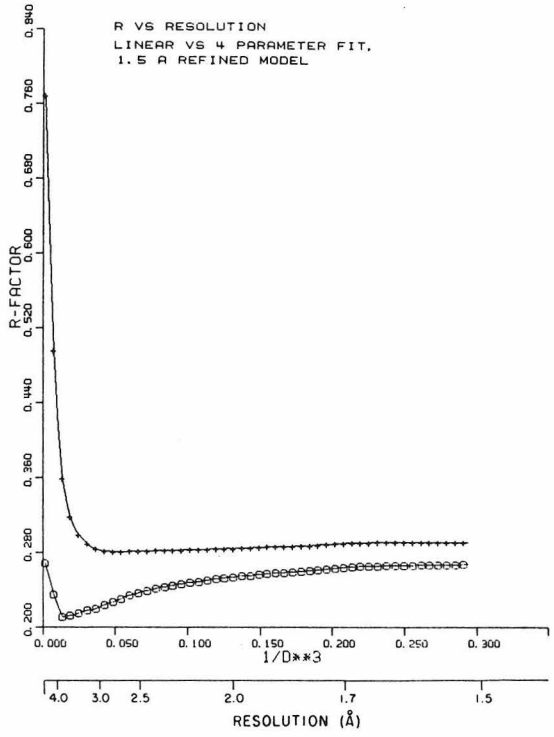
R VS RESOLUTION
LINEAR VS 4 PARAMETER FIT,
1.5 A REFINED MODEL
R-FACTOR
0.840
0.760
0.680
0.600
0.520
0.440
0.360
0.280
0.200
0.000
0.050
0.100
0.150
0.200
0.250
0.300
1/D**3
4.0
3.0
2.5
2.0
1.7
1.5
RESOLUTION (Å)

Figure 4

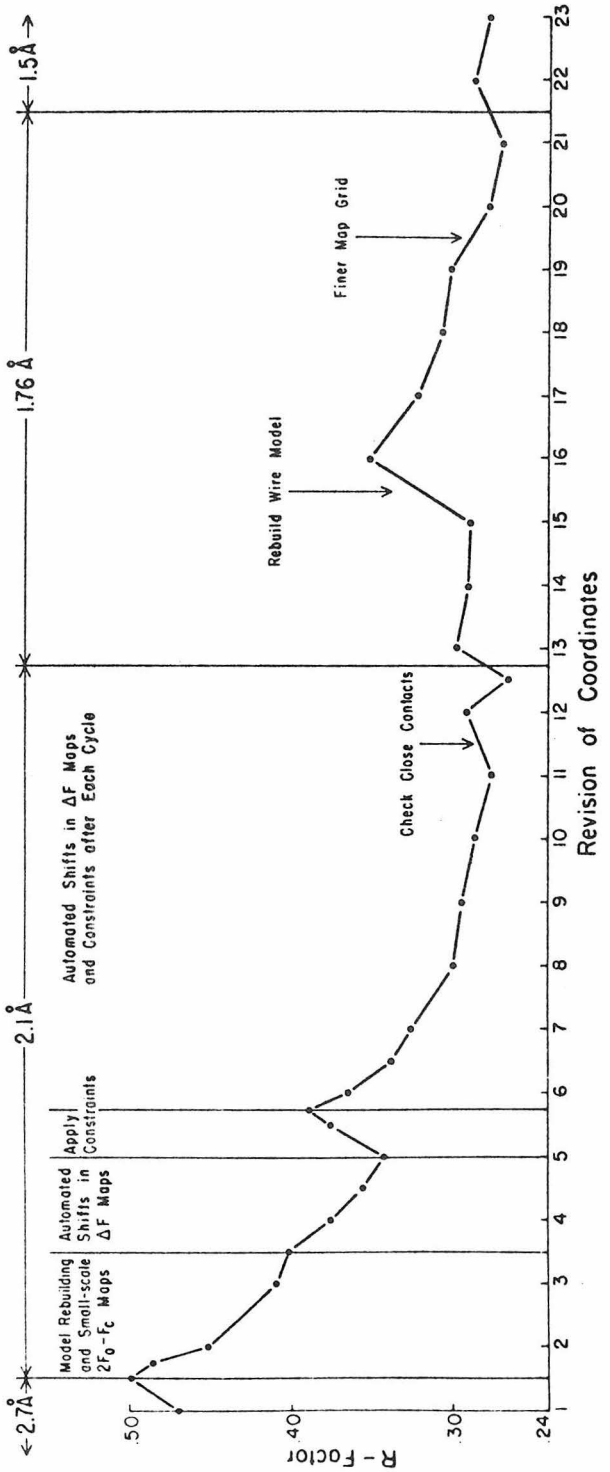
2.7Å
2.1Å
1.76 Å
1.5Å
Model Rebuilding and Small-scale $2F_o-F_c$ Maps
Automated Shifts in ΔF Maps
Apply Constraints
Automated Shifts in ΔF Maps and Constraints after Each Cycle
Check Close Contacts
Rebuild Wire Model
Finer Map Grid
R - Factor
.50
.40
.30
1 2 3 4 5 6 7 8 9 10 11 12 13 14 15 16 17 18 19 20 21 22 23 24
Revision of Coordinates

Figure 5

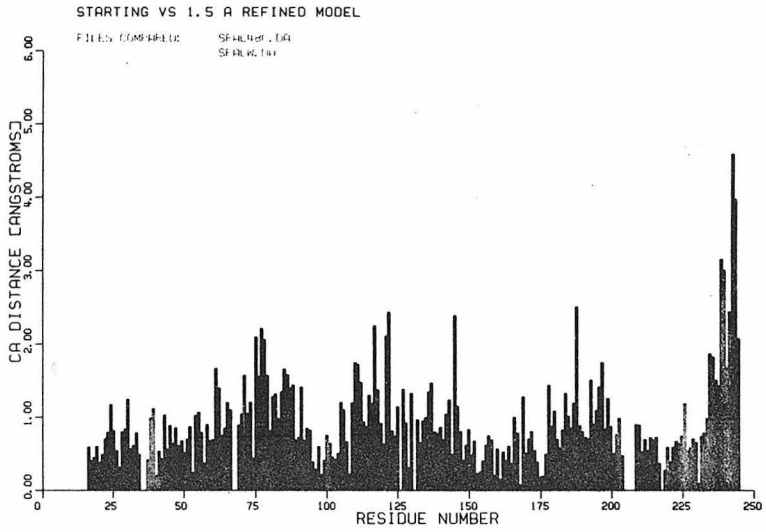
STARTING VS 1.5 A REFINED MODEL
CA DISTANCE (ANGSTROMS)
0.00
1.00
2.00
3.00
4.00
5.00
6.00
0
25
50
75
100
125
150
175
200
225
250
RESIDUE NUMBER

Figure 6a

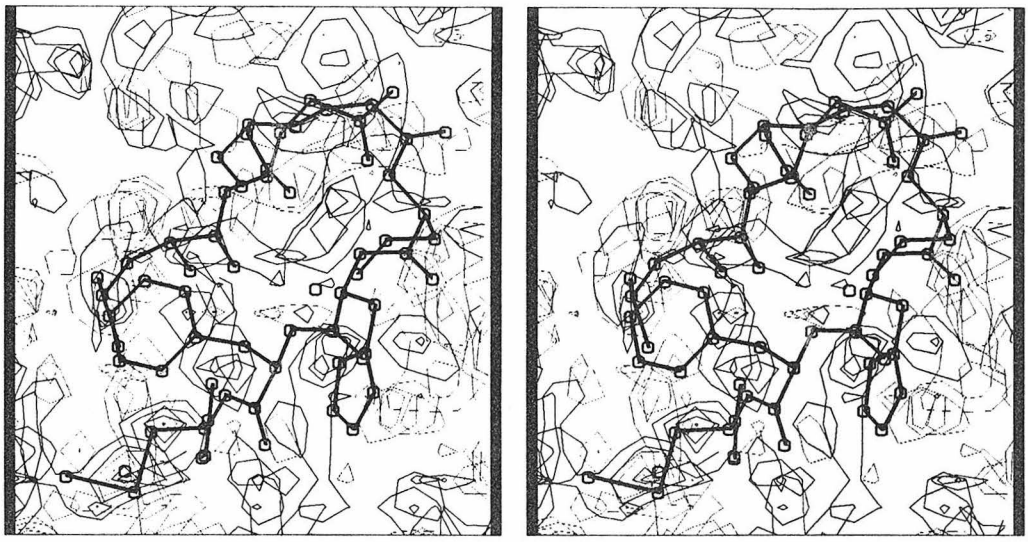

Figure 6b

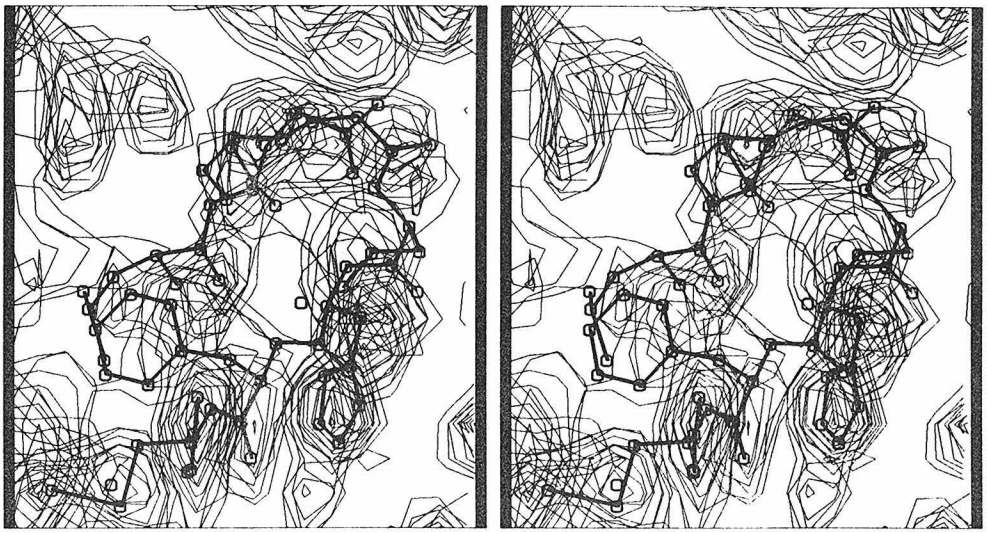

Figure 6c

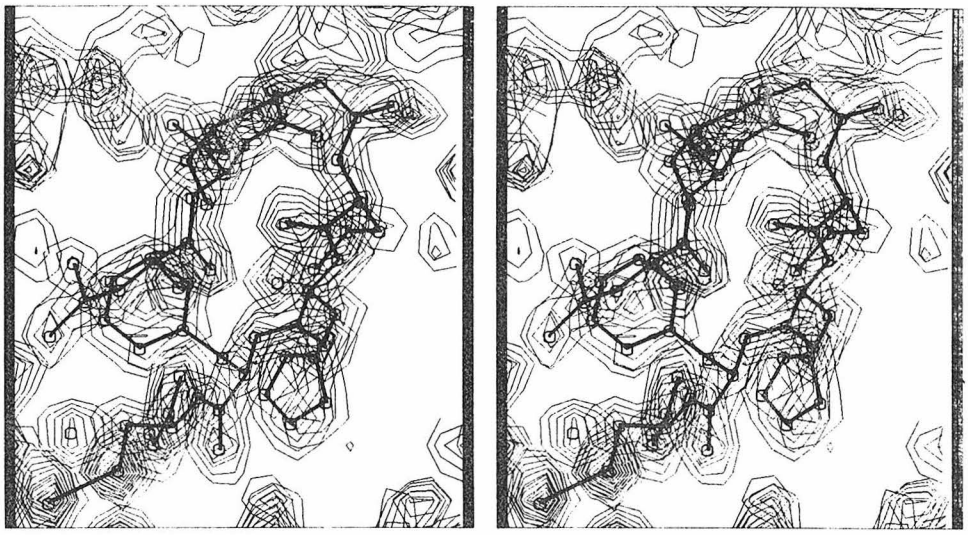

Figure 6d

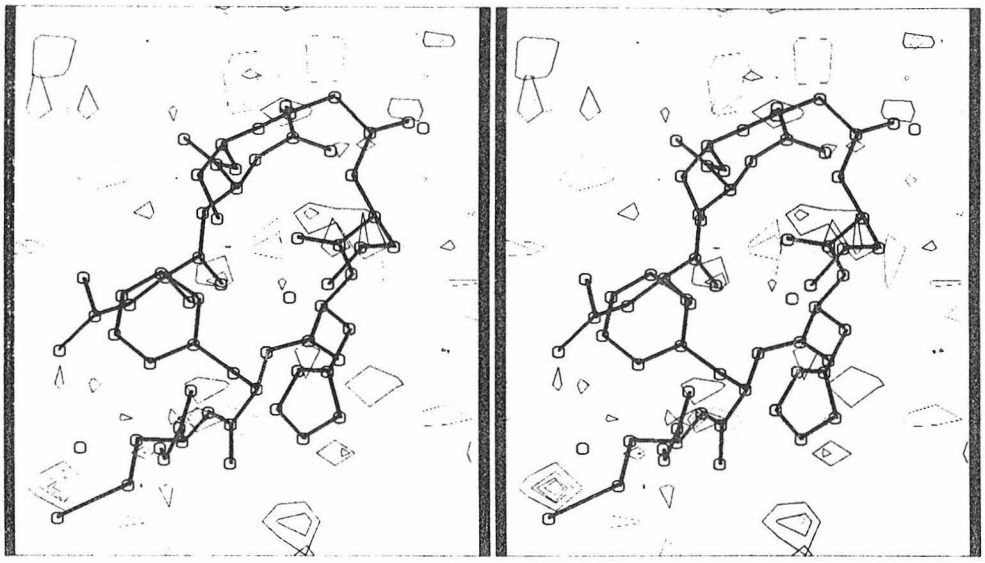

Figure 7

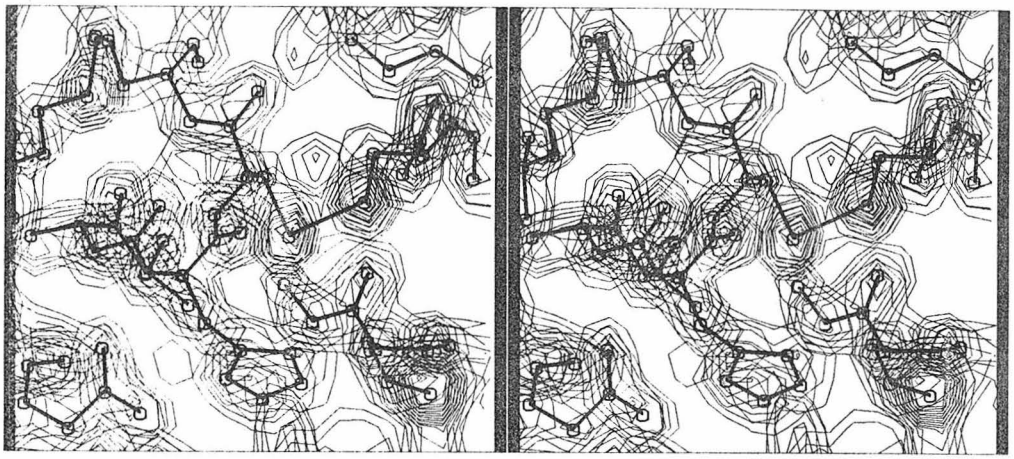

Figure 8

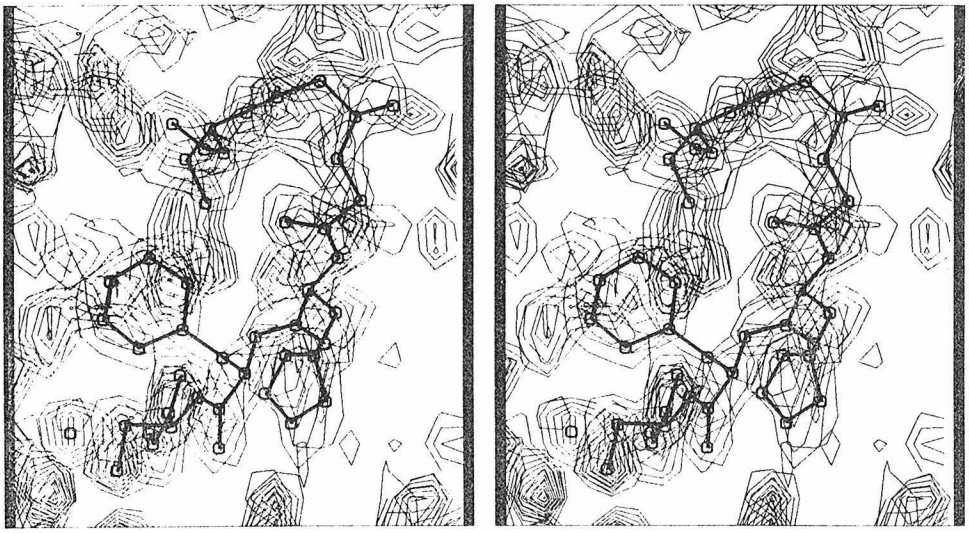

Appendix 7

One Picture is Worth a Thousand Words:

A Trypsin Pictorial Assay

This appendix consists mainly of stereo figures of the refined trypsin structure, generated with the system described in Chapter III. The electron density syntheses used for these figures were all computed with phases (ϕ_c) calculated from the current model. Except where noted, the observed structure factor amplitudes (F_o) for DIP-trypsin to 1.5 Å resolution were used, and contour levels were approximately 0.5e/Å^3 x 0.5e/Å^3 (i.e., proceed from 0.5e/Å^3 in 0.5e/Å^3 increments).

The atoms of the DIP-trypsin catalytic site are shown superposed on the F_o, ϕ_c electron density in Figure 1. The Fourier series was terminated at 6 Å, 4.5 Å, 3 Å, and 1.5 Å nominal resolution in frames a, b, c, and d, respectively. There are a number of interesting and informative features in this series. First, these density maps are essentially "best-case" maps; the amount of detail visible at each resolution is about as much as can be expected for a protein structure of medium size.

Second, the appearance of structural information can be followed as a function of resolution. At 6 Å (Figure 1a)*, the main chain of the protein cannot be readily traced; the 3_{10} loop containing the His 57 imidazole is seen as a pillar rather than a loop. Moreover, no side chain information is visible (with the exception of a large peak for the DIP-group). At 4.5 Å (Figure 1b), it is possible to trace the path of the main chain, although the orientation of amide

---

* In view of the existence of a well-defined saddle-point in the 6 Å electron density above the His 57 imidazole, the high-occupancy site in Ag^+-trypsin will henceforth be referred to as "high-o. silver."

planes cannot be easily determined. Density is present for only the larger side chains (e.g., His 57). Ripples in the electron density, apparently resulting from series termination, can be seen; for example, there is little density for the main chain from residue 195 to 196, in back of the DIP-group. At 3 Å (Figure 1c), there are protrusions in the main-chain density for carbonyl groups, and all of the side chains are visible, although interpretation of 3 Å density is in practice often ambiguous. At 1.5 Å (Figure 1d), individual atoms have begun to be resolved, and interpretation is straightforward.

A third and very important point about this resolution series is that in the interpretation of low- and medium-resolution maps (e.g., when constructing a wire model), placement of atoms should not necessarily follow the highest density. An obvious example is that the density tends to be highest at the center of rings and disulfide bridges rather than at the atomic sites themselves, at resolutions above 2.5 Å. Some more subtle cases, however, are apparent in Figures 1b and 1c. At 4.5 Å, the disulfide bridge is not at all centered in the density. This arises mainly from overlap with the density of the Phe 41 side chain in the upper right and the main-chain density in the upper left. In the 3 Å map the Cβ of His 57 appears uncentered due to overlap between the main chain density and that of the imidazole ring. Overlap of the Asp 102 carboxyl-group density with that of the His 57 imidazole and of Ser 214 Oγ (just below the lower boundary of the picture) causes the carboxyl to look somewhat miscentered, and was a major factor in the original placement of these

groups such that the His 57 $N\delta_1$ pointed between the two carboxyl oxygens (1). Even in the 1.5 Å map atoms should not necessarily be positioned in maximum density. For instance, in the case of carbonyl oxygens the maximum density is displaced toward the carbonyl carbon. This result serves to emphasize the value of difference syntheses in protein structure refinement performed in electron-density space. The orientation of the catalytic groups Asp 102, His 57, and Ser 195 can be seen quite clearly in this figure.

Figure 2 is a view down the z axis of the DIP-serine. Its resemblance to the postulated tetrahedral intermediate is apparent; the oxygen atom corresponding to the carbonyl oxygen of a specific substrate is well stabilized in its position by hydrogen bonds to the main-chain amides of Gly 193 and Ser 195. Also visible in the upper right is the salt bridge between the carboxyl of Asp 194 and the amino terminus, which is formed upon activation of trypsinogen.

The region around His 40, approximately the same region as shown in Figures 6 and 8 of Appendix 6 but computed with more recent phases, is pictured in Figure 3. The orientation of the amide planes in this loop was highly ambiguous in the starting (MIR) map.

The fit of some typical aromatic side chains to the refined density is illustrated in Figures 4, 5, and 6. The indole ring in Figure 4 is part of the side chain of Trp 141. The $N\varepsilon_1$ is hydrogen bonded to the Asp 71 carbonyl oxygen, which can be seen in the upper right. In the lower left, part of the His 40 imidazole ring and the C=O of Gly 193 are visible. Two well-ordered solvent molecules are

also shown. Figures 5 and 6 are two different views of Tyr 234, down x and down z, respectively. The ring and associated peptide chain are very well defined, to the point of resolving the individual atoms.

Figures 7 and 8 are pictures of one of the regions most in need of further refinement--the primary Ca^{2+} site. The manner in which the polypeptide chain forms a pocket for the Ca^{2+} ion can readily be seen in stereo in Figure 7. Because of the high degree of crowding, this figure was contoured at a very high level--from $0.80e/Å^3$ in $0.55e/Å^3$ steps. The occupancy of the bound ion (solid black in this picture) has increased dramatically during the last few refinement cycles, and it now appears likely that this ion is indeed Ca^{2+}. Although the positions of the six ligands are for the most part well defined, the orientation of the Glu 70 (to the left and below the ion) and Glu 80 (to the left and above the ion) side chains is still not completely clear.

The nearly octahedral coordination of the bound ion can be observed more closely in Figure 8. Frame 8a was drawn from the current set of coordinates and phases; frame 8b is based on interpretation of the first 1.76 Å map. The view in each frame is down z. There has been a significant change in placement of the Glu 80 side chain; however, as suggested above, the interpretation for this group is still tentative. There is a high degree of negative charge surrounding this site, the positive ion contributing to neutralization of charge on three different Glu side chains.

Thus, the refinement, although in its final stages, is still continuing. Additional DIP-trypsin data have been measured to 1.35 Å ($2\theta = 69.6°$, CuK_α radiation), and these data will soon be incorporated. The DIP-trypsin coordinates have been deposited with the Brookhaven Protein Data Bank, Brookhaven National Laboratory, Upton, Long Island, New York 11973, from whom copies can be obtained.

I am grateful to Dr. Charles Cantor for suggesting the resolution series.

References

1. Krieger, M., Kay, L.M., and Stroud, R.M. (1974). J. Mol. Biol. 83, 209-230.

Figure Legends

FIGURE 1. Resolution series, viewed down the y axis, of the DIP-trypsin catalytic site. Each map is an F_o, ϕ_c synthesis with terms included to the indicated resolution.

a) 6.0 Å, contoured from 0.05e/Å^3 in 0.05e/Å^3 steps.

b) 4.5 Å, contoured from 0.10e/Å^3 in 0.10e/Å^3 steps.

c) 3.0 Å, contoured from 0.35e/Å^3 in 0.30e/Å^3 steps.

d) 1.5 Å, contoured from 0.50e/Å^3 in 0.50e/Å^3 steps.

FIGURE 2. View down z of the "oxyanion hole" and N-terminal salt bridge.

FIGURE 3. View down y of the area around His 40.

FIGURE 4. Trp 141 and neighboring atoms, down z.

FIGURE 5. The region around Tyr 234, down x. Contours are from 0.60e/Å^3 in steps of 0.4e/Å^3.

FIGURE 6. Tyr 234, down z. Part of the His 91 imidazole is visible in the lower left.

FIGURE 7. The primary Ca^{2+} binding site. This loop was almost a solid ball of density in the starting 2.7 Å map. There are several

very well ordered solvent molecules in this area, as well as the bound ion, which is totally black in this picture.

FIGURE 8a. A closer view of the metal ion, which has recently refined to an occupancy nearly that expected for fully occupied Ca^{2+}. The six ligands are arranged in a nearly octahedral fashion. The ion is in a position to take part in charge neutralization of three different Glu carboxyl groups--those of Glu 70, Glu 77, and Glu 80.

b) A drawing of the metal ion site based on interpretation of the first 1.76 Å map. The largest changes have been in the occupancy of the ion and the position of the Glu 80 side chain, as described in the text.

Figure 1a

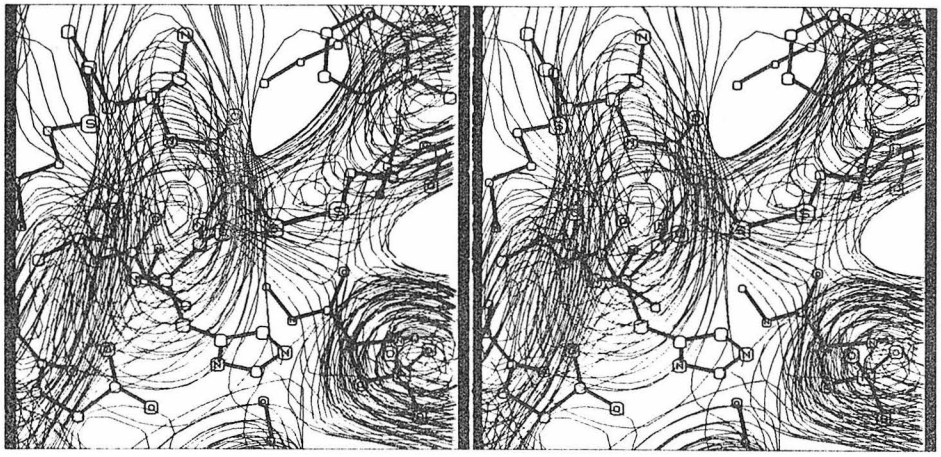

Figure 1b

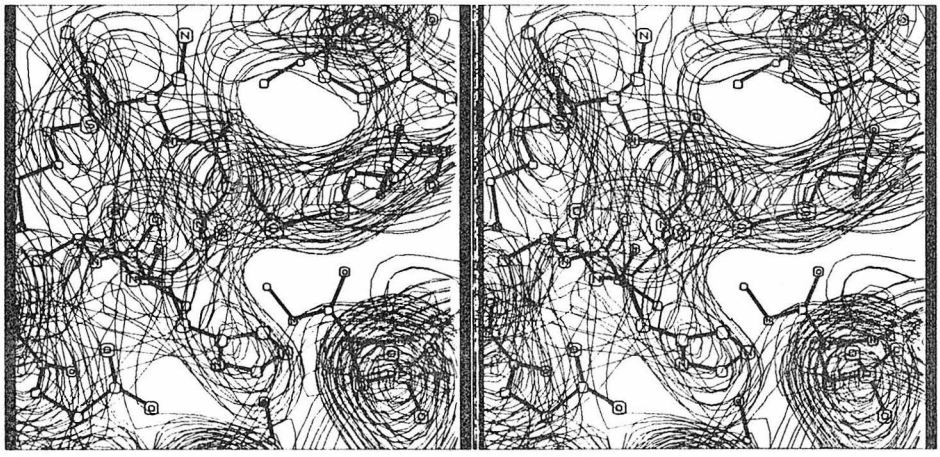

Figure 1c

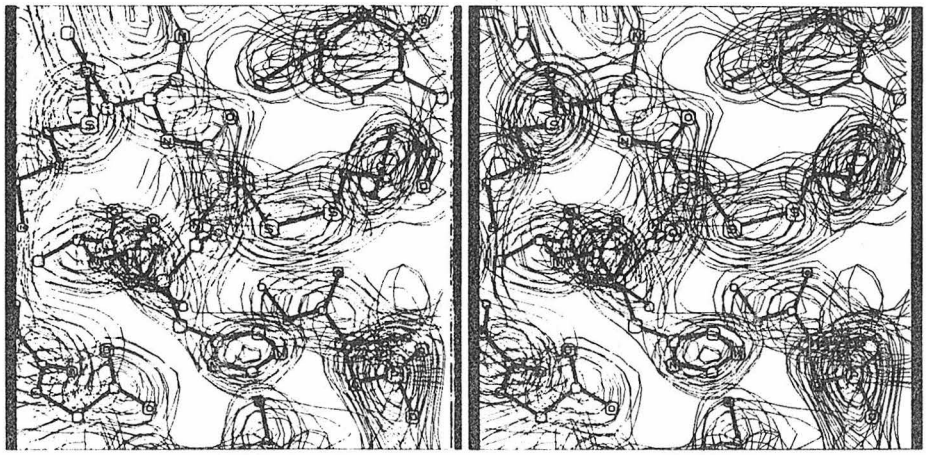

Figure 1d

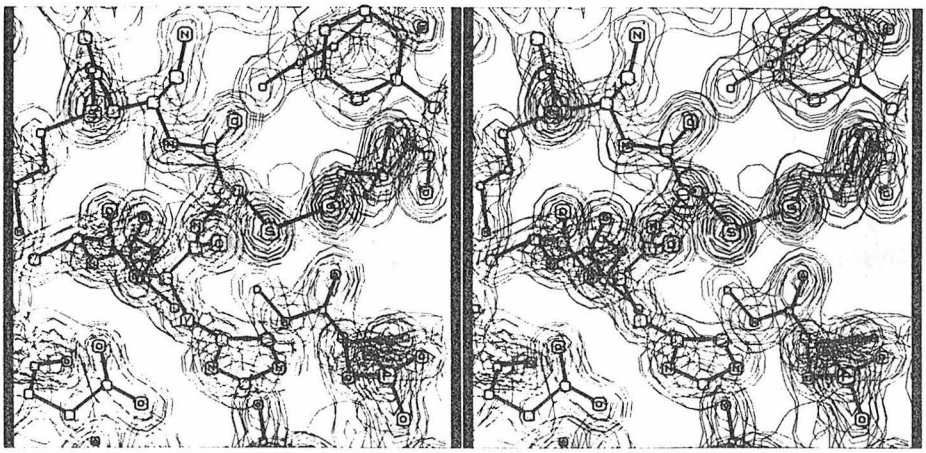

Figure 2

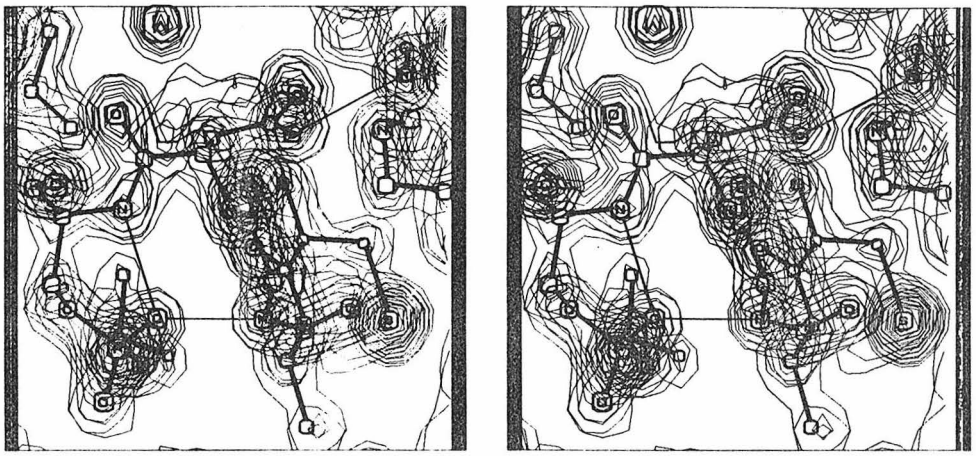

Figure 3

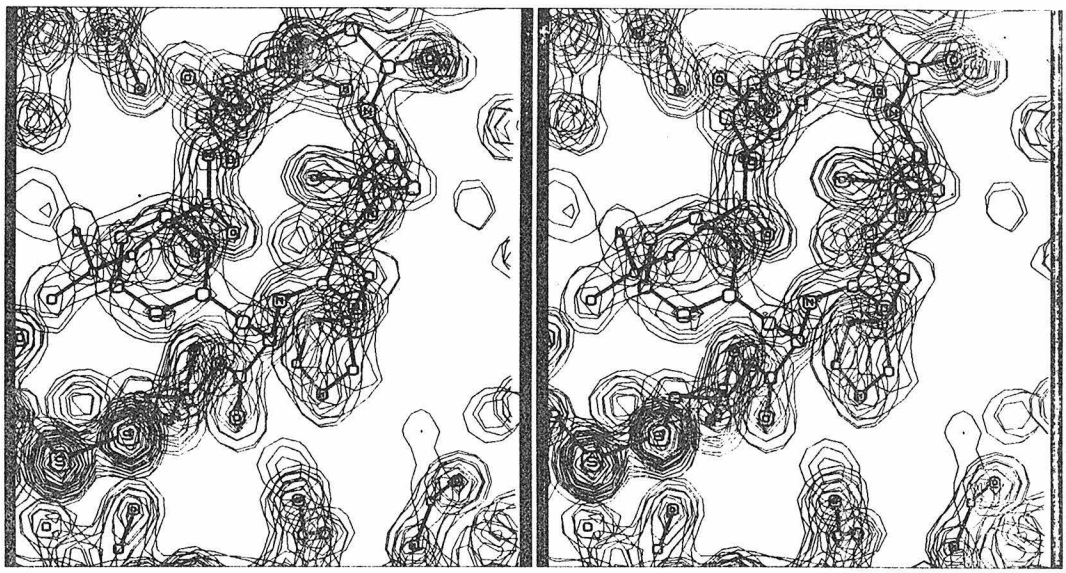

Figure 4

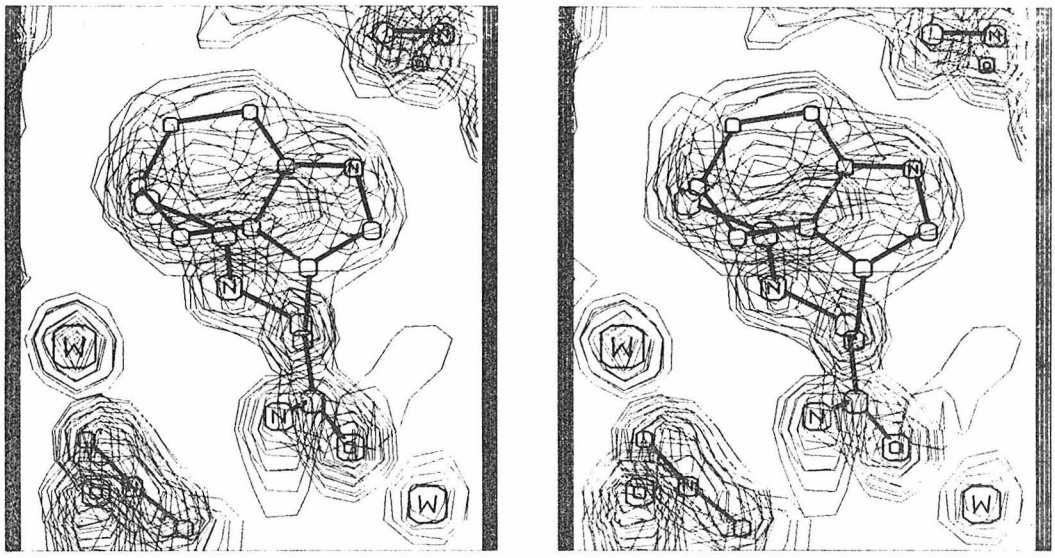

Figure 5

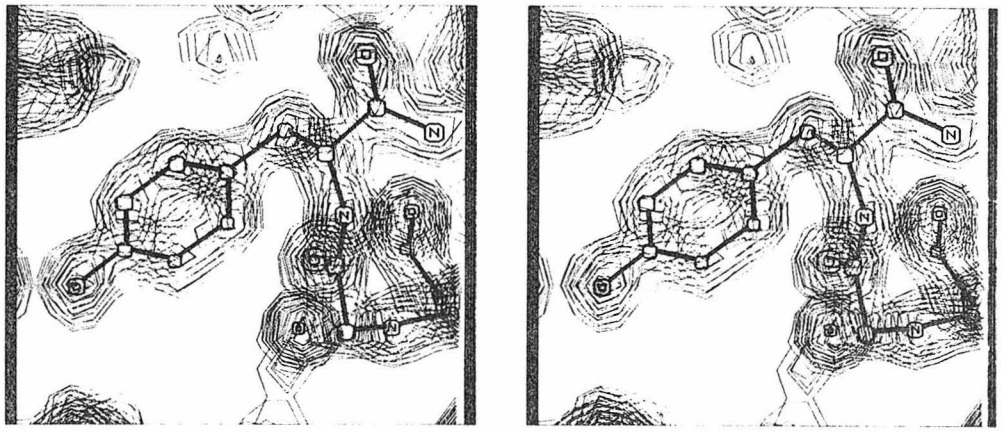

Figure 6

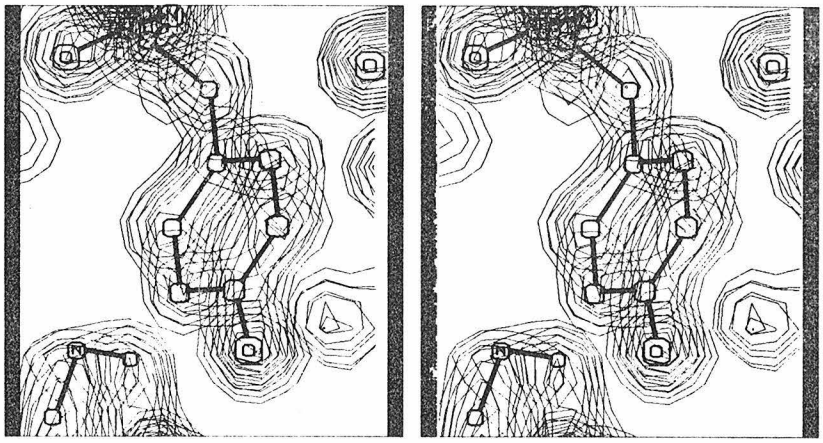

Figure 7

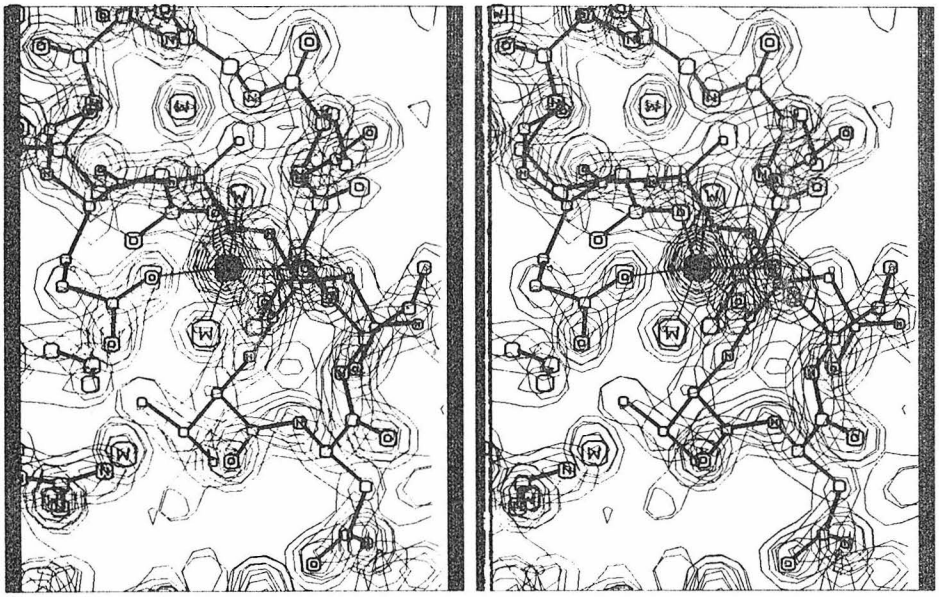

Figure 8

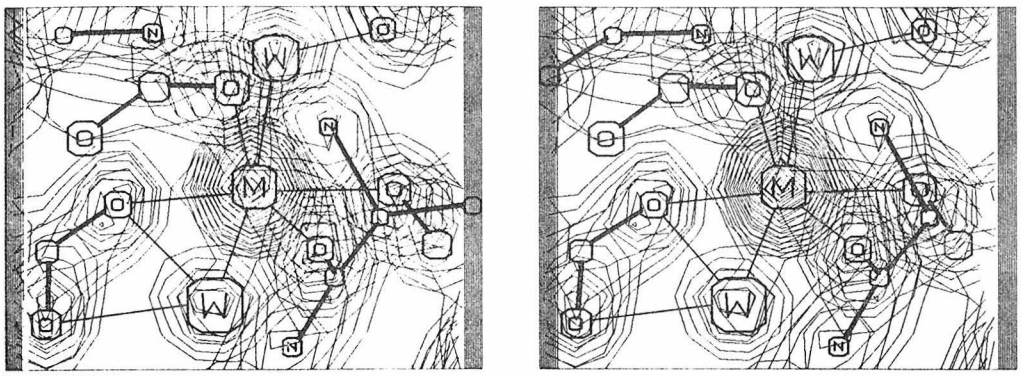

(a)

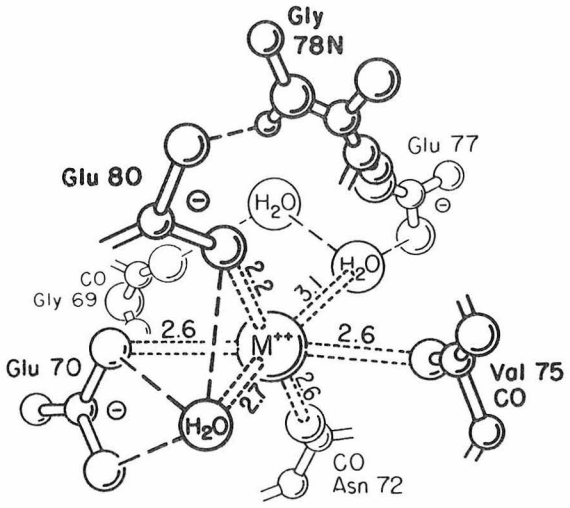
Gly
78N
Glu 77
Glu 80
H2O
H2O
CO
Gly 69
2.2
3.1
2.6
M++
2.6
Glu 70
Val 75
CO
2.7
2.6
H2O
CO
Asn 72

(b)